의학박사 학위논문

Contributions of Ras hyperactivation in neuron and astrocyte to memory deficits in mouse models of RASopathy

신경세포와 교세포의 Ras 경로 과활성화가
Ras 관련 신경발달장애 생쥐 모델의
기억장애에 미치는 영향

2023년 8월

서울대학교 대학원
의과학과 생리학전공

강 민 경

Contributions of Ras hyperactivation in neuron and astrocyte to memory deficits in mouse models of RASopathy

지도 교수: 이 용 석

이 논문을 의학박사 학위논문으로 제출함
2023년 4월

서울대학교 대학원
의과학과 생리학전공
강 민 경

강민경의 의학박사 학위논문을 인준함
2023년 7월

위 원 장 _____ (인)

부위원장 _____ (인)

위 원 _____ (인)

위 원 _____ (인)

위 원 _____ (인)

Contributions of Ras hyperactivation in neuron and astrocyte to memory deficits in mouse models of RASopathy

Advisor: Yong-Seok Lee

A dissertation submitted to the
Department of Biomedical Science
at the Seoul National University College of Medicine

By Minkyung Kang

in partial fulfillment of the requirements
for the Degree of Doctor of Philosophy

April 2023

Approved by Thesis Committee
July 2023

Chair _____ (인)

Vice Chair _____ (인)

Examiner _____ (인)

Examiner _____ (인)

Examiner _____ (인)

Preface

This dissertation consists of a couple of works that I involved as a first author. Review in chapter 1 has been published in Molecular brain (Kang and Lee, 2019). Results in chapter 2 has been published in Scientific reports (Ryu and Kang et al., 2020). Most of the results described in chapter 3 are in preparation for publication.

Kang, M & Lee, Y.S. The impact of RASopathy-associated mutations on CNS development in mice and humans. *Molecular Brain*, 12:96 (2019).

Ryu, H.H & Kang, M et al. Neuron type-specific expression of a mutant KRAS impairs hippocampal-dependent learning and memory. *Scientific Reports*, 10:17730 (2020).

Abstract

Contributions of Ras hyperactivation in neuron and astrocyte to memory deficits in mouse models of RASopathy

Minkyung Kang
Department of Biomedical Science
The Graduate School
Seoul National University College of Medicine

The RAS-ERK signaling pathway plays critical roles in brain function, including cellular processes, synaptic transmission, and learning and memory in central nervous system. Germline mutations of molecules in the RAS-ERK signaling pathway are associated with a series of developmental disorders, collectively called RASopathy, which includes neurofibromatosis type 1, Noonan syndrome, cardio-facio-cutaneous syndrome, and Costello syndrome. Most mutations associated with RASopathy enhance the activity of RAS-ERK signaling pathway, and therefore, most cases with RASopathies share representative clinical characteristics, especially, cognitive impairments. Recent studies using various mouse models of RASopathies have shown that each RAS-ERK signaling component may have a distinct molecular and cellular pathophysiology depending on cell type-specificity. In this dissertation, I hypothesized that each neuronal and astroglial cell type might have distinct roles that contribute to the cell type-specific pathophysiology in RASopathy-related cognitive deficits. To answer the question, I investigated the cellular mechanisms underlying learning and memory impairments in two types of RASopathy mouse models, *KRAS*^{G12V} and *BRAF*^{K499E}.

In chapter 1, I reviewed the previous literatures that investigated the impact of RASopathy-associated mutations on central nervous system development in mice and humans, which provided understandings and insights into the specific roles of RAS-ERK signaling genes to central nervous system and

the subsequent effect on cognitive function in adult mice.

In chapter 2, I investigated the impacts of neuron type-specific manipulation of RAS-ERK signaling by expressing *KRAS*^{G12V} in the hippocampus. I found that the expression of *KRAS*^{G12V} in either hippocampal excitatory or inhibitory neurons results in spatial learning and memory deficits in adult mice, each for different reasons. In inhibitory neurons, *KRAS*^{G12V} induced enhanced GABAergic inhibitory synaptic transmission, and impaired long-term potentiation, which could be restored by picrotoxin treatment. In contrast, in excitatory neurons, *KRAS*^{G12V} induced neuronal cell death, which might be responsible to the behavioral defects. This result showed that both inhibitory and excitatory neurons are involved in *KRAS*-associated learning impairments in adult via distinct mechanisms.

In chapter 3, I investigated how the aberrant *Braf* signaling affects cognitive functions by using CFC syndrome-associated *Braf* mutations. Expressing the *Braf*^{K499E} under control of Nestin-Cre, resulted in severe hippocampal memory deficits in mice, whereas *Braf*^{K499E} in either excitatory or inhibitory neurons did not alter learning and memory. Intriguingly, I found that the *Braf*^{K499E} and subsequently activated ERK signaling renders astrocytes being in reactive-like status. Importantly, astrocyte-specific expression of the mutant BRAF in adult was sufficient to induce cellular and behavioral deficits in mice, which are accompanied by hyperactive Ca^{2+} fluctuations in astrocyte. Finally, the learning deficits of Nestin;*Braf*$^{KE/+}$ mice can be reversed by normalizing RAS-ERK signaling solely in astrocytes. This study demonstrates that the reactive-like astrogliosis may underlies the severe cognitive deficits in CFC syndrome.

In conclusion, I demonstrated that the RASopathy-associated genes are differentially affect functional properties of each cell type in central nervous system, which may be responsible for the cell type-specific pathophysiology of individual RASopathy patient. By showing the neuronal contribution in

mutant *KRAS*-mediated learning deficits, and astrocytic contribution in mutant *BRAF*-mediated learning deficits, these results strongly suggest that both neuron and astrocyte are responsible for RASopathy-related cognitive impairments in each gene-specific manner. Furthermore, this study will provide insight to identify cell types as well as underlying mechanism accounting for the cognitive deficits in other RASopathies not covered here.

Keyword: RAS-ERK signaling, neurodevelopmental disorders, learning and memory, hippocampus
Student Number: 2017-37022

Table of Contents

List of Figures and Table

Chapter 1

The impact of RASopathy-related mutations on CNS in human and mice

1. RAS-ERK signaling and RASopathy

The RAS-extracellular signal-regulated kinase (ERK) pathway is well identified signaling cascade that transduce signals from membrane receptors to the cytoplasm and nucleus by protein-protein interaction and phosphorylation (1-3). This highly conserved pathway plays pivotal roles in controlling numerous biological processes such as cell growth, proliferation, and differentiation in developing and adult organs (2, 4). RAS-ERK signaling is initiated by the binding of growth factors to G-protein coupled receptors, such as receptor tyrosine kinases (RTKs), and triggered by a sequential activation of RAS, RAF, MEK, and MAPK (Figure 1). First, RAS protein is composed of a three multigene family that includes HRAS, KRAS, and NRAS. These RAS proteins encode a small guanosine nucleotide-bound GTPase protein, and switch the cycles between an active GTP-bound state and inactive GDP-bound state during the signal transduction. The process is facilitated by guanine nucleotide exchange factors (GEFs) and GTPase-activating proteins (GAPs). SOS1 is a well known GEF that activate RAS, whose activity is regulated by multiple adaptor proteins, including GAB1 and GRB2 (5). On the other side, NF1 is a representative GAP that switch RAS into inactive state by hydrolyzing GTP to GDP. Sequentially, activated RAS induces the activation of direct downstream effector, RAF, by association with the RAS-binding domain. *RAF*, which consist of ARAF, BRAF, and RAF1, encodes a serine/threonine kinase. Phosphorylation of RAF stimulates its kinase activity, initiating sequential phosphorylation, and activates the MAPK/ERK kinase 1/2 (MEK1/2). In turn, MEK1/2 activates ERK1 and ERK2, homologous subtypes of the ERK family, by phosphorylation of tyrosine and threonine residues (6). As final effectors of the RAS-ERK cascade, ERK1 and ERK2 exert influence on various downstream molecules, such as transcription factors (7).

Due to essential roles of RAS-ERK signaling pathway in diverse cellular and biological processing, germline dysregulations of RAS-ERK signaling pathway results in a class of developmental disorders, that are collectively assorted RASopathy (3, 8, 9). Representatively, RASopathy includes neurofibromatosis type 1 (NF1), Noonan syndrome, cardio-facio-cutaneous (CFC) syndrome, LEOPARD syndrome, Legius syndrome, and Costello syndrome (CS), and so on. In most cases, RASopathy patients share typical clinical features, including a short stature, developmental delays, craniofacial dysmorphism, cardiac defects, and neurological deficits (10). These typical characteristics expressed in RASopathy patients are summarized in table 1. Although most of RASopathy share major clinical symptoms, each RASopathy also exhibit distinct and unique characteristics, depending on the mutated RAS-ERK signaling components (3, 11). Consistently, several studies have demonstrated the disease- and gene-specific impairments in central nervous system (CNS) development and function in each RASopathy animal model (Table 2). In this chapter, I review the distinctive roles of RAS-ERK signaling genes in CNS features that have been revealed by examining the defects in CNS development of RASopathies. Furthermore, I also review how RASopathy-related mutations affect neurological function in mice and human.

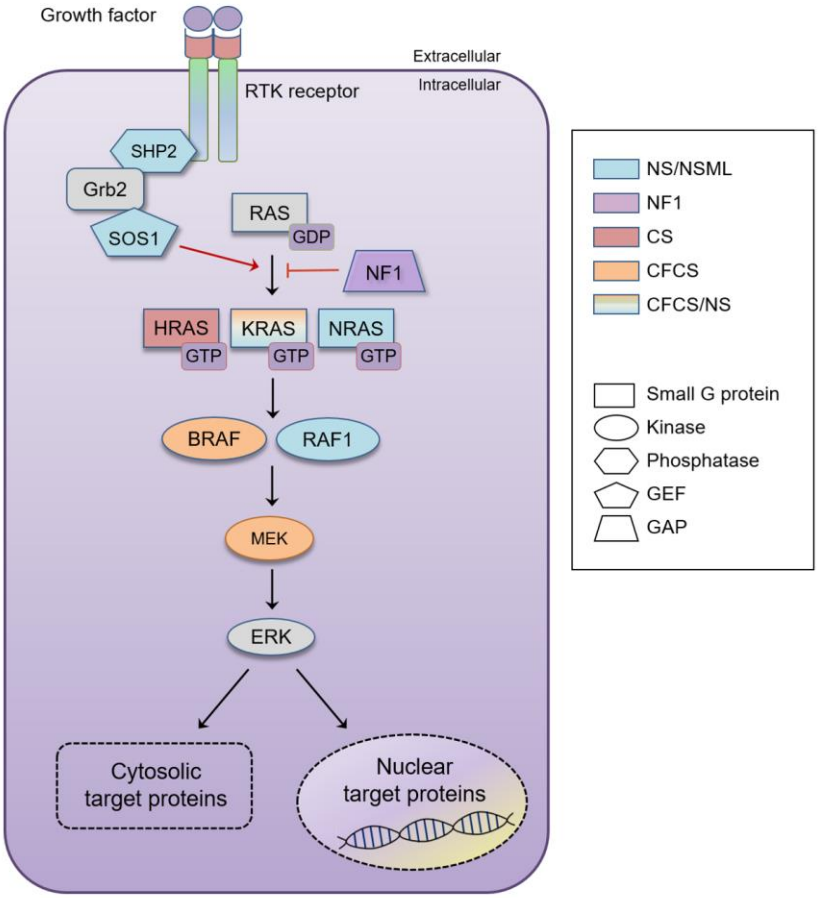

Figure 1. The RAS-ERK signaling pathway and related neurodevelopmental disorders. Genes frequently mutated in RASopathies are colored on each disorder and are presented as a polygon depending on their functional categories. NS/NSML, Noonan syndrome/Noonan syndrome with multiple lentigines; NF1, Neurofibromatosis type 1; CS, Costello syndrome; CFCS, Cardio-facio-cutaneous syndrome; GEF, guanine exchange factor; GAP, GTPase activating protein.

Disease	Associated genes	CNS structural phenotypes	Other phenotypes
NF1	*NF1* (95%) (12)	Neurofibromas , abnormal cortical development (13), abnormal glial development (14), macrocephaly	Below-average IQ, ADHD, impaired executive functioning, deficits in visual-spatial skills (15, 16), hyperpigmentation of melanocytes, hamartomas of the iris (17, 18), bone malformation, cardiac defects (19, 20)
NS /NSML	*PTPN11* (>50%) (21), *RAF1* (3-17%) (22, 23), *SOS1* (9-13%) (24), *KRAS* (<2%) (25, 26), *BRAF* (<2%) (22), *MEK1/2* (<2%) (27)	Cerebellar ectopia (28, 29), temporal lobe anomaly, hydrocephalus, cerebral abscess (30-32), epilepsy, cortical dysplasia (33)	Neurocognitive delay (33-35), typical facial abnormalities, short stature, motor delay, increased risk of cancer, cardiac defects (34-40)
CFCS	*BRAF* (43-78%) (41-43), *MEK*1/2 (7-11%) (42, 43), *KRAS* (5-8%) (25, 43)	Ventriculomegaly, hydrocephalus (44-50), atrophy (44, 46, 51-54), migration and myelination abnormalities, agenesis of corpus callosum (50, 52, 55-57)	Neurological abnormalities, seizures, tactile defensiveness, learning disabilities (4, 50, 55), craniofacial defects, cardiac defects (4, 58, 59), motor delay, hypotonia (4, 50, 55)
CS	*HRAS (85-90%)* (60-62), *KRAS* (7%) (63), *BRAF* (4-6%) (27), *MEK*1/2 (2-3%) (27)	Ventricular abnormalities (64-67), cerebral malformations (64, 65, 67-71), cerebellar abnormalities (66, 69, 71-74), macrocephaly (59, 60)	Mental retardation (59, 60), facial features, loose skin, severe failure to thrive, predisposition to tumors (59, 60)

NF1, Neurofibromatosis type 1; NS, Noonan syndrome; NSML, Noonan syndrome with multiple lentigines; CFCS, Cardio-facio-cutaneous syndrome; CS, Costello syndrome; IQ, intelligence quotient; ADHD, attention deficit hyperactivity disorder;

Table 1. Human patients with RASopathies and their representative phenotypes.

Gene	Mouse model	CNS structural phenotypes	Other phenotypes
Nf1	*Nf1* homozygous KO	Defects in the neural tube, hyperplasia of neural crest-derived ganglia (75)	Embryonic lethality, heart defects, delay in organ development (76, 77)
	Nf1 heterozygous KO	Increased astrocyte number (78, 79)	Impaired synaptic plasticity, impaired spatial learning, Heart defects (80-82)
	Synapsin 1-dependent *Nf1* ablation	Reduced size of forebrain, reduced cortical thickness, increased gliogenesis (83)	Learning deficits, growth retardation (83, 84)
	hGFAP-dependent *Nf1* ablation	Increased gliogenesis, enlarged cerebral cortex, defective GNP migration and proliferation (85-88)	Postnatal lethality, growth retardation (86, 87)
	BLBP-dependent *Nf1* ablation	Increased glial lineage proliferation, abnormal neuronal differentiation (89)	Postnatal lethality (89)
	Nestin-dependent *Nf1* ablation (induction in adulthood)	Unlocked oligodendrocyte lineage (latent), defective GNP proliferation and migration, increased adult neurogenesis (88, 90, 91)	Spontaneous antidepressive-like behavior (91)
Ptpn11	Nestin-dependent *Ptpn11* ablation	Decreased neural stem cell proliferation, lamination defects, reduced number of neurons, increased number of astrocytes (92)	Postnatal lethality, growth retardation (92)
	Olig1-dependent *Ptpn11* ablation	Decreased number of OLC precursors and mature oligodendrocytes, reduced axonal myelination (93)	Developmental abnormalities (93)
	Olig2-dependent *Ptpn11* ablation	Decreased number of oligodendrocyte precursors, hypomyelination (94)	Postnatal lethality, severe shivering (94)
	Olig2-dependent *Ptpn11*^{Q79R} KI	Increased number of oligodendrocyte precursors, abnormal myelination (94)	Not known
	Nestin-dependent *Ptpn11*^{E76K} KI	Hydrocephalus, aberrant development of ependymal cells, reduced proliferation, enhanced glial differentiation (95)	Postnatal lethality, dome-shaped head, reduced anxiety behavior, hyperactivity, impaired motor function (95)
	Ptpn11^{D61G} herozygous KI	Increased neurogenesis, decreased gliogenesis (96)	Impaired synaptic plasticity, / spatial learning, craniofacial dysmorphia (97, 98)

Kras	Synapsin1-dependent *Kras*^{G12V} KI	Enhanced GABAergic synaptogenesis (99)	Increased inhibitory tone, impaired spatial learning (99)
Hras	*Hras*^{G12V} homozygous KI	Hypertrophy of the brain and pyramidal neurons (100)	Impaired spatial learning, facial dysmorphia, cardiac defects (100)
	aCaMKII-dependent *Hras*^{G12V} KI	Increase in docked vesicles (101)	Increased synaptic plasticity, enhanced spatial learning (101)
Braf	Nestin-dependent *Braf* ablation	Impaired neuronal differentiation, dysmyelination, defective oligodendrocyte differentiation (102, 103)	Postnatal lethality, growth retardation, defective motor coordination, neuromuscular defects (102, 103)
	Braf^{V600E} heterozygous KI	Increased number of GFAP positive cells in the DG (104)	Reduced life span, growth retardation, facial dysmorphia, epileptic seizures (104)
Raf1	*Raf1* heterozygous KO	Small granule cell volume, increased cell death, reduced neuronal maturation (105)	Postnatal lethality, growth retardation, apoptosis in the lung and liver, limbs coordination problems (106)
	Raf1^{L613V} heterozygous KI	Increased density of astrocytes, enhanced OPCs density (107)	Enhanced learning and memory (107)
Mek1/2	*Mek1*^{Y130C} homozygous KI	Increased astrocyte density, increased number of cortical oligodendrocytes (108)	Pulmonary artery stenosis, cranial dysmorphia (108)
	Nestin-dependent *Mek1/2* ablation	Decrease of astrocyte precursors and OPCs, failure of gliogenesis (109)	Early postnatal lethality (109)
	hGFAP-dependent *Mek1/2* ablation	Suppressed generation of astrocyte precursors and OPCs, failure of gliogenesis (109)	Postnatal lethality (109)
	hGFAP-dependent *Mek1*^{S218E,S222E}	Increase in astrocyte precursors and mature astrocytes, reduction of neuron number (109)	Not known

hGFAP, human glial fibrillary acidic protein; BLBP, brain lipid binding protein; GNP, granule neuron progenitor; DG, dentate gyrus; OPCs, oligodendrocyte progenitor cells;

Table 2. RASopathy mouse models and their representative phenotypes.

2. RASopathy and central nervous system features

2. 1 Neurofibromatosis type 1

Neurofibromatosis type 1 (NF1) is an autosomal dominant disorder caused by loss of function mutations in NF1 gene, and relatively common developmental disease that occurs in approximately 1 in 3,000 individuals (20, 110). NF1 affects multiple organs, mainly skin, bone, and brain, and is diagnosed by both somatic and behavioral symptoms. NF1 is caused by loss of function mutations in *NF1* gene, which encodes a GAP for RAS, thus negatively regulating the RAS-ERK signaling pathway (10, 110, 111). Therefore, loss of function mutations in NF1 induce aberrant hyperactivation of RAS-ERK signaling. As mutations in the *NF1* gene lead to abnormal cell growth, proliferation, and differentiation, individuals with NF1 frequently exhibit neurofibromas, hyperpigmentation of melanocytes, and hamartomas of the iris (17, 18). Additionally, common characteristics of NF1 include bone malformations, cardiac defects, and neurocognitive impairments (19, 20). Notably, since NF1 is most abundantly expressed in the nervous system, a wide range of cognitive deficit is associated with NF1. More than 75% of NF1 patients suffer from cognitive impairments, such as below-average IQ and specific deficits in attention, executive functioning, visuospatial perception, social function and function (15, 16).

As shown in table 2, there are numerous studies that reported large range of features in NF1 mouse models. As *Nf1* homozygous knockout mice ($Nf1^{-/-}$) die *in utero* because of severe cardiac malformations, a delay in renal, hepatic, and skeletal muscle development, and hyperplasia of neural crest-derived sympathetic ganglia (76, 77), a heterozygous knockout mouse line ($Nf1^{+/-}$) has been extensively used to investigate the cellular mechanisms underlying NF1 etiology (80, 81, 83, 84, 112, 113). Along with human patients, *Nf1* heterozygous knockout mice displayed developmental abnormalities in the heart and neural crest-derived tissues (76, 79).

As RAS-ERK signaling components play distinct roles in each cell type in brain, there are several studies that investigate the effects of *Nf1* in cell type-specific manner. Ablation of *Nf1* only in neurons by using the Synapsin I promoter (*Nf1*^{Syn1}) led to growth delay, including reduced body weight and size, that was sustained into adulthood (83). *Nf1*^{Syn1} conditional knockout (CKO) mice also exhibited reduced size and weight of the forebrain, but not other brain regions (83). Histological analyses of CKO mice also revealed noticeable defects in the cerebral cortex, such as a reduction in cortical thickness (83). These results indicate that *Nf1* has an indispensable role in CNS development (83, 114). Studies dealing with human GFAP (hGFAP)-Cre transgenic mouse line also have suggested that *Nf1* plays an essential role in CNS development. As GFAP expression is initially detected in radial glial cell, which give rise to both glial and neuronal lineage cells, *Nf1*^{hGFAP} CKO mice lack *Nf1* in the majority of their neurons and astrocytes (115). These mutant mice were born in normal rate, but became remarkably smaller than their littermates after bitrh, and died within 4 months (86, 87). *Nf1*^{hGFAP} CKO mice showed increased brain to body weight ratio due to enlarged cerebral cortex, though cerebellum was notably smaller compared with littermates (85, 88). Moreover, the mutant mice displayed defective migration and proliferation of granule neuron progenitors, and failure in cortical barrel formation in somatosensory cortex (87). However, deleting *Nf1* using GFAP-Cre did not impair either learning or synaptic plasticity in adult mice (84).

Recent studies reported that *Nf1* is involved in cell fate specificity and cellular processes such as proliferation and differentiation in both the developmental stage and adulthood. *Nf1*^{hGFAP} CKO mice exhibited increased gliogenesis at the expense of neurogenesis in the early neonatal period and adulthood (85). Due to the altered populations of glia and neurons, *Nf1*^{hGFAP} CKO mice showed a smaller olfactory bulb and an enlarged corpus callosum (85). Likewise, *Nf1* ablation in neuroglial progenitors using a brain

lipid binding protein (BLBP)-Cre mouse line also resulted in increased glial proliferation and abnormal neuronal differentiation *in vivo* (89). Moreover, inactivation of *Nf1* in adult neural stem cells (NSCs) unlocked a latent oligodendrocyte lineage and allowed NSCs to give rise to all three lineages *in vivo* (90). Similarly, postnatal *Nf1* ablation using Nestin-CreERT2 induced defective granule neuron progenitors (GNPs) proliferation, and migration (88). Moreover, ablation of *Nf1* in adult hippocampal neural progenitor cells resulted in elevated proliferation rate and an increased number of newly born neurons in the dentate gyrus (91). How does *Nf1* alter cell fates? It has been demonstrated that *Nf1* ablation in neural stem/progenitor cells promotes the expression of *Olig2*, a basic-helix-loop-helix transcription factor that is required for cell fate determination (116). $Nf1^{hGFAP}$ CKO and $Nf1^{BLBP}$ CKO mutant mice showed increased *Olig2* expression, suggesting that *Nf1* suppresses *Olig2* expression and the oligodendrocyte progenitor lineage in neonatal SVZ progenitor cells (85, 117). Consistent with the neonatal study, inactivation of *Nf1* in adult NSCs also resulted in increased *Olig2* expression (90).

Since *Nf1* is also known as a tumor suppressor gene, studies in diverse cell types have insisted that *Nf1* loss of function mutations are associated with abnormal cellular growth, such as increased proliferation of oligodendrocyte precursors in the embryonic spinal cord (118) and Schwann cells (119). Especially, $Nf1^{-/-}$ and $Nf1^{+/-}$ NSCs highly produced morphologically abnormal, immature astrocytes compared to normal NSCs *in vitro* (120). The increase in proliferating cells seen *in vitro* was also observed in $Nf1^{-/-}$ and $Nf1^{+/-}$ embryonic brains and $Nf1^{+/-}$ adult brains *in vivo* (120). In addition, $Nf1^{-/-}$ NSCs from the brainstem exhibit increased proliferation and glial cell differentiation *in vitro* and *in vivo*; however, the lack of effect on neocortex suggests that the effects of *Nf1* gene ablation are brain region-specific (117). Since *Nf1* mutant mice recapitulate in large range of the CNS features reported in NF1 human individuals, these studies unveiled the pivotal roles

of NF1 in CNS development, including the gross morphology and proper formation of brain region structures, and the regulation of cell fate decision.

Along with structural abnormalities in CNS, *Nf1*-related mouse models have been used to investigate the mechanisms underlying the cognitive deficits. As a pioneered work, heterozygous *Nf1* mice exhibited impaired hippocampal-dependent spatial learning, in addition to a hippocampal LTP deficit and increased inhibitory synaptic transmission (81, 112). The authors showed that attenuating RAS-ERK signaling activity is able to restore LTP and learning impairments in $Nf1^{+/-}$ mice, insisting that the impairments in NF1 cases are caused by hyperactive RAS-ERK signaling (112). Interestingly, the lack of *Nf1* only in inhibitory neurons was sufficient to result in impairments in learning and synaptic plasticity, suggesting the essential roles of *Nf1* in regulation of inhibitory synaptic function (84). Another model, which ablated exon 23a of *Nf1*, also exhibited impairments in spatial learning and contextual discrimination (82). Similarly, specific ablation of exon 9a in Nf1 reproduced the features of the $Nf1^{+/-}$ mice, involving hippocampal LTP defict, enhanced inhibitory synaptic transmission, and learning impairments (121).

Recently, transcriptome profiling analyses of mouse brain have revealed the enriched *Nf1* transcripts in inhibitory neurons rather than the in excitatory neurons, and provided a insight as to how *NF1* dominantly roles in inhibitory synaptic function (122). Furthermore, accounts for the conserved distribution pattern of *NF1* in human brain, it is demonstrated that the enriched expression of *NF1* in inhibitory neurons may underlie cell type-specific pathophysiology and cognitive deficits in NF1 (123).

2. 2 Noonan syndrome and Noonan syndrome with multiple lentigines

Noonan syndrome (NS), familial and sporadic forms of autosomal dominant genetic disorder, is relatively common among RASopathies with an incidence of 1 in 2,500 live births (31, 124, 125). Mutations in RAS-ERK signaling genes have been reported to be found in NS patients, such as the gain of function mutations in *protein tyrosine phosphatase non-receptor type 11* (*PTPN11*), *son of sevenless homolog 1* (*SOS1*), *Kirsten rat sarcoma viral oncogene homolog* (*KRAS*), *neuroblastoma RAS viral oncogene homolog* (*NRAS*), *Raf-1 proto-oncogene* (*RAF1*), *BRAF*, *soc-2 suppressor of clear homolog* (*SHOC2*), and *MEK1*, and the loss of function mutations in *Cbl proto-oncogene* (*CBL*) (25, 63, 126). Among the NS-linked mutations, gain of function mutations in the *PTPN11* gene, which encodes the non-receptor protein phosphatase SHP2, are highly responsible for most of NS cases (126). Individuals with NS show characteristic appearances, such as short stature, broad forehead, sparse eyebrows, a low-set and posteriorly rotated ear, and a webbed neck (34-40). The patients are also diagnosed by other important symptoms include a motor delay, increased risk of cancer, and heart defects (34-40). Similarly, individuals with Noonan syndrome with multiple lentigines (NSML) share large part of clinical symptoms observed in patients with NS, but they also exhibit high penetrance of hypertrophic cardiomyopathy and lentigines (127). Interestingly, contrary to NS, loss of function mutations of *PTPN11* gene are associated with NSML (127).

Approximately 30% to 50% of NS individuals display a large range of neurocognitive impairments, but little is known about CNS abnormalities in NS patients (34, 35). There are several cases of NS that report cerebellar ectopia, temporal lobe anomaly, hydrocephalus, cerebral abscess, cortical dysplasia and malignant Schwannoma (28-33). Not only structural defects, severe mental retardation and intractable epilepsy are also reported in NS patients (33).

Mutant mice harboring NS-associated *Sos1*^{E846K}, *Kras*^{V14I}, or *Raf1*^{L613V} mimic characteristic features of NS patients, short stature, facial dysmorphia, growth retardation, and cardiac defect (128-131). Since *PTPN11* mutations are responsible for the majority of NS cases, Shp2 mutant mice are widely used models of NS (96-98, 132, 133). A large subset of NS patients have a constitutively active gain of function mutation Shp2^{D61G} that increase the phosphatase activity of Shp2 (134, 135). The homozygous expression of Shp2^{D61G} variant eventually induced embryonic lethality, as the embryos were severely hemorrhagic and edematous, had heart defects and showed decreased organ size (98). However, heterozygous Shp2^{D61G} mutant mice that carried only one copy of the mutant variant highly survived, and exhibited characteristic NS features, such as short stature, wide-set eyes, a broad forehead, and a triangular face (98). Interestingly, heterozygous Shp2^{D61G} mice also displayed impairments in spatial learning and memory and synaptic plasticity (97). Mutant mice harboring a milder form of mutation, Shp2^{N308D}, showed cardiac defects and moderate impairment in spatial learning and memory that was consistent with human patient cases (97, 98). Moreover, there are several studies that carried out cell type-specific manipulations of NS-associated Shp2 mutations. Neural crest cell-specific expression of Shp2^{Q79R} induced craniofacial defects and growth delay (129). NSC-specific Shp2^{E76K} expression induced hydrocephalus may be associated to abnormal ependymal cell development (95). In behavioral level, Shp2^{E76K}-expressing mice displayed hyperactivity, reduced anxiety-like behavior, and impaired locomotive function (95). Whole body Shp2^{D61Y}-expressing mice were embryonically lethal, and epiblast-specific Shp2^{D61Y} expression resulted in embryonic cardiac defects (132).

SHP2 is a growth factor-modulated phosphatase that regulates both the RAS-ERK and the JAK-STAT signaling pathways (136, 137). Since both signaling pathways play essential roles in cellular processes, several studies suggested that SHP2 affects cell proliferation and differentiation in varied

cell types (138-142). For instance, SHP2 mediates initiation of retinal neurogenesis and it regulates retinal progenitor factors and cell proliferation (143). SHP2 also modulates cell migration, focal adhesion formation and neurite outgrowth, and subsequently regulates the differentiation-induced activation of FAK, Src, paxillin, and ERK1/2 (144). Similarly, mutant mice in which Shp2 is selectively deleted in neural precursor cells showed early postnatal lethality, reduced proliferation of NSCs, demonstrating that SHP2 is an important player in mammalian brain development (92).

Recent studies have also demonstrated that Shp2 is implicated in oligodendrocyte development. *In vivo* role of Shp2 in oligodendrocyte differentiation was studied by using mutant mice with a Olig2 expressing cell-selective Shp2 deletion in the ventral spinal cord (93). These mice showed a significant decrease in the number of both oligodendrocyte precursor cells and mature oligodendrocytes, and reduced axonal myelination, indicating the critical role of Shp2 in oligodendrocyte development (93). Similarly, Olig2-specific Shp2 null mice also displayed a dramatic reduction in oligodendrocyte progenitor cell number, in both embryonic and postnatal stages, and showed decreased myelination (94). On the contrary, Olig2-selective expression of NS-linked mutation $Shp2^{Q79R}$ increased the number of oligodendrocyte precursor cells in embryonic and postnatal brain, but resulted in aberrant myelination and fewer myelinated axons (94).

Since SHP2 promotes neurogenesis and suppressed gliogenesis by repression of the JAK-STAT pathway, SHP2 has been shown to role as a cell fate regulator. Indeed, $Shp2^{D61G}$ heterozygous mutant mice exhibited fewer astrocytes and more neurons in the forebrain at postnatal day 2, suggesting that Shp2 mutations disrupt the balance of cell type populations (96). Similarly, mice in which Shp2 is selectively deleted in neural precursor cells displayed defective neuronal differentiation and modestly enhanced astrogliogenesis, supporting the idea that Shp2 roles as a cell fate

determinant (92).

As well as Shp2 mutant mice, there are various NS mouse models. Heterozygous *Raf1*-deficient mice showed reduced neuronal maturation and decreased volumes of granule cell layer due to increased rate of cell death at early postnatal period, and a high proportion of abnormally fast dividing cells in the subgranular zone (105). Mice expressing *Raf1*^{L613V} had a increased density of GFAP-positive astrocytes in the cortex and the hippocampus, and the number of oligodendrocyte progenitor cells were also increased in the cortex (107). As mentioned above, SHP2^{D61G} promote the differentiation into neuronal lineage rather than glial lineage, by direct interaction with JAK-STAT pathway, which is inconsistent result with *Raf1*^{L613V} mice (96). Although the underlying mechanism for the discrepancy in cellular phenotypes is not clear, these results suggest that there are distinct pathophysiologies according to each NS-associated mutation. Interestingly, *Raf1*^{L613V} mice showed enhanced performance in several learning tasks (107). NS-associated *Kras*^{G12V} mutant mice showed enhanced GABAergic synaptogenesis and impaired spatial learning when the mutation was selectively expressed in synapses (145).

2. 3 Cardio-facio-cutaneous syndrome

Cardio-facio-cutaneous syndrome (CFC syndrome) is a rare and severe form of RASopathy that is related to the downstream genes of *RAS*, including *BRAF* (41, 42), *KRAS* (41), and *MEK1/2* (42). Among these genes, *BRAF* mutations are responsible for over 70% of CFC syndrome patients (58). *BRAF* encodes a serine/threonine kinase, and both the kinase-active and kinase-impaired mutations of *BRAF* are found in CFC syndrome individuals (41, 42). In addition to *BRAF*, mutations in *MEK1* and *MEK2* are responsible for approximately 25% of CFC syndrome patients (58). *MEK1* and *MEK2* are threonine/tyrosine kinases, and all of CFC-associated *MEK* mutations are kinase-active mutations (42, 146). CFC syndrome patients share the multiple congenital symptoms with NS and Costello syndrome (58). CFC syndrome individuals display NS-like faces, with macrocephaly, low-set ears, a short nose, a broad forehead, and down-slanting palpebral fissures with ptosis (4, 59). Moreover, cardiac defects are also similar to those of NS and Costello syndrome, with pulmonic stenosis, septal defects, and hypertrophic cardiomyopathy (HCM) showing high prevalence (59). Neurological impairments, including hypotonia, motor delay, seizures, tactile defensiveness, speech delay, and learning disabilities, are present at large range of degrees (4, 50, 55). Physical retardation caused by gastrointestinal dysfunction, including vomiting, oral aversion, reflux, and constipation, is also typical characteristic in CFC syndrome infancy (50). Especially, CNS malformations are another important diagnostic symptoms of CFC syndrome. Previous studies reported the malformations in CNS structures, including ventriculomegaly and hydrocephalus, in CFC syndrome cases (44-50). Volume loss in the brain due to cortical atrophy, cerebral atrophy, brain stem atrophy, and white matter atrophy have also presented in a part of CFC syndrome patients (44, 46, 51-54). Additionally, defects in migration and myelination, and corpus callosum abnormalities, such as hypoplasia and lipoma were also emerged by brain imaging (50, 52,

55-57). In accordance with CNS structural malformations, most CFC syndrome patients are diagnosed with a large range of cognitive deficits and intellectual disabilities (50).

Recently, patient-derived induced pluripotent stem cells (iPSCs) have made advancements in the understanding of disease-related mutations. iPSC from a patient harboring *BRAF*^{Q257R}, the most frequent CFC syndrome mutation, showed depletion of neural progenitor pool, induced by decreased phosphorylation of AKT, and early neuronal maturation (147). Caused by the depletion of progenitors, the number of late-born cells, such as the upper-layer cortical neurons and glia, was significantly decreased (148). Moreover, the number of GABAergic interneurons was elevated, demonstrating that the high prevalence of epilepsy in CFC syndrome cases may be linked to imbalance between excitation and inhibition ratio (148).

Since *BRAF* mutations have the highest incidence in CFC syndrome, a majority of animal studies in CFC syndrome have been concentrated on *Braf*. To identify the roles of *Braf* in various biological processes, there are several studies with loss of function *Braf* mutations. First, *Braf*-deficient cultured embryonic neurons did not survive in the presence of neurotrophic factors while *Raf1*-lacking neurons survived, suggesting the critical role of *Braf* in cellular survival (149). A *Braf* null mutant mice were embryonically lethal due to the vascular defects at midgestation (150). In addition, the deletion of *Braf* in NSCs by using Nestin-Cre line induced malformation of the CNS, including a decreased cerebellum with blurred granule cell layer borders and a diminished hippocampus granule cell layer, due to decreased differentiation into mature granule cells (102). Nestin-specific *Braf*-lacked mice also showed dysmyelination and defective oligodendrocyte differentiation, indicating that the *Braf* has critical role in postnatal CNS development (103). Forebrain excitatory neuron-specific *Braf* deletion resulted in deficits in hippocampal LTP and hippocampal-dependent learning and memory, while the impact of *Braf* deletion in aspects of CNS

structure or development in these mice remains to be investigated (151).

Transgenic mice harboring CFC-linked gain of function mutations successfully recapitulated multiple features of human CFC syndrome individuals (108, 152). The knock-in mice expressing constitutively active *Braf*^{V600E} mimicked several CFC syndrome phenotypes, such as reduced life span, growth retardation, facial dysmorphia, cardiomegaly, and epileptic seizures (104). Mice expressing *Braf*^{L597V} mutation also recapitulated CFC syndrome characteristics of a short stature, facial dysmorphia, and cardiac enlargement (153). The most prevalent CFC-linked *Braf* mutation, *Braf*^{Q241R}, showed different phenotypes in each genetic background. In C57BL/6J background, mice showed embryonic/neonatal lethality with embryonic skeletal abnormalities, lymphatic defects, cardiac defects, and liver necrosis (152, 154). In BALB/c and C57BL/6J mixed background, mice showed lethality between birth and 24 weeks, growth retardation, sparse and ruffled fur, liver necrosis, and atrial septal defects (152, 154). In addition, *Braf*^{Q241R} mice in ICR background showed growth retardation, a hunched appearance, craniofacial dysmorphism, and learning deficits (152). Not only *Braf* mutation knockin, mutant mice harboring *Mek1*^{Y130C}, the most frequently found *MEK1* mutation in CFC syndrome individuals, displayed pulmonary artery stenosis, cranial dysmorphia, and neurological anomalies (108). Moreover, homozygous *Mek1*^{Y130C} knockin mice showed a higher density of GFAP-positive astrocytes and Olig2-positive oligodendrocytes in the sensory cortex and hippocampal CA1 regions compared to control mice (108). As addressed above, iPSCs containing *BRAF*^{Q257R} exhibited decreased late-born glial populations, while CFC-linked *Mek1*^{Y130C} expressing adult mice showed an increased density of GFAP-positive cells in hippocampal and cortical areas (104, 108, 147). In spite of kinase-active property of *BRAF*^{Q257R} mutation, the ERK activity was decreased in neural progenitor cells, indicating the cell context-dependent role of *BRAF* (147). Therefore, in *BRAF*^{Q257R} iPSCs, decreased ERK activation may be

responsible for the decreased number of glia population, which could explain the discrepancy between *BRAF*^{Q257R} iPSCs and *Mek1*^{Y130C} mice (108, 147).

In addition to mouse models, zebrafish models harbording CFC-associated *Braf* or *Mek* variants were also investigated, and these mutant alleles interfered with convergence-extension cell movements during gastrulation, suggesting the CFC-related developmental phenotypes (146). Taken together, CFC-associated genes, representatively *BRAF* and *MEK*, play critical roles in various cellular processes during CNS development, including precursor maturation and proliferation, myelination, and differentiation. However, our knowledge regarding the detailed causal relationship between CNS abnormalities and cognitive function in CFC syndrome is remained to be investigated. Further studies using mutant animals with more specific temporal and spatial manipulation of CFC syndrome genes would provide understanding of the pathophysiology of cognitive deficits in CFC syndrome.

2. 4 Costello syndrome

Costello syndrome (CS) is a rare multiple congenital abnormality syndrome that affects 1 in 1,250,000 people and shares many features with other RASopathies (155-157). CS is mostly caused by gain of function mutations in the *HRAS* gene, most of which have been previously reported as somatic or oncogenic mutations in various tumors (60, 62, 158). *HRAS* activating mutations are highly prevalent in CS individuals; they disrupt guanine nucleotide binding and induce a decrease in intrinsic and GAP-induced GTPase activity, allowing mutant HRAS proteins to remain in the active state (159). In addition, *BRAF*, *KRAS*, and *MEK1* mutations are also associated with a small population of CS individuals (27, 63, 160). CS patients are typical characterized by coarse facial features, redundant and loose skin, severe failure to thrive, mental retardation, cardiomyopathy, and a predisposition to tumors (59, 60). There is no single feature that is unique to CS, and this syndrome phenotypically overlaps with NF1, NS, NSML, and CFC syndrome (60, 161). Typical and coarse facial features associated with CS involve macrocephaly with a prominent forehead, a short nose with a depressed nasal bridge and a broad base, and low-set, posteriorly rotated ears with thickened helices and lobes. Most CS patients have cardiac abnormalities, including hypertrophic cardiomyopathy, valve abnormalities, septal defects, and arrhythmia (162). Failure to thrive due to gastrointestinal dysfunction often involves reflux, oral aversion, and constipation during early infancy (67, 157). Structural and electrophysiological neurological malformations are also common in CS. For example, ventricular abnormalities, such as mild ventricular dilatation, are observed in more than 40% of CS individuals (64-67). Cerebral malformations in CS include cerebral atrophy, leukomalacia, poor gray-white matter differentiation, a small corpus callosum, and MRI signal abnormalities (64, 65, 67-71). Cerebellar abnormalities include malformation, cerebellar atrophy, deviation of the cerebellar tonsils, and demyelinization of the basal tonsil (66, 69, 71-

74).

Krencik and colleagues have shown that human iPSC carrying *HRAS*^{G12S} that were derived from CS patients exhibited hyperplasia and differentiated into astroglia more rapidly *in vitro* than iPSC derived from control cell lines with normal *HRAS*. CS-derived iPSC also generated an abundance of extracellular matrix remodeling factors and proteoglycans (163). Moreover, *HRAS*^{G12S} iPSC-derived neurons had a longer progenitor phase, unlike the phenotype reported in *BRAF*^{Q257R} iPSC-derived neurons that originated from CFC syndrome patients (147, 164). Thus, postnatal progressive cerebellar overgrowth of the brain in CS individuals could be caused by the extended progenitor phase (165).

As with CFC syndrome, only few animal models were generated for CS. Both homozygous and heterozygous *Hras*^{G12V} knock-in mice closely phenocopied some of the features observed in individuals with CS, including facial dysmorphia, cardiomyopathies, and alterations to the homeostasis of the cardiovascular system (166). In addition, later studies with homozygous *Hras*^{G12V} knock-in mice demonstrated that they have neurocognitive deficits, such as hyperactivity, increased anxiety-like behavior and mild deficit in spatial memory (167). However, Viosca and colleagues did not observe significant changes in either the activity or the expression of downstream of Hras such as phospho-CREB and *c-fos* (167). Transgenic mice with forebrain excitatory neuron-specific expression of *Hras*^{G12V} under the control of the αCaMKII promoter displayed several synaptic phenotypes, including a high density of docked neurotransmitter vesicles in glutamatergic terminals and increased synaptic plasticity which may be associated with the dramatically enhanced hippocampal-dependent learning (101). Schreiber and colleagues have also shown that the homozygous *Hras*^{G12V} knock-in mice exhibit spatial learning deficits, which are accompanied by robust upregulation of Erk signaling in hippocampal lysates, neuronal hypertrophy, increased brain volume, and impaired

mGluR-dependent long-term depression (LTD) (100). Notably, mice expressing CS-associated *Hras*^{G12V} or *Hras*^{G12S} mutations in cortical precursors displayed promoted precursor cell proliferation and premature gliogenesis, but inhibited neurogenesis (168). Consistently, either form of *Hras* mutations also promoted precursor cell proliferation and astrogenesis, but inhibited neurogenesis in cultured cortical precursors (168). These findings from multiple experimental systems such as iPSCs, mice models and cultured cells commonly suggest the essential role of *HRAS* in neural precursor cell proliferation and gliogenesis, which might strongly affect the structure and function of CNS including increased brain volume in CS patients.

2.5 Further questions

In chapter 1, I reviewed the literatures that demonstrate dysregulation in different components of the RAS-ERK signaling pathway with different RASopathies have distinct impact on features of central nervous system in a cell type-specific manner. However, it is still remained unclear how some RASopathy mutations affect neurons and others affect glia.

One hypothesis is that during the development process, each signaling component begins to be expressed in different period. Although there has been no study that have examined the expression patterns of RAS-ERK signaling genes during the developmental phase in detail, most of the key RAS-ERK components, such as NF1, SHP2, BRAF, and MEK are emerged before either embryonic day 10 or 15, which are initiation time points of neurogenesis or astrogliogenesis, repectively. Therefore, examining the expression profiles of RAS-ERK molecules during brain development in high temporal resolution would be worthful to find out detailed participation of the molecules in neurogenesis and astrogliogenesis over time.

Another hypothesis is that the expression of RAS-ERK signaling components are remarkably different between cell types. Recently, it has been shown that the RAS-ERK signaling network is constructed differently between excitatory and inhibitory neurons in mouse hippocampus (122). Thus, it would be interesting to investigate whether the spatial expression pattern of signaling components are changed or remained over different phase of developmental stages. Moreover, comparing expression pattern of RAS-ERK molecules between neuron and glia as well as between excitatory and inhibitory neurons might provide impotant clues to define neuron- or glia-specific phenotypes of several RASopathy mutations.

Furthermore, the studies described above may also provide insight to understand the mechanisms underlying neuron type-, or glia-specific phenotypes in RASopathies not covered here.

2. 6 Purpose of this study

In this dissertation, I hypothesized that the different RASopathy-related mutations affect neuron and astrocyte differently in cognitive deficits. To answer the question, I investigated the cell type-specific mechanisms underlying learning and memory impairments in two types of RASopathy mouse models. First, according to previous studies that reported the dominant roles of *KRAS* in neuronal properties (99), I investigated the effect of $KRAS^{G12V}$ on learning and memory in neuron types. Second, I investigated the effect of $BRAF^{K499E}$ on learning and memory not only in neurons, but also in astrocytes.

Chapter 2

Neuron type-specific expression of a RASopathy-related KRAS mutation impairs spatial learning and memory

Introduction

The nervous system is composed of various type of neural cells, including astrocytes, microglia, oligodendrocytes, and neurons. For that reason, the investigations of signaling pathways from the whole brain might not reflect the actual physiological role of signaling pathway. Therefore, it is noteworthy to understand cell type-specific role and effect of the signaling pathway. Especially, recent studies suggested that RAS-ERK signaling components have distinct effects in several cell types in the mammalian brain. For example, it has been shown that expressing NS-associated SHP2 mutant only in excitatory neurons, but not in inhibitory neurons, resulted in cognitive impairments (122). In addition, increased excitatory synaptic transmission was found in mutations in *Ptpn11* and *Hras* (97). Similarly, mutations in *Syngap1* were also shown to affect excitatory synaptic function (169). RASopathy-associated deficits are not restricted to excitatory neurons. On the other hand, haploinsufficiency of *Nf1* enhanced RAS-ERK signaling primarily in GABAergic neurons and showed an enhanced synaptic function in GABAergic neurons (80, 84). A mutant mouse harboring an NS-associated KRAS mutation showed elevated RAS-ERK signaling specifically in GABAergic interneurons (145). Therefore, to selectively target the molecules in the affected cell types to gain specificity and effectiveness, understanding the cell type-specific roles and molecular and cellular mechanisms affected by specific genetic mutations in the RAS-ERK signaling might be important.

There are three *RAS* genes that code for highly homologous RAS proteins, NRAS, HRAS, and KRAS. All of the isoforms are enriched in neurons, and have same effector binding domains and are able to interact with the identical set of downstream effectors, however, due to differences in their posttranslational modifications, they may have access to different effector pools and may be capable of generating distinct signal outputs (170, 171).

Functional significance of *NRAS* in brain is not deeply investigated yet, but it is considered that *NRAS* and *KRAS* may interact with *NF1* in the presynaptic neuron at inhibitory synapses (112). Consistently, *KRAS*-mediated signaling is implicated in modulation of inhibitory tone and GABAergic synaptogenesis (99). Endogenous *HRAS* is expressed dominantly in presynaptic neurons, and therefore *HRAS* plays roles in presynaptic function such as synaptic vesicle release via phosphorylation of synapsin I (101). Moreover, *HRAS* is also involved in regulating extracellular matrix remodeling and astrocyte proliferation in brain (163). Among RAS-ERK signaling components, to date, 91 KRAS mutations have been identified in NS and 28 have been identified in CFC syndrome (NSEuroNet database, https://nseuronet.com), and all patients with NS caused by KRAS mutations exhibit the severe intellectual disability (25). Point mutations in codon 12 of the KRAS gene, such as G12V, accounts for approximately 80% of KRAS mutations in cancer, and some of those are also reported in rare cases of RASopathies (172). Previous studies demonstrated that conditional knock-in mice expressing a constitutively active KRAS mutation under control of synapsin promoter show abnormal behavioral as well as memory deficits in the test of spatial learning and working memory (145). These mutant mice also showed LTP impairment and increased inhibitory postsynaptic currents, suggesting that Kras may be involved in regulating presynaptic function at GABAergic synapses and mediate the excitatory / inhibitory balance (145). Defects in development of GABAergic inhibitory neurons were also founded, which may contribute to behavioral deficits in the mutant mice (145). These synapsin-specific KRAS mutant mice showed significantly increased GABAergic synaptogenesis, indicating the KRAS is involved in synaptogenesis during early development stage, and subsequently impairs memory in adulthood. Notably, although KRAS is also expressed in the adult mouse brain, the physiological functions of KRAS in adult neuron type remain unclear. Moreover, how

does KRAS affect neurological function in each cell type -specific manner is also unknown.

In this chapter, I investigated the cell type-dependent effects of KRAS on learning and memory by expressing the mutant $KRAS^{G12V}$, a constitutively active mutant, either in hippocampal excitatory or inhibitory neurons in adult mice. As a result, expression of the mutant KRAS either in excitatory or inhibitory neurons impaired learning and memory depending on distinct cellular abnormalities.

Material and method

1. Mice

αCaMKII-Cre (JAX 005359) and vGAT-IRES-Cre (JAX 016962) mice were maintained by breeding with wild-type C57Bl/6J mice at the SNU Specific Pathogen Free centre. Animals were group-housed (four mice per cage) on a 12-hour light/dark cycle in the vivarium at SNU. Both female and male mice (2-7 months old) were used for all experiments. All studies were approved by the Seoul National University Institutional Animal Care and Use Committee.

2. AAV packaging

AAV packaging was performed as described previously (122). Briefly, EYFP or hemagglutinin (HA) tagged-$KRAS^{G12V}$ were inserted into the pAAV-EF1a-DIO-WPRE plasmid. For AAV packaging, HEK 293T cells (7×10^{12}) were cultured on dishes (Thermo Fisher 157150) with 15 mL DMEM (Thermo Fisher Scientific SH30243.01) containing 10% fetal bovine serum (Thermo Fisher Scientific SH30919.03) and penicillin/streptomycin (GIBCO 15140-122) at 37 ℃ and 5% CO_2. p5E18-RxC1 (13 μg), pAd-ΔF6 plasmid (26 μg), and pAAV plasmid (EYFP or $KRAS^{G12V}$; 13 μg) were transfected into HEK 293T cells using polyethylenimine (PEI, Polysciences, Inc.) transfection method. The transfection medium was replaced with 20 mL fresh medium. After 72 h, the culture medium was harvested for AAV purification. The supernatants were layered in an ultracentrifuge tube (Beckman 324214) in the following order: culture medium from each dish, 6 mL of 15% iodixanol (Opti-Prep; Axis-shield 1045) solution [1 M NaCl, 1 mM $MgCl_2$, 2.5 mM KCl, and 25% Opti-prep in phosphate-buffered saline (PBS)], 5 mL of 25% solution (2.5 mM KCl, 0.2% phenol red, 1 mM $MgCl_2$, and 42% Opti-prep in PBS), 5 mL of 40% solution (2.5 mM KCl, 1 mM $MgCl_2$ and 67% Opti-prep in PBS)

and 4 mL of 60% solution (2.5 mM KCl, 1 mM $MgCl_2$, and 0.2% phenol red in Opti-prep). The iron seared tubes were centrifuged at 69,000 rpm for 1 h using the Beckman UltimaTL-100K ultracentrifuge and 70Ti rotor. The 40% solution was harvested from the centrifuged column using a syringe. The harvested solution was diluted with PBS, filtered with the Amicon ultra-15 filter tube (Millipore UFC910024). The filter was washed 3 times with 15 mL PBS. The viral particles in the solution were quantified via qPCR.

3. Stereotaxic viral injection

Stereotaxic surgery was performed as previously described (122). Mice were anesthetized with ketamine solution and mounted on a stereotaxic frame. The hippocampal CA1 region was targeted using the following coordinates: anterior-posterior (AP): -1.8 mm, medial-laterl (ML): ±1.0 mm, dorsal-ventral (DV): -1.7 mm/AP: -2.5 mm, ML: ±2.0 mm, DV: -1.8 mm. AAV was injected into each point. All mice were allowed to recover for a minimum of 3 weeks before further use in experiments.

4. Open field test

Open field test was performed as described previously (173). A cube-shaped acrylic box (32 cm by 32 cm by 32 cm) was used as an arena. After a short acclimation, each mouse was released into the box and allowed to freely explore the arena for 15 minutes. Movement of mice were analyzed with tracking software (EthoVision; Nodulus).

5. Morris water maze (MWM) test

The MWM test was performed as previously described (174). Briefly, mice were handled for 2 minutes at the same time of each day for 7 consecutive days before the test. The maze consisted of a gray opaque cylindrical tank (diameter, 120 cm) in a room with multiple visual cues, which are the animal's navigational references for locating the platform. The tank was

filled with water (20 ℃ to 22 ℃) and painted white. The tank was divided into four invisible quadrants (target quadrant, opposite quadrant, right quadrant, left quadrant) and a platform, which was submerged 1 cm under the surface of the water, was placed at the centre of the target quadrant. Before the initial trial on day 1, each mouse was placed onto the platform for 30 seconds. On training days, mice were released at the edge of the tank facing the inner wall, and start position was chosen randomly for each trial. When mice failed to reach the platform within 60 seconds of trial, they were gently guided onto the platform and rescued from the maze after 10 seconds. When mice successfully reached the platform, they were rescued from the maze after 10 seconds. Mice were trained with six trials per day 4 consecutive days, and interval between trial 3 and 4 was 45 minutes to 1 hour. In probe test, platform was absent, and mice were tracked for 60 seconds. Movement was analyzed with tracking software (EthoVision 11.5; Nodulus). The visible platform-version of MWM was performed after the hidden platform test. The platform was tagged with a visible flag, and latency to reach the platform was assessed. Experimenters were blinded to the genotype of mice or type of injected viral vectors.

6. Object-place recognition (OPR) test

OPR test was performed as described previously (174). Mice were handled for 5 min for four consecutive days and habituated in a cube-shaped opaque acrylic box (32 cm by 32 cm by 32 cm) for 15 minutes for another 2 days before performing the training and test. In the training session, mice were placed in the arena containing two identical 50 ml glass bottles and were allowed to explore the objects for 10 minutes. In the test session, 24 hours after training, mice were placed in the same arena containing one object that stayed in the same location and the other object relocated to a new position. All locations for the objects were counterbalanced among groups, and objects and arena were cleaned between trials. Sessions were recorded and

later analyzed manually. Experimenters were blinded to the genotype of mice or type of injected viral vectors.

7. Classical fear conditioning

Fear conditioning test ws performed as previously described (174). Briefly, mice were trained with three pairs of a tone and a co-terminating scrambled foot shock [tone: (2800 Hz, 85 dB, 30 s), shock: (2 s, 0.6 mA)] in a conditioning chamber (Coulbourn Instruments, Whitehall, PA, USA). After training, mice were re-exposed to the same conditioning chamber without any tone or foot shock for three consecutive days. Each re-exposure was separated by 24 h. The percentage of freezing behavior was scored by using an automated software (Freeze Frame, ActiMetrics, Wilmette, IL, USA). Experimenters were blinded to the genotype of mice or type of injected viral vectors.

Results

2. 1 Ectopic expression of KRAS^{G12V} in hippocampal inhibitory neurons

Previous work had reported that expression of *Kras* gene is significantly higher in vGAT^{+} inhibitory neurons than in αCaMKII^{+} excitatory neurons in the adult wild type mouse hippocampus (122). To assess the effects of neuronal type-specific role of KRAS^{G12V} on hippocampal-dependent spatial learning and memory in adult mice, I injected a Cre recombinase–dependent adeno-associated virus (AAV) vector encoding KRAS^{G12V}–hemagglutinin (HA) into the dorsal hippocampus of vGAT-IRES-Cre transgenic mice for inhibitory neuron-specific manipulation (175). Examining the immunolabeling of HA, the AAV was highly expressed in the CA areas (CA3 – CA1), but not in the dentate gyrus (Figure 2A). Before I proceed the tasks for assessing learning and memory, I tested whether the basal locomotive activity and anxiety-like behavior are affected by KRAS^{G12V} expression. Open field analyses revealed that KRAS^{G12V} expression in vGAT^{+} inhibitory neurons elevated total distance traveled during the test, while anxiety-like behavior measured by the time spent in the center zone remained unchanged (Figure 2, B to D).

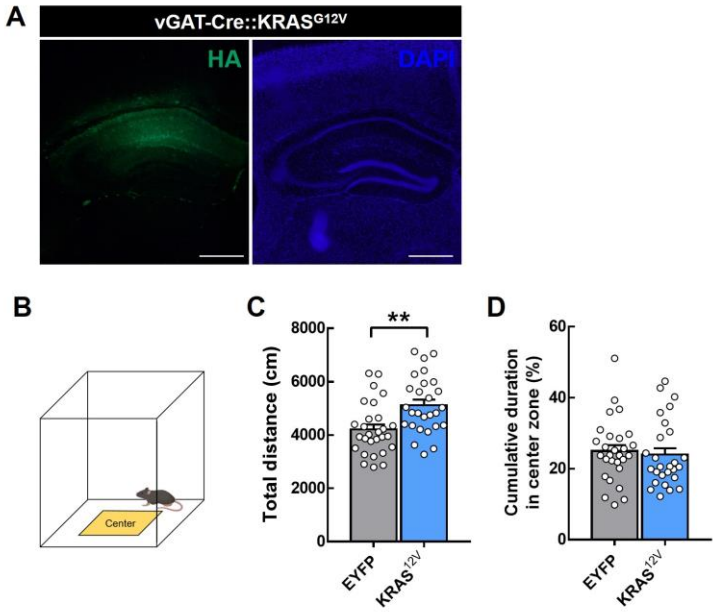

Figure 2. Ectopic expression of KRAS^{G12V} in inhibitory neurons. (A) Expression of adeno-associated virus (AAV) expressing KRAS^{G12V}-HA in the dorsal hippocampus of adult vGAT-Cre mouse. 4',6-diamidino-2-phenylindole (DAPI) staining was used to identify nuclei. Scale bars, 200 μm. (B) The schematic diagram showing center zone of the open field test. (C) vGAT-Cre::KRAS^{G12V} mice showed increased total distance moved in the open field test (n = 28, 27; $^{**}p$ = 0.0017 by unpaired *t* test). (D) Both group of mice showed comparable cumulative duration in center zone in open field test (n = 28, 27; p = 0.6795 by unpaired *t* test). Data are expressed as the mean ± SEM.

2. 2 Ectopic expression of $KRAS^{G12V}$ in inhibitory neurons impairs hippocampal-dependent spatial learning and memory

To investigate the role and effect of inhibitory neuron-specific expression of $KRAS^{G12V}$ on hippocampal-dependent spatial learning and memory, I subjected vGAT-Cre::$KRAS^{G12V}$ mice to hidden-platform version of the Morris water maze (MWM) test (Figure 3A). During the training sessions, the vGAT-Cre::$KRAS^{G12V}$ mice exhibited a greater escape latencis to find the hidden platform (Figure 3B). In the probe test, vGAT-Cre::$KRAS^{G12V}$ mice spent significantly shorter time in the target quadrant in which the platform was located during the training sessions compared to the vGAT-Cre::EYFP mice, and showed chance-level performances, demonstrating that the vGAT-Cre::$KRAS^{G12V}$ mice failed to recall the position of hidden platform (Figure 3, C and D). Furthermore, vGAT-Cre::$KRAS^{G12V}$ mice swam farther from the platform and visited the platform fewer times than vGAT-Cre::EYFP mice, suggesting that sole expression of $KRAS^{G12V}$ in $vGAT^{+}$ inhibitory neurons in the adult hippocampus is sufficient to result in spatial learning and memory deficits (Figure 3, E and F).

Next, I carried out the object-place recognition test, another well-known hippocampus-dependent task (176). 24 hours after training session, vGAT-Cre::EYFP mice significantly prefered the relocated object (new), whereas vGAT-Cre::$KRAS^{G12V}$ mice did not, suggesting the spatial learning deficit of $KRAS^{G12V}$-expressing mice (Figure 3, G and H).

Classical fear conditioning is extensively used Pavlovian learning and memory task in which mice associate aversive unconditioned stimuli, such as an electric foot shock, with non-aversive conditioned stimuli, such as context or an auditory tone (177). The amygdala is pivotally involved in classical fear conditioning task, especially in auditory version of fear conditioning (177). Next, contextual and auditory fear memory were assessed by measuring freezing behavior when the conditioned mice were exposed to the same context or the same tone. vGAT-Cre::EYFP and vGAT-

Cre::KRAS^{G12V} mice showed comparable levels of freezing in both contextual and auditory tests which were performed 24 and 48 hours after conditioning (Figure 3, I to K). In conclusion, these results indicate that the constitutive activation of KRAS in vGAT^{+} hippocampal inhibitory neurons impairs spatial learning and memory in adult mice.

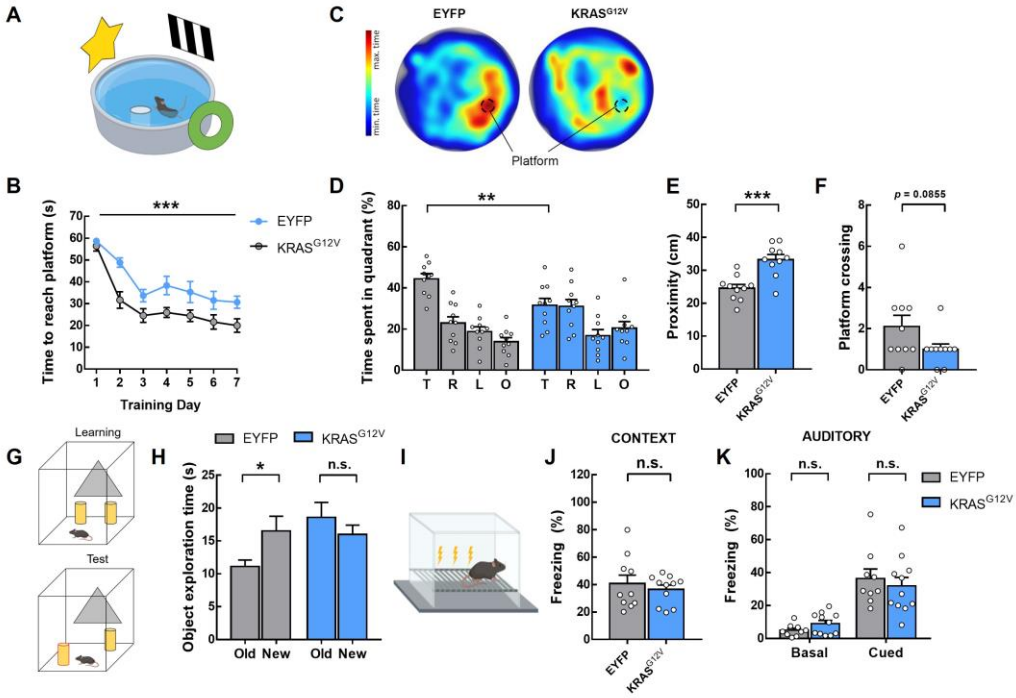

Figure 3. Ectopic expression of KRAS^{G12V} in inhibitory neurons causes spatial memory deficits. (A) The schematic diagram of Morris water maze. (B) Learning curve showed that the latency to find the hidden platform during the training sessions was significantly increased in vGAT-Cre::KRAS^{G12V} mice compared to vGAT-Cre::EYFP control mice (n = 10, 10; $F_{1,18}$ = 21.53, ***p = 0.0002 by two-way repeated measures ANOVA). (C) Representative heat map summary of MWM probe test. Platform position during the training trials is indicated by the dotted circle. (D) Time spent in each quadrant during the probe test. vGAT-CRE::KRAS^{G12V} mice spent significantly less time in the target quadrant compared to vGAT-Cre::EYFP mice (comparison of target quadrant occupancy, **p = 0.0063 by unpaired t-test). Moreover, vGAT-Cre::EYFP mice selectively searched for the platform in the target quadrant, while KRAS^{G12V} did not (n = 10, 10; **p = 0.0063 by unpaired t test). T, target quadrant, R, right to target, L, left to target, O, opposite to target. (E) Proximity to target platform (average distance to the platform's former location during the probe trial) was longer in vGAT-Cre::KRAS^{G12V} mice (***p = 0.0003 by unpaired t test). (F)

Number of platform crossing during the probe trial was tend to be decreased in vGAT-Cre::KRAS^{G12V} mice (p = 0.0855 by unpaired t test). (G) Schematic diagram of object-place recognition test. (H) In object-place recognition test, vGAT-Cre::EYFP mice showed significant preference to the relocated (new) object, while vGAT-Cre::KRAS^{G12V} mice showed similar preference between old and new object (n = 26, 27; *p = 0.0112, p = 0.1223 by paired t test) New, new location; old, object location used in training session. (I) Schematic diagram of classical fear conditioning. (J) In contextual and (K) cued fear memory test, two groups showed comparable levels of freezing (contextual test, n = 10, 11; p = 0.534 by unpaired t test; cued test, n = 9, 11; p = 0.1157 for basal freezing before tone presented, p = 0.5690 for freezing in response to tone by unpaired t test). Data are expressed as the mean ± SEM.

2. 3 Ectopic expression of KRAS^{G12V} in inhibitory neurons increases inhibitory synaptic transmission

To examine whether the KRAS^{G12V} expression in inhibitory neurons alter electrophysiological properties, we assessed spontaneous inhibitory postsynaptic currents (sIPSC) in the hippocampal pyramidal neurons of KRAS^{G12V}-expressing mice. By using whole cell patch recording, we found the significant increase of sIPSC frequency in vGAT-Cre::KRAS^{G12V} mice compared to vGAT-Cre::EYFP mice with no difference in amplitude (Figure 4, A and B). Spontaneous excitatory postsynaptic currents (sEPSC) were also recorded with no differences in mean amplitude or frequency observed in the vGAT-Cre::KRAS^{G12V} mice (Figure 4, C and D). These finding suggest that the observed behavioral deficits may be linked to an increase of the inhibitory synaptic transmission in the hippocampus. Next, to test whether these alterations in inhibitory synaptic transmission influenced to hippocampal synaptic plasticity, we measured field excitatory postsynaptic potentials (fEPSPs) in the Schaffer-collateral pathway. vGAT-Cre::KRAS^{G12V} mice showed significantly decreased the input-output relationship of fEPSPs, indicating impaired basal synaptic transmission (Figure 4E). Moreover, paired-pulse facilitation ratio was reduced at 5 ms of inter-stimuli interval in vGAT-Cre::KRAS^{G12V} mice compared to control (Figure 4F). Long-term potentiation is a form of synaptic plasticity that is thought to be a cellular mechanism underlying learning and memory (178). Notably, strong stimulation-induced LTP was significantly decreased in vGAT-Cre::KRAS^{G12V} mice (Figure 4, G and H). Then we tested whether the LTP impairment is caused by alteration of inhibitory synaptic function. LTP was induced in the presence of a $GABA_A$ receptor antagonist, picrotoxin, and picrotoxin treatment restored LTP impairments in vGAT-Cre::KRAS^{G12V} mice (Figure 4, I and J). These results demonstrate that the KRAS^{G12V} expression in inhibitory neuron induces impairments of synaptic plasticity which might be due to increased inhibitory synaptic trnasmission.

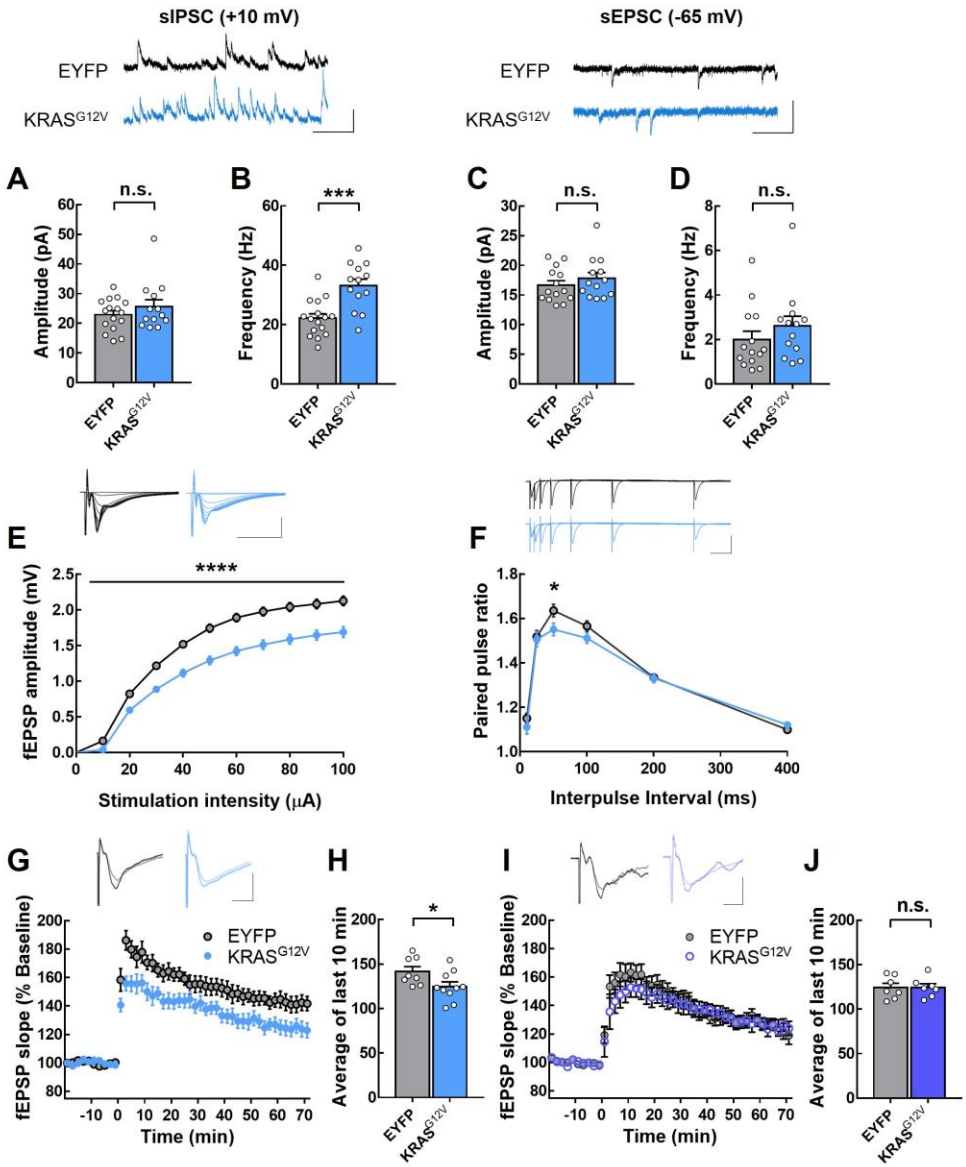

Figure 4. Ectopic expression of KRAS^{G12V} in inhibitory neurons elevates inhibitory synaptic transmission and impairs LTP. (A, B) KRAS^{G12V} expression in the inhibitory neurons increased the frequency of sIPSC, but did not alter amplitude of sIPSC in hippocampal pyramidal neurons (n = 16 cells from 3 mice, 13 cells from 3 mice; p = 0.2883, ***p = 0.0003 by unpaired t test). Vertical bar, 50 pA; horizontal bar, 200 ms. (C, D) KRAS^{G12V} expression in the inhibitory neurons did not affect either the frequency or the amplitude of sEPSC in hippocampal pyramidal neurons (n

= 14 cells from 3 mice, 13 cells from 3 mice; p = 0.3528, p = 0.3044 by unpaired t test). Vertical bar, 50 pA; horizontal bar, 200 ms. (E) vGAT-Cre::KRAS^{G12V} mice showed significantly decreased the input-output relationship of the fEPSP at CA3-CA1 synapse compared to EYFP mice (n = 20 slices from 10 mice, 23 slices from 10 mice; ****p > 0.0001 by two-way repeated measures ANOVA). (F) vGAT-Cre::KRAS^{G12V} showed significantly decreased paired pulse facilitation ratio at 50 ms interpulse interval compared to EYFP group (n = 20 slices from 10 mice, 23 slices from 10 mice; *p = 0.0403 by unpaired t test). Vertical bar, 1 mV; horizontal bar, 50 ms. (G) Inhibitory neuron-specific expression of KRAS^{G12V} significantly impaired LTP induced by the strong stimulation protocol (n = 8 slices from 5 mice, 10 slices from 5 mice). (H) The averages of fEPSP slope of 61 to 70 minutes after LTP induction were compared (*p = 0.0422 by unpaired t test). Vertical bar, 1 mV; horizontal bar, 5 ms. (I) Picrotoxin (10 μM) treatment restored the TBS-induced LTP impairments in vGAT-Cre:: KRAS^{G12V} mice (n = 7 slices from 4 mice, 7 slices from 3 mice). (J) The averages of fEPSP slope of 61 to 70 minutes after LTP induction were compared. Vertical bar, 1 mV; horizontal bar, 5 ms. Data are expressed as the mean ± SEM. *Hyun-Hee Ryu and Kyoung-Doo Hwang performed electrophysiology.*

2. 4 Ectopic expression of KRAS^{G12V} in hippocampal excitatory neurons

In adult mice, *Kras* is expressed not only in inhibitory neurons but also in excitatory neurons (122). To assess the effects and roles of ectopic KRAS^{G12V} expression in the hippocampal excitatory neurons, I injected AAV-KRAS^{G12V}–HA into the dorsal hippocampus of αCaMKII-Cre mice, thereby allowing the selective expression of KRAS^{G12V} in the excitatory neurons (Figure 5A). I then subjected the mice to open field test to assessing the basal locomotive activity and anxiety-like behaviors (Figure 5B). Interestingly, αCaMKII-Cre::KRAS^{G12V} mice exhibited hyperactivity and avoided the center zone in the open field test (Figure 5, C and D)

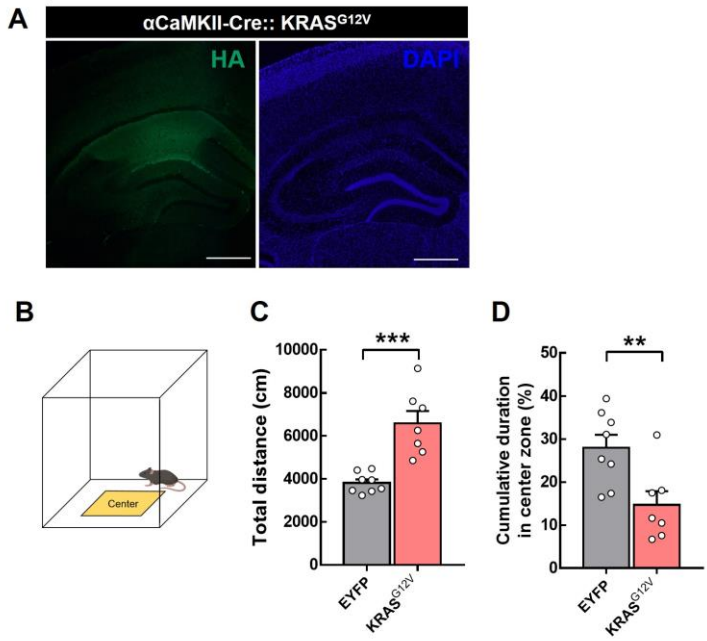

Figure 5. Ectopic expression of KRAS^{G12V} in excitatory neurons. (A) Expression of adeno-associated virus (AAV) expressing KRAS^{G12V}-HA in the dorsal hippocampus of adult αCaMKII-Cre mouse. 4',6-diamidino-2-phenylindole (DAPI) staining was used to identify nuclei. Scale bars, 200 μm. (B) The schematic diagram showing center zone of the open field test. (C) αCaMKII-Cre::KRAS^{G12V} mice showed increased total distance moved in open field test (n = 8, 7; ***p = 0.0003 by unpaired t test). (D) αCaMKII-Cre::KRAS^{G12V} mice showed increased cumulative duration in center zone in open field test (n = 8, 7; **p = 0.0096 by unpaired t test). Data are expressed as the mean ± SEM.

2. 5 Ectopic expression of KRAS^{G12V} in hippocampal excitatory neurons impairs hippocampal-dependent spatial learning and memory

To assess the hippocampal-dependent spatial learnind and memory, I subjected the mice to the MWM test (Figure 6A). αCaMKII-Cre::KRAS^{G12V} mice showed a significantly longer escape latencies during the training sessions of the MWM test, suggesting that KRAS^{G12V} expression in the hippocampal excitatory neurons severely impairs spatial learning (Figure 6B). In probe trial after training sessions, αCaMKII-Cre::KRAS^{G12V} mice failed to identify and reach the target quadrant, whereas the control αCaMKII-Cre::EYFP mice spent a significantly longer time in the target quadrant, suggesting that KRAS^{G12V} expression in the adult hippocampal excitatory neurons also impairs spatial memory (Figure 6, C and D). Moreover, KRAS^{G12V}-expressing mice swam farther from the platform location (Figure 6E) and crossed the platform fewer times than the EYFP-expressing control mice (Figure 6F).

Next, I carried out classical fear conditioning to assess the contextual and auditory fear memory of the mice (Figure 6G). αCaMKII-Cre::KRAS^{G12V} mice showed significantly lower freezing time compared to αCaMKII-Cre::EYFP mice in contextual test, but not in auditory test in the classical fear conditioning (Figure 6, H and I), showing that expressing KRAS^{G12V} in excitatory neurons impairs hippocampus-dependent memory without affecting amygdala-dependent memory.

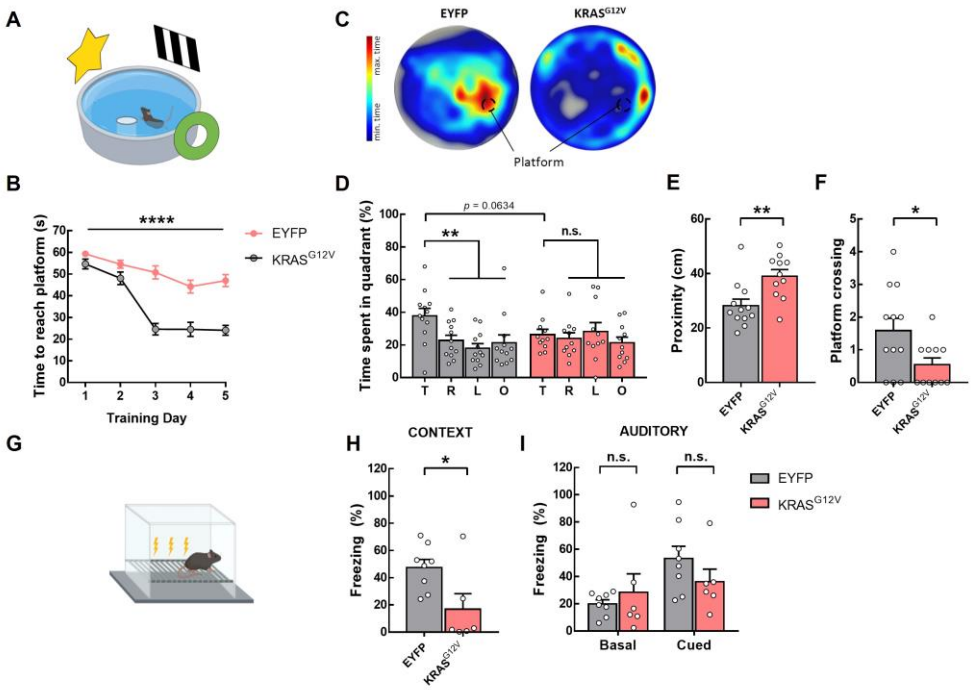

Figure 6. Ectopic expression of KRAS^{G12V} in excitatory neurons impairs spatial memory. (A) The schematic diagram of Morris water maze. (B) Learning during training trials is significantly slower in KRAS^{G12V}-injected mice compared to EYFP-injected controls (n = 12, 11; $F_{1,21}$ = 69.63, ****p < 0.001 by two-way repeated measures ANOVA). (C) Representative heat map summary of MWM probe test. Platform position during the training trials is indicated by the dotted circle. (D) Time spent in each quadrant during the probe test. αCaMKII-Cre::EYFP mice selectively searched for the platform in the target quadrant, while KRAS^{G12V} did not (n = 12, 11; $F_{3,44}$ = 0.2765, **p = 0.0055, $F_{3,40}$ = 0.799, p = 0.6384 by one-way ANOVA). αCaMKII-Cre::KRAS^{G12V} mice tend to spend less time in the target quadrant compared to EYFP-injected control mice (p = 0.0634 by unpaired t test). T, target quadrant, R, right to target, L, left to target, O, opposite to target. (E) αCaMKII-Cre::KRAS^{G12V} mice swam significantly farther than αCaMKII-Cre::EYFP mice during probe trials (n = 12, 11; **p = 0.0047 by unpaired t test). (F) αCaMKII-Cre::KRAS^{G12V} mice crossed the former platform position significantly less than αCaMKII-Cre::EYFP mice during

probe trials (n = 12, 11; *p = 0.0290 by unpaired t test). (G) Schematic diagram of classical fear conditioning. (H) In contextual fear memory test, αCaMKII-Cre::KRAS^{G12V} mice showed significantly reduced freezing behavior compared to αCaMKII-Cre::EYFP mice (n = 8, 6; *p = 0.0247 by unpaired t test). (I) The freezing level of αCaMKII-Cre::KRAS^{G12V} in response to the conditioned tone (cue) was not statistically different from that of αCaMKII-Cre::EYFP mice (n = 8, 6; p = 0.5026 for basal freezing level before tone played, p = 0.2178 for cued freezing by unpaired t test). Data are expressed as the mean ± SEM.

2. 6 Ectopic expression of $KRAS^{G12V}$ in hippocampal excitatory neurons induces neuronal death

During the histological assay (data not shown), we have observed the morphological alterations such as decreased cell density and the expansion of the hippocampal cell layer in αCaMKII-Cre::$KRAS^{G12V}$ hippocampus. Since a decreased cell number and abnormal cell layer have high probability to mean cell death, we hypothesized that the excitatory neuron-specific expression of $KRAS^{G12V}$ results in neuronal death. To test the hypothesis, we assesed the expression of cleaved caspase-3, a cell death marker. The number of cleaved caspase-3^{+} neurons was dramatically increased in the αCaMKII-Cre::$KRAS^{G12V}$ hippocampus compared to αCaMKII-Cre::EYFP hippocampus (Figure 7, A and B). Interestingly, $KRAS^{G12V}$ expression in inhibitory neuron-specific manner did not result in neuronal death (Figure 7, C and D).

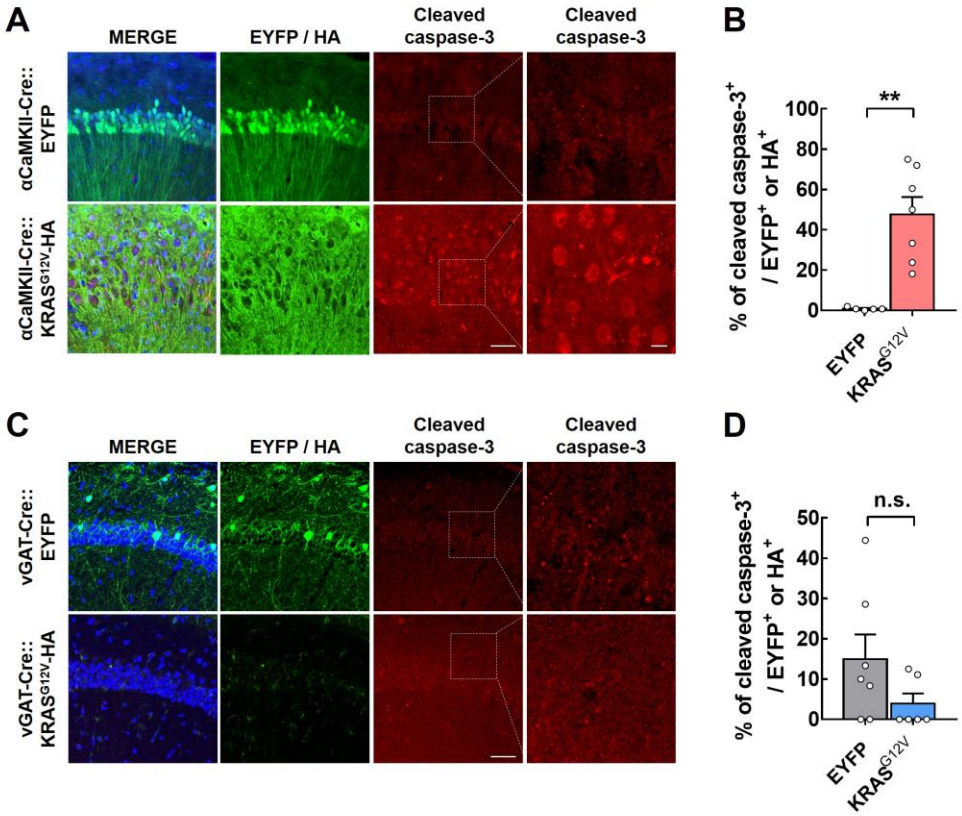

Figure 7. KRAS^{G12V} induces neuronal death in excitatory neurons, but not in inhibitory neurons. (A) Representative immunostained images for HA (green), cleaved caspase-3 (red), and DAPI (blue) in αCaMKII-Cre::KRAS^{G12V} mice. Scale bar, 50 μm, 20 μm. (B) The percentage of cleaved caspase-3 positive neurons was significantly increased in the KRAS^{G12V}-expressing hippocampal slices (n = 5 slices from 3 hippocampi, 7 slices from 3 hippocampi; $^{**}p$ = 0.0012 by unpaired *t* test). (C) Representative immunostained images for HA (green), cleaved caspase-3 (red), and DAPI (blue) in vGAT-Cre:: KRAS^{G12V} mice. Scale bar, 50 μm, 20 μm. (D) The percentage of cleaved caspase-3 positive neurons was comparable between vGAT-Cre::KRAS^{G12V} and vGAT-Cre::EYFP mice (n = 6 slices from 3 hippocampi, 6 slices from 4 hippocampi; p = 0.2488 by upaired *t* test). Data are expressed as the mean ± SEM. *Hyun-Hee Ryu and I performed immunohistochemistry.*

Discussion

In this chapter, to investigate the cellular mechanisms of cognitive impairments in KRAS-associated RASopathies, I used a strong gain of function mutation of KRAS, G12V, to mimic severe cases of RASopathy. Previously, Papale et al. had generated synapsin-specific $KRAS^{G12V}$ knockin mice and reported several notable features, including learning deficits and synaptic impairments (99). In these mice, suppression of hyperactivated RAS-ERK signaling in adult period is not sufficient to restore the behavioral and synaptic impairments, insisting that the overactivation of RAS-ERK signaling is responsible for the developmental defects (99). However, the effects of cell type-specific activation of RAS-ERK signaling in the adult hippocampus have not been fully investigated, and it remained uncertain whether the $KRAS^{G12V}$ in mature neurons is responsible to behavioral and synaptic deficits. Therefore, I assessed the effects of $KRAS^{G12V}$ in adult hippocampal neuron types on hippocampal-dependent learning and synaptic properties, and found that the expression of $KRAS^{G12V}$ in either hippocampal excitatory or inhibitory neurons results in spatial learning deficits in adult mice, each for different reasons.

As mentioned in introduction, mutations in the genes of RAS-ERK signaling pathway have cell type-specific roles on the downstream signaling activation as well as synaptic function. One of hypotheses for cell type-specific effect of RAS-ERK signaling is the distinct expression profiles of RAS-ERK signaling genes between excitatory and inhibitory neurons (122). Supporting this, the NF1 mRNA is significantly enriched in inhibitory neurons versus in excitatory neurons in both mice and humans, which may explain its essential roles in mediating inhibitory synaptic function (84, 122, 123). Similarly, expression profile has shown that the Kras transcripts were higher in hippocampal inhibitory neurons rather than in excitatory neurons, and previous study reported that the synapsin-specific $KRAS^{G12V}$ knockin

mice show increased inhibitory function (99, 122). Consistently, I found that KRAS is involved in regulating GABAergic inhibitory synaptic function, and subsequently impairs learning and memory. I also found the significant suppression of input-output curve of fEPSP in inhibitory neuron-specific $KRAS^{G12V}$-expressing mice, which might be due to increased inhibitory tone. Although the enhanced RAS-ERK signaling pathway increases GABA release by phosphorylation of synapsin I at the hippocampal inhibitory synapse, a detailed molecular mechanism how the KRAS regulates the spontaneous GABA release should be identified (84). It is widely known that the enhanced GABAergic inhibitory synaptic transmission is able to result in LTP impairment. vGAT-Cre::$KRAS^{G12V}$ mice showed LTP deficit which is restored by picrotoxin treatment, demonstrating the increased inhibition-induced LTP impairment.

Notably, $KRAS^{G12V}$ resulted in neuronal death only in excitatory neurons, but not in inhibitory neurons, suggesting the another distinct role of KRAS in excitatory neurons. $KRAS^{G12V}$ also induced histological malformation, such as an expanded hippocampal cell layer, which might be induce complex behavioral alterations. RAS-ERK signaling is widely known as anti-apoptotic regulator, but it also functions as pro-apoptotic regulator. For example, previous study has shown that nestin-specific $KRAS^{G12V}$ expression induces cell death in neural progenitor cells, contributing to generation of brain edema in zebrafish (179). RAS-ERK signaling activation is thought to be able to bring out either cell death or cell survival depending on context and conditions, the detailed cellular mechanisms are remained unknown. Moreover, the mechanisms how $KRAS^{G12V}$ resulted in cell death only in excitatory neurons, but not in inhibitory neurons remained to be investigated. Since RAS-ERK signaling is composed of distinct networks in excitatory and inhibitory neurons, I speculated that KRAS-ERK signaling is not linked to pro-apoptotic regulation in inhibitory neurons. Recent study reported the discovery of a pan-KRAS inhibitor that

inactivates common KRAS proteins without needing to be covalently anchored to a specific mutant amino acid (180). It would be worthwhile to investigate whether the defects due to $KRAS^{G12V}$ are reversible. Taken together, gain of function mutation of KRAS in adult hippocampal neurons affects function and survival of inhibitory and excitatory neurons. These findings may provide advances of understanding in physiological roles of KRAS in adult neurons.

Chapter 3

Aberrant *BRAF* signaling impairs learning and memory via reactive-like astrogliosis

Introduction

Among RAS-ERK signaling genes, BRAF is a serine/threonine protein kinase which is a direct downstream effector of RAS of which mutations have been associated with cancers as well as multiple RASopathies (22, 27, 41-43, 181). To date, 417 *BRAF* mutations have been identified in CFC syndrome (NSEuroNet database, https://nseuronet.com), a rare and severe form of RASopathy with a high prevalence of intellectual disabilities (50, 59, 182). In a previous study, forebrain-specific *Braf* knockout mice showed impairment in spatial learning and hippocampal LTP without altering synaptic transmission or the paired-pulse facilitation ratio, suggesting the pivotal roles of *Braf* in learning and memory (151). As mentioned above, gain of function mutations of the *BRAF* gene are highly associated with CFC syndrome, and there are several mouse models harboring *BRAF* mutations were successfully recapitulated developmental malformations observed in CFC syndrome involving craniofacial, cardiac abnormalities, and growth delay (104, 152-154). Notably, heterozygous knockin mice expressing *Braf*^{Q241R} showed learning deficits in contextual fear conditioning (152). However, as fewer animal models of CFC syndrome have been reported likely due to its lower prevalence (approximately 1 in 810,000) compared to other RASopathy, molecular and cellular mechanism such as cell type specificity underlying cognitive deficits associated with *BRAF* mutations remains unknown.

Recently, several studies have reported that the RASopathy-linked mutations are related with astroglial differentiation in model organisms (107, 147, 163). For example, the mutant mice expressing either *Mek1*^{Y130C} or *Raf1*^{L613V} RASopathy-associated mutation showed increased glial number in the cortex and hippocampus (108). On the contrary, a recent study with induced pluripotent stem cells (iPSCs) harboring *BRAF*^{Q257R} reported the decreased number of glial cells (147). Astrocytes are related to several key

physiological processes in the central nervous system, and there are emerging evidences of astrocytic dysfunction in neurological disorders involving cognitive disabilities. However, how the RAS-ERK signaling is involved in regulatory system of astroglial properties and finally affects cognition was poorly understood.

In this study, I investigated mechanisms for learning and memory deficits in CFC syndrome by generating and characterizing a series of cell type-specific conditional knock-in mouse lines expressing a CFC syndrome-associated constitutive active *Braf*^{K499E} mutation (41). I found that the expression of *Braf*^{K499E} in neural stem cells under control of Nestin-Cre resulted in severe hippocampal memory deficits in mice, whereas expressing the K499E mutant *Braf* either in excitatory or in inhibitory neurons does not. Notably, *Braf*^{K499E} mutation resulted in aberrant reactive-like astrogliosis in hippocampus and cortex when the variant is expressed in neural stem cells. Moreover, expressing *Braf*^{K499E} variant in adult astrocytes is sufficient to induce hippocampal learning and memory which accompanied by hypertrophy and hyperactive Ca^{2+} fluctuation of astrocytes. These defective phenotypes were restored by astrocyte-specific attenuation of RAS-ERK signaling activity. Furthermore, reducing RAS-ERK activity selectively in astrocyte was also able to recover the learning and memory deficits in Nestin;*Braf*$^{K499E/+}$ mice, demonstrating that the increased RAS-ERK activity in astrocyte results in dysfunction of astrocytes, and subsequently causes learning and memory deficits in CFC syndrome.

Material and method

1. Mice

To construct the targeting vector for inducible *Braf*^{K499E} knockin mice, the K499E (exon 11) mutation, marked by a unique BstBI site, was introduced by site-directed mutagenesis. A splice acceptor sequence, a Braf cDNA fragment encoding wild type exon 10-22, and a pGK-Neo gene were positioned between two loxP sites. *Braf*$^{K499Efl/+}$ mice were crossed to αCaMKII-Cre mice (JAX 005359), vGAT-IRES-Cre (JAX 016962), Nestin-Cre (JAX 003771) or GFAP-CreER^{T2} (JAX 12849) mice. Three to six-month-old male and female mice were used. For AAV experiments, three to four-month-old male C57Bl/6N mice were used. All experiments used littermates as control group, and were carried out and analyzed with the experimenters blinded to genotype. Animals were group housed (two to five mice per cage) on a 12-hour light-dark cycle in vivarium at SNU. All studies were approved by the Animal Research Committee at SNU (SNU-220107-2-1).

2. Morris water maze (MWM) test

MWM test was performed as described in Chapter 2.

3. Object-place recognition (OPR) test

OPR test was performed as described in Chapter 2.

4. Open field test

Open field test was performed as described in Chapter 2.

5. Three-chamber social test

Mice were habituated to the three-chamber apparatus for 15 minutes for 2 consecutive days. When the habituations were completed, the mice were

released to the center chamber of apparatus which containing a wired cup with stranger mouse and an empty cup. For each set of experiment, the location of two cups was counterbalanced. The movement of mice was tracked for tracking software (EthoVision; Nodulus).

6. Tissue preparation and immunohistochemistry

Mice were fully anesthetized and transcardially perfused with cold 4% paraformaldehyde and PBS. Then brains were dissected, post-fixed with 4% PFA overnight, dehydrated with 30% sucrose for following 2 days, and sectioned on a cryotome. Tissue sections (20 μm thick) were collected in cryoprotectant solution (50% 0.1 M sodium phosphate buffer, 25% ethylene glycol, and 25% glycerol), and incubated in a blocking solution consisting of Normal goat serum (or donkey serum) and Triton X-100 in PBS. Sections were then incubated with primary antibody [anti-GFAP rabbit IgG (Abcam, ab7260); anti-GFAP mouse IgG (Cell signaling, #3670); anti-NeuN mouse IgG (Millipore, MAB377); anti-S100β rabbit IgG (Abcam, ab52642); anti-Iba1 rabbit IgG (WAKO); anti-Ki67 rabbit IgG (Invitrogen, MA5-14520); anti-PV mouse IgG (Millipore, MAB1572); anti-SOM rat IgG (Millipore, MAB354)] were `in blocking solution and incubated with tissue sections at 4 ℃ for 24 hours to 48 hours followed by incubation in secondary antibodies for 2 to 4 hours at room temperature. Images were acquired on the FV-3000 confocal microscope (Olympus, Japan) with FV31S software.

7. Sholl analysis

Sholl analysis was performed on serially stacked confocal images as previously described (183). Images of hippocampal sections immunostained with GFAP antibody were used for Sholl analysis. The Sholl analysis plugin was applied in ImageJ (NIH). The serial concentric circles were automatically drawn at 1 μm intervals from the center of the soma to the end of the most distant process in each single astrocyte. Number of intersections

and sum of process intersections were analyzed.

8. Western blotting

Cortices and hippocampi were dissected and lysed in protein lysis buffer (10 mM Tris-HCl, 1.6% SDS) containing phosphatase inhibitor cocktails and protease (Sigma). Supernatants were collected and protein concentration was measured using a BCA assay kit (Thermo). Equal amounts of proteins (5 - 10 ug) were loaded on a SDS-PAGE gel, and transferred to nitrocellulose membranes. After blocking with 5% skim milk in TBST solution (Tris-buffer saline containing 0.1% Tween-20) for 40 minutes at room temperature. Then membranes were hybridized with each primary antibody [anti-GRIA1 mouse IgG (Millipore, MAB2263); anti-GRIA2 mouse IgG (Millipore, MAB397); anti-GRIN1 rabbit IgG (Millipore, AB9864); anti-GRIN2A rabbit IgG (Millipore, 04-901); anti-GRIN2B rabbit IgG (Millipore, AB1557P); anti-gephyrin mouse IgG (Synaptic Systems, 147 111); anti-vGAT mouse IgG (Synaptic Systems, 131 011); anti-synapsin rabbit IgG (Abcam, ab64581); anti-vGLUT1 rabbit IgG (Synaptic Systems, 135 302); anti-PSD95 mouse IgG (Abcam, ab2723); anti-p-ERK1/2 rabbit IgG (Cell signaling, 9101); anti-ERK rabbit IgG (Cell signaling, 9102)] in 5% skim milk overnight at 4 ℃. After washing with TBST, membranes were incubated with a secondary antibody in 5% skim milk for 1 hour at room temperature. Signals were visualized by ECL solution (Thermo).

9. Tamoxifen administration

Stock solution of tamoxifen (Sigma-Aldrich) was made at concentration of 20 mg/ml in sunflower seed oil (Sigma-Aldrich). Dose of 100 mg/kg tamoxifen was administered into control or double transgenic mice (male and female) by intraperitoneal (i.p.) injection per day for consecutive 5 days.

10. Stereotaxic viral injection

Virus was generated from the Institute for Basic science virus facility (IBS virus facility). Mice were anesthetized with ketamine solution and mounted on a stereotaxic frame. The hippocampal CA1 region was targeted using the following coordinates: anterior-posterior (AP): -1.8 mm, medial-lateral (ML): ±1.0 mm, dorsal-ventral (DV): -1.7 mm/AP: -2.5 mm, ML: ±2.0 mm, DV: -1.8 mm. AAV was injected into each point. All mice were allowed to recover for a minimum of 3 weeks before further use in experiments.

Results

3. 1 *Braf*^{K499E} expression in either excitatory neurons or inhibitory neurons does not impair learning and memory

To investigate the mechanism for severe intellectual disability in *Braf*-associated neurodevelopmental disorders, we generated an inducible knock-in mice harboring Braf K499E allele in which the expression of the K499E variant is under the control of Cre-dependent recombination (Figure 8). Previous studies have shown that BRAF is highly expressed in neurons (122). Deleting BRAF in forebrain excitatory neurons impairs hippocampal learning and memory, suggesting that BRAF may play critical roles in excitatory neurons (151). However, a recent study showed that BRAF expression is relatively higher in inhibitory neurons than in excitatory neuron in the hippocampus (122). To examine which neuron type is responsible for the learning impairments associated with the BRAF mutation, I crossed the floxed BRAF K499E mice with Cre lines expressing the Cre recombinase under the control of alpha Ca^{2+}/calmodulin-dependent kinase II (αCaMKII) or vesicular GABA transporter (vGAT) promoter, allowing excitatory neuron or inhibitory neuron-specific expression of BRAF K499E, respectively (Figure 9A).

Majority of CFC syndrome patients show learning disability, and especially, individuals harboring Braf K499E (KE) mutations show severe difficulty in education and academic performance (50). To examine the impact of Braf KE expression restricted to excitatory or inhibitory neurons on hippocampus-dependent learning and memory, I subjected αCaMKII;*Braf*$^{KE/+}$ and vGAT;*Braf*$^{KE/+}$ mice to the hidden platform version of the Morris water maze (Figure 9B)(184). During the training sessions, αCaMKII;*Braf*$^{KE/+}$ and vGAT;*Braf*$^{KE/+}$ mice showed a comparable latency to find the hidden platform compared to control groups (Figure 9, C and I). In probe trials wherein the platform is removed, contrary to our expectation,

αCaMKII;*Braf*$^{KE/+}$ and vGAT;*Braf*$^{KE/+}$ performed equivalently to control mice (Figure 9, D-F and J-L), with comparable swimming speed (Figure 10, D-F and J-L). Next, the mice were subjected to the object-place recognition (OPR) test, which is another hippocampal-dependent learning and memory task (Figure 9G). 24 hours after training, both αCaMKII;*Braf*$^{KE/+}$ and vGAT;*Braf*$^{KE/+}$ mice showed preference toward the relocated object and did not show significant difference from the littermates, demonstrating that spatial recognition memory is intact in both mutant mice (Figure 9, H and M). These data suggest that BRAF K499E expression either in αCaMKII^{+} excitatory or in vGAT^{+} inhibitory hippocampal neuron is not critically involved in the learning and memory deficits associated with CFC syndrome.

In addition to intellectual disability, RASopathy individuals with *BRAF* mutations often display a large range of behavioral disability such as locomotor impairments, increased anxiety and decreased sociability (58, 185). Therefore, we first characterized those neurobehavioral characteristics in each conditional knock-in mice line. Neither αCaMKII;*Braf*$^{KE/+}$ nor vGAT;*Braf*$^{KE/+}$ mutant mice displayed a significant difference compared to their littermate control mice in total distance moved or time spent in the center zone of a novel square arena, indicating normal voluntary locomotive activity and anxiety-like behavior (Figure 10, A and B, G and H). As recent clinical investigations reported a high prevalence of autism spectrum disorders among RASopathy patients (185), I evaluated innate sociability of mutant mice. Both αCaMKII;*Braf*$^{KE/+}$ and vGAT;*Braf*$^{KE/+}$ showed normal sociability by presenting strong preference for social target (Figure 10, C and I).

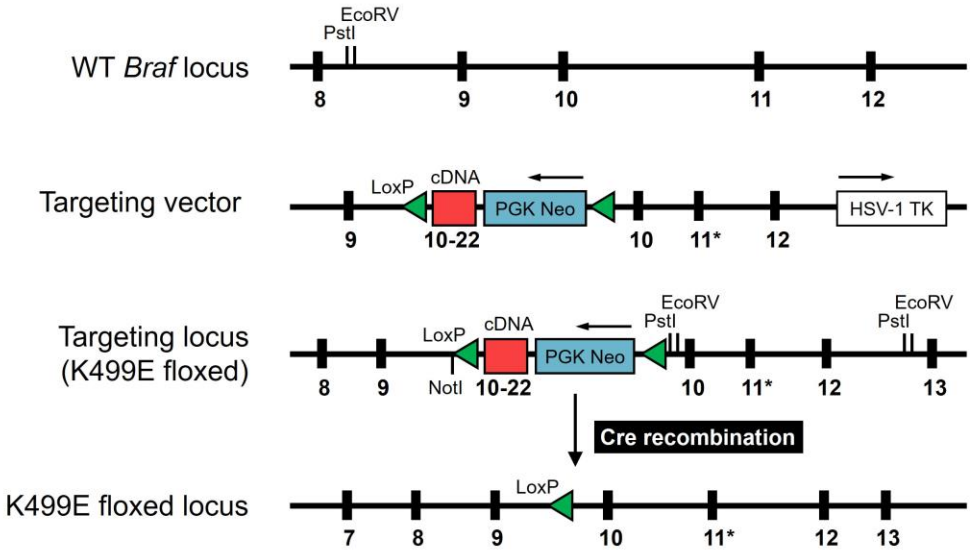

Figure 8. Targeting strategy for generating inducible *Braf*^{K499E} knockin mice. Structures of the *Braf* locus, targeting vector, mutant allele and location of probes for Southern blotting are shown. *Erica Tiberia generated Braf*$^{K499E\ floxed}$ *mice (New York University).*

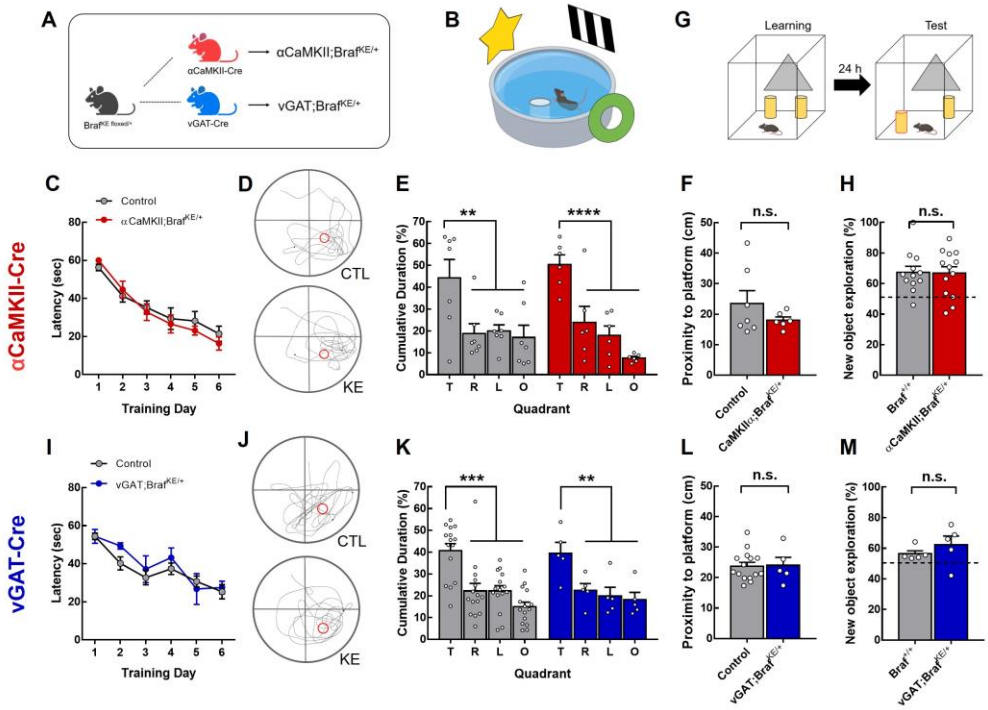

Figure 9. *Braf*^{K499E} in excitatory neurons or inhibitory neurons does not cause learning deficits. (A) Schematic diagram of breeding strategy. (B) Schematic illustration of Morris water maze. (C) Learning curve showing that the latencies to find the hidden platform during the Morris water maze (MWM) training trials was comparable between control and αCaMKII;*Braf*$^{KE/+}$ (n = 7, 6). (D) Representative swimming trajectory of WT and αCaMKII;*Braf*$^{KE/+}$ mice in the probe trial of MWM. Platform position during the training trials is indicated by the red-colored circle. (E) Quadrant occupancy analysis for the probe test. Both genotype spent more time in target quadrant than three other quadrants (n = 7, 6; $F_{3, 24} = 5.037$, $^{**}p = 0.0076$, $F_{3, 20} = 14.58$, $^{****}p < 0.0001$ by one-way ANOVA). (F) Proximity to target platform occupied by both group (n = 7, 6) was similar ($p = 0.2656$ by unpaired *t* test). (G) Schematic illustration of object-place recognition test. (H) Time exploring the relocated (new) object in OPR test was similar between genotypes (n = 12, 13; $^{***}p = 0.0002$, $^{***}p = 0.0006$ by unpaired *t* test, respectively, compared to a hypothetical 50%). (I)

Learning curve showing that the latencies to find the hidden platform during the MWM training trials was comparable between control and vGAT;*Braf*$^{KE/+}$ (n = 15, 5). (J) Representative swimming trajectory of WT and vGAT;*Braf*$^{KE/+}$ mice in the probe trial of MWM. (K) Quadrant occupancy analysis for the probe test (n = 15, 5; $F_{3, 56} = 14.75$, ****$p < 0.0001$, $F_{3, 16} = 6.306$, **$p = 0.0050$ by one-way ANOVA). (L) Proximity to target platform occupied by both group (n = 15, 5) was similar ($p = 0.9273$ by unpaired *t* test). (M) Both genotype (n = 5, 5) spent longer time to explore the novel object than the old object (*$p = 0.0118$, $p = 0.0616$ by unpaired *t* test, respectively, compared to a hypothetical 50%). T, target quadrant; R, right quadrant; L, left quadrant; O, opposite quadrant. Data are expressed as the mean ± SEM.

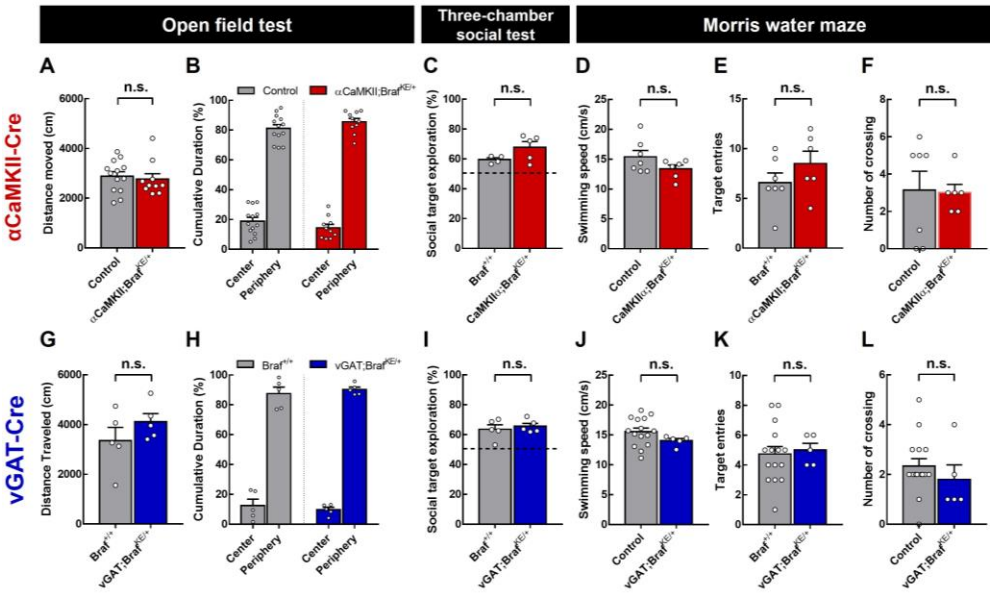

Figure 10. *Braf*^{K499E} in excitatory neurons or inhibitory neurons does not have significant effect on behaviors. (A) Control mice (n = 13) and αCaMKII;*Braf*$^{KE/+}$ mice (n = 10) showed comparable length of total distance traveled during open field test (p = 0.6807 by unpaired t test). (B) Both groups preferred to stay in the periphery zone of open field arena. (C) Both genotypes spent longer time to explore the social target in social interaction test (n = 4, 5; ***p = 0.0003, **p = 0.0019 by unpaired t test, respectively, compared to a hypothetical 50%, equal preference for social target and empty cup). (D) In probe test of Morris water maze, both genotypes had comparable swimming speeds (n = 7, 6; p = 0.1479 by unpaired t test). (E) Number of target zone entries in the probe trial was comparable between both groups (p = 0.2388 by unpaired t test). (F) Number of crossing were similar in both groups (p = 0.9052 by unpaired t test). (G) *Braf*$^{+/+}$ (n = 5) and vGAT;*Braf*$^{KE/+}$ (n = 5) showed comparable distance traveled during open field test (p = 0.2681 by unpaired t test, p = 0.2625 by unpaired t test). (H) Both groups preferred to stay in the periphery zone of open field arena. (I) Three chamber social interaction test. Both genotypes (n = 5, 5) spent longer time to explore the social target than the empty cup (**p = 0.0020, ****p < 0.0001 by unpaired t test, respectively, compared to a hypothetical

50% equal preference for social target and empty cup). (J) Control group (n = 15) and vGAT;*Braf*$^{KE/+}$ (n = 5) showed similar swim speeds in probe test (p = 0.1834 by unpaired t test). (K) Number of target zone entries in the probe trial was comparable between both group (p = 0.7749 by unpaired t test). (L) Number of crossing were similar in both groups (p = 0.4026 by unpaired t test). Data are expressed as the mean ± SEM.

3. 2 BRAF K499E expression in neural stem cell impairs learning and memory

As BRAF K499E expression in αCaMKII^{+} excitatory neuron or vGAT^{+} inhibitory neuron did not impair hippocampus-dependent learning and memory, we hypothesized that other cell type, not neuronal subtypes, might be responsible for mutant BRAF-associated deficits in learning and memory. I generated mice expressing BRAF mutation in neural stem cells in brain by crossing Braf K499E floxed mice with Nestin-cre mice. Different from αCaMKII or vGAT, Nestin promoter allows early expression of the target gene which is initiated by the embryonic period in neural stem cells, which subsequently will be differentiated into both neurons and glia (186). Therefore, Nestin;*Braf*$^{KE/+}$ might be ideal to model developmental neurological phenotypes reported in CFC syndromes such as brain malformation (56, 187). To investigate whether the Braf K499E affects gross morphology, brain volume and width are measured by sequential magnetic resonance (MR) imaging. Nestin;*Braf*$^{KE/+}$ showed increased brain volume and width, whereas they showed decreased body weight compared to wild type (WT) littermates, which is parallel to relative macrocephaly found in patients with CFC syndrome (Figure 11, A to D) (188, 189). However, the volume of the hippocampus was comparable to that of WT (Figure 11, E and F). Western blot analysis revealed that the phosphorylated ERK1/2 (p-ERK1/2) expression was significantly increased in mutant hippocampus, showing the overactivation of RAS-ERK signaling in Nestin;*Braf*$^{KE/+}$ mice (Figure 11G).

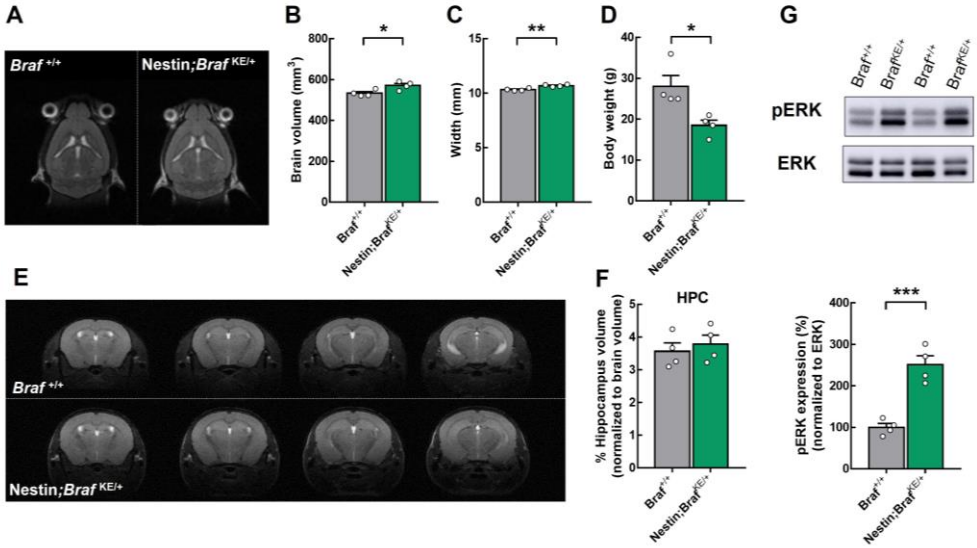

Figure 11. *Braf*^{K499E} in neural stem cells results in enlarged brain volume and hyperactive RAS-ERK signaling activity. (A) Representative horizontal image of structural magnetic resonance imaging (MRI). (B, C) Brain volume and width were increased in Nestin;*Braf*$^{KE/+}$ brain, (D) while body weight was decreased (n = 4, 4, **p* = 0.0251, ***p* = 0.0025, **p* = 0.0185 by unpaired *t* test). (E) Representative coronal MRI image of hippocampus. (F) Hippocampal volume which is normalized to whole brain volume was unaltered in Nestin;*Braf*$^{KE/+}$ (*p* = 0.5803 by unpaired *t* test). (G) Representative immunoblot image of hippocampal lysates. p-ERK1/2 expression were increased in Nestin;*Braf*$^{KE/+}$ lysates (n = 4, 4; ****p* = 0.0007 by unpaired *t* test). Data are expressed as the mean ± SEM.

Prior to assessing learning and memory, we evaluated general behavior of Nestin;*Braf*$^{KE/+}$. In open field test, mutant mice showed normal basal locomotive activity and anxiety-like behavior (Figure 12, A and B). In addition, Nestin;*Braf*$^{KE/+}$ mice showed intact sociability, indicating that BRAF KE in neural stem cells does not alter general behaviors (Figure 12C).

I next asked if Nestin;*Braf*$^{KE/+}$ mice are impaired in hippocampal learning and memory tasks (Figure 13, A and B). Interestingly, in contrast to excitatory or inhibitory neuron type-specific BRAF KE mutants, Nestin;*Braf*$^{KE/+}$ mice show severe deficits in the Morris water maze task. Nestin;*Braf*$^{KE/+}$ mice showed greater escape latencies during the training sessions (Figure 13C). Importantly, the mutant showed chance-level performances in the probe trial test, while WT littermates spent significantly longer time in target quadrant, demonstrating that the mutant mice failed to learn and recall the location of the platform position (Figure 12, D to F and figure 13, D to F). In addition, Nestin;*Braf*$^{KE/+}$ mice also showed a significant deficit in the OPR task (Figure 13, G and H). These data strongly suggest that Nestin;*Braf*$^{KE/+}$ mice recapitulate structural and intellectual deficits associated with CFC syndrome. I used this mutant to investigate the mechanism of learning and memory deficits in CFC syndrome.

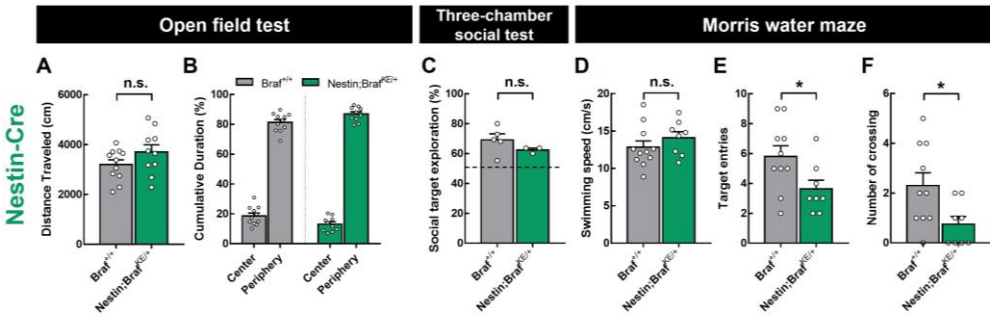

Figure 12. *Braf*^{K499E} in neural stem cells does not have significant effect on general behaviors. (A) Wild type mice (n = 11) and Nestin;*Braf*$^{KE/+}$ mice (n = 10) showed comparable length of distance moved during open field test (p = 0.1454 by unpaired t test). (B) Both groups preferred to stay in the periphery zone of open field arena. (C) Both genotypes spent longer time to explore the social target in social interaction test (n = 5, 3; **p = 0.0014, ***p = 0.0005 by unpaired t test, respectively, compared to a hypothetical 50%, equal preference for social target and empty cup). (D) Control group (n = 11) and Nestin;*Braf*$^{KE/+}$ (n = 8) showed similar swim speeds in probe test (p = 0.3096 by unpaired t test). (E) Number of target zone entries of Nestin;*Braf*$^{KE/+}$ was less than WT mice in the probe trial (*p = 0.0402 by unpaired t test). (F) Nestin;*Braf*$^{KE/+}$ (n = 8) showed less number of crossing than *Braf*$^{+/+}$ mice (*p = 0.0288 by unpaired t test). Data are expressed as the mean ± SEM.

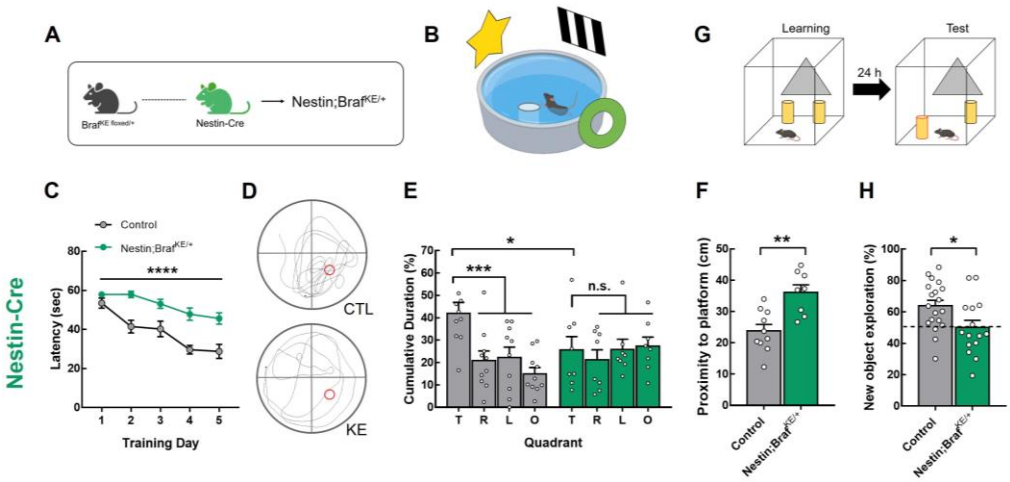

Figure 13. *Braf*^{K499E} in neural stem cells causes learning deficits. (A) Schematic diagram of breeding strategy. (B) Schematic illustration of Morris water maze. (C) Learning curve showing that the latencies to find the hidden platform during the MWM training trials of Nestin;*Braf*$^{KE/+}$ was significantly longer than those of control (n = 10, 8; $F_{1, 17} = 35.64$, ****$p < 0.0001$ by Two-way repeated measures ANOVA). (D) Representative swimming trajectory of WT and Nestin;*Braf*$^{KE/+}$ mice in the probe trial of MWM. (E) Quadrant occupancy analysis for the probe test (n = 10, 8; $F_{3, 36} = 7.743$, ***$p = 0.0004$, $F_{3, 28} = 0.3142$, $p = 0.8149$ by one-way ANOVA; *$p = 0.0461$ by unpaired *t* test). (F) Proximity to target platform occupied by Nestin;*Braf*$^{KE/+}$ mice was longer than the *Braf*$^{+/+}$ mice (n = 10, 8; **$p = 0.0014$ by unpaired *t* test). (G) Schematic illustration of object-place recognition test. (H) *Braf*$^{+/+}$ (n = 17) spent longer time to explore the relocated object, but Nestin;*Braf*$^{KE/+}$ mice (n = 13) did not (***$p = 0.0009$, $p = 0.7754$ by unpaired t test, respectively, compared to a hypothetical 50%). T, target quadrant; R, right quadrant; L, left quadrant; O, opposite quadrant. Data are expressed as the mean ± SEM.

3. 3 BRAF K499E drives increased reactive-like astrogliosis in the hippocampus

Individuals with RASopathy display developmental abnormalities in central nervous system including structural malformation, imbalance of neuron-glial population, ectopia and atrophy that might contribute to neurobehavioral phenotypes (29, 34, 35, 44, 46, 190). To investigate the cellular mechanism of the learning and memory impairments in the Nestin;*Braf*$^{KE/+}$ mice, we performed histological analyses. When I analyzed the numbers of NeuN^{+} neuron and areas of GFAP^{+} astrocyte in the hippocampus CA1 region, the relative area of GFAP^{+} astrocytes was significantly increased in Nestin;*Braf*$^{KE/+}$ mice compared to littermate controls while the NeuN^{+} neuronal populations are unaltered (Figure 14, A to D). Recently, several studies have reported that the RASopathy-related genetic modifications in rodent model result in a selective loss of parvalbumin^{+} interneurons (191, 192). However, Nestin;*Braf*$^{KE/+}$ mice showed an altered number of neither parvalbumin^{+} nor somatostatin^{+} interneurons in the hippocampus CA1 suggesting that the *Braf* mutation did not affect inhibitory neuronal development at least in the hippocampus (Figure 15). Reactive astrocytes are astrocytes that undergo morphological, molecular, and functional remodeling in response to external stimulus (193) and GFAP and S100β are the most widely used marker of reactive astrocytes (194, 195). Notably, the numbers of GFAP^{+} and S100β^{+} cells are both increased in the hippocampus of the mutants, suggesting reactive-like astrogliosis in mutant hippocampus (Figure 14, E to H). Next, I performed a detailed Sholl analysis to quantify morphological and structural changes in an individual GFAP^{+} astrocyte, and observed number and sum of intersects were significantly increased in Nestin;*Braf*$^{KE/+}$ mice (Figure 14, I to K). One possibility to explain the observed abnormal increase in astrogliosis is a neuroinflammation or injury, which is frequently accompanied by microglial activation (196). To investigate this possibility, I immunolabled for the

activated microglial marker, Iba1. I found that the number and morphology of Iba1^{+} microglia in hippocampus CA1 region did not significantly differ from those of littermate controls, suggesting that the reactive-like astrocytes were not caused by local inflammatory responses (Figure 14, L to N). A similar increase in relative density and area of GFAP^{+} astrocyte with unchanged neuronal density was also found in the somatosensory cortex (Figure 16, A to D). Additionally, no change in relative density of Iba1^{+} microglia was detected in mutant cortex (Figure 16, E to G). Same as in the hippocampal lysates, p-ERK1/2 expression also was increased in cortical lysates, indicating BRAF K499E-mediated RAS-ERK signaling overactivation in the cortex (Figure 16H).

It is known that changes in neurons are often involved in altering or maintaining the state of astrocytes (83, 197). To examine whether the neuronal expressions of the mutant BRAF also induce reactive-like astrogliosis, we analyzed the GFAP^{+} astrocytes in the hippocampi of αCaMKII;*Braf*$^{KE/+}$ and vGAT;*Braf*$^{KE/+}$ mutant mice. Both mutant mice did not exhibit alterations in the relative area of GFAP^{+} cells, indicating neuronal expression of Braf K499E does not affect astrocytic populations (Figure 17).

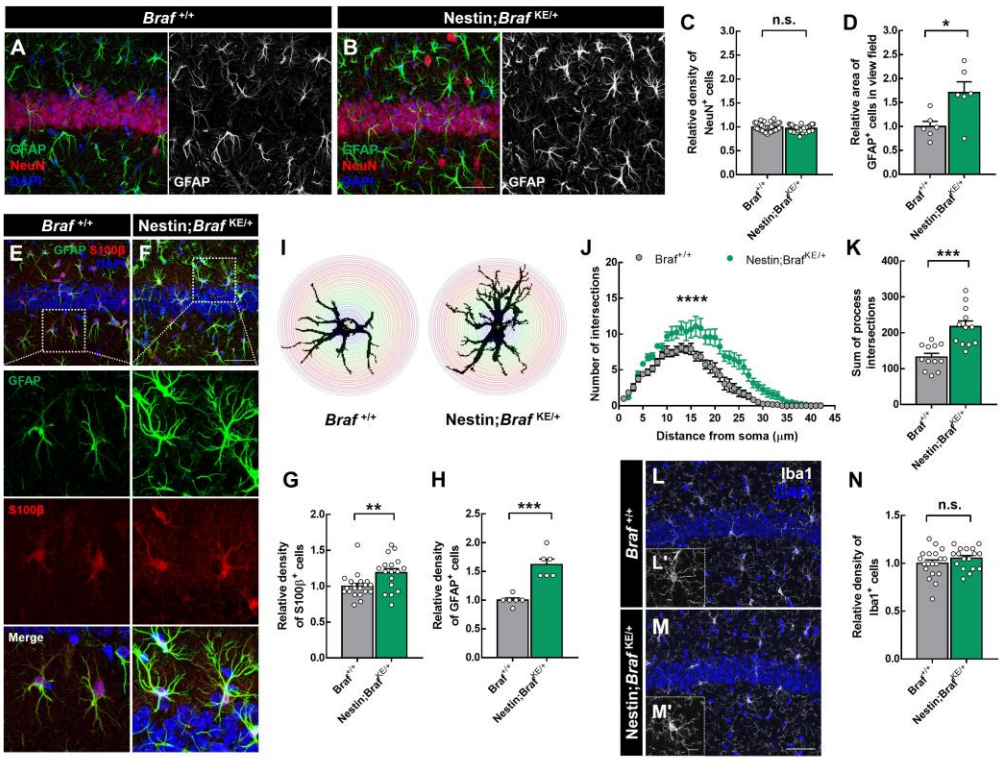

Figure 14. Nestin;*Braf*$^{KE/+}$ mutant exhibit significant increase of GFAP expression in hippocampus. (A, B) Representative confocal images of GFAP (green) and NeuN (red) immunolabeling in adult hippocampus CA1. Scale bars, 50 μm. (C) Number of NeuN-positive cells was unchanged (n = 35 images from 8 mice, 36 images from 7 mice; p = 0.1122 by unpaired t test). (D) Nestin;*Braf*$^{KE/+}$ brain showed increased area of GFAP-expressing cells compared with *Braf*$^{+/+}$ brain (n = 6 images from 3 mice, 6 images from 3 mice; *p = 0.0187 by unpaired t test). (E, F) Representative confocal images of GFAP (green) and S100β (red) immunolabeling in adult hippocampus CA1. Scale bars, 50 μm. (G) Nestin;*Braf*$^{KE/+}$ brain showed increased density of S100β-expressing cells compared with *Braf*$^{+/+}$ brain (n = 20 images from 5 mice, 17 images from 5 mice; **p = 0.0084 by unpaired t test). (H) Nestin;*Braf*$^{KE/+}$ brain showed increased density of GFAP-expressing cells compared with *Braf*$^{+/+}$ brain (n = 6 images from 3 mice, 6 images from 3 mice; ***p < 0.0001 by unpaired t test). (I) Representative

image for Sholl analysis of an astrocyte in the stratum radiatum from the GFAP-stained image. (J) The number of process intersections and (K) the sum of process intersections of $GFAP^{+}$ astrocytes were increased in the stratum radiatum of Nestin;*Braf*$^{KE/+}$ mice (9 cells from 3 mice, 9 cells from 3 mice; p = 0.0335 by unpaired t test). (L, M) Representative confocal images of Iba1 (white) immunolabeling in hippocampus CA1. Scale bars, 50 μm; 10 μm. (N) Both genotypes showed comparable number of Iba1-positive cells in CA1 (n = 19 images from 5 mice, 17 images from 5 mice; p = 0.2364 by unpaired t test). Data are expressed as the mean ± SEM.

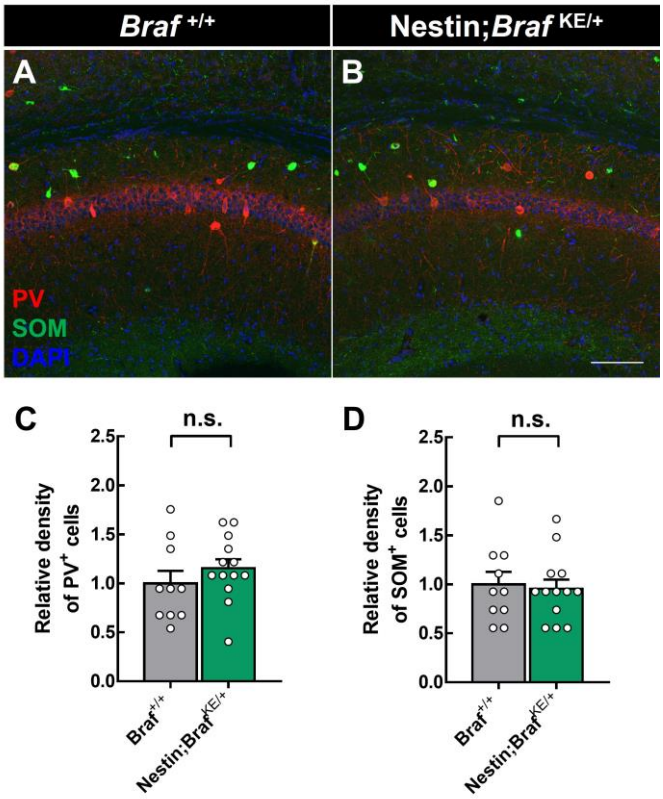

Figure 15. Nestin;*Braf*$^{KE/+}$ mice showed comparable number of PV-, and SOM-positive hippocampal inhibitory neuronal subtypes. (A, B) Representative confocal images of PV and SOM immunolabeling in the adult hippocampus CA1. Scale bars, 100 μm. (C) Nestin;*Braf*$^{KE/+}$ mice did not displayed significantly altered number of PV-positive or (D) SOM-positive cells in the CA1 (10 images from 3 mice, 13 images from 3 mice; $p = 0.3284$; $p = 0.7701$ by unpaired t test).

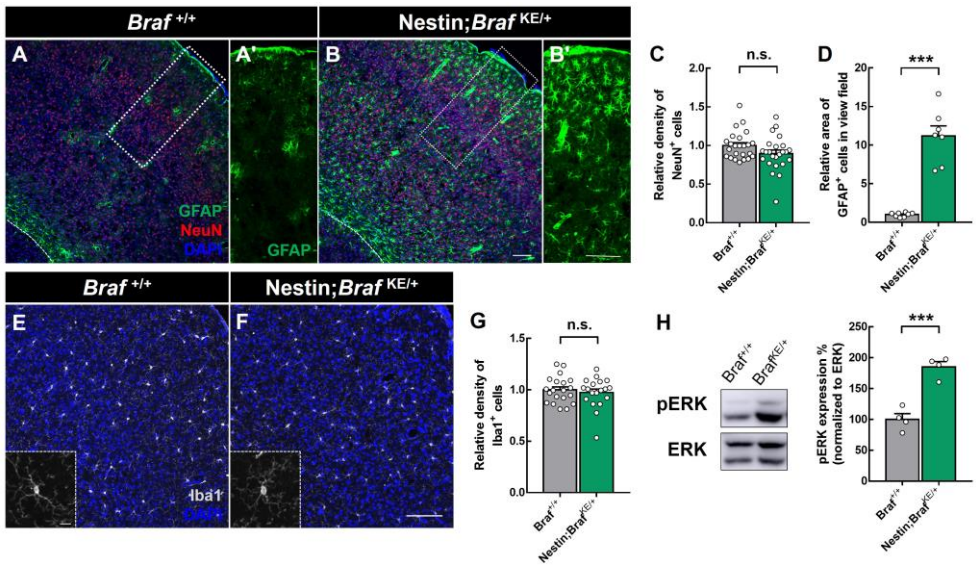

Figure 16. Nestin;*Braf*$^{KE/+}$ mutant exhibit significant increase of GFAP expression in somatosensory cortex. (A, B) Representative confocal images of GFAP and NeuN immunolabeling in adult somatosensory (S1) cortex. Scale bars, 100 μm. (C) Number of NeuN-positive cells was unchanged (n = 24 images from 3 mice, 24 images from 3 mice; $p = 0.0804$ by unpaired *t* test). (D) Nestin;*Braf*$^{KE/+}$ brain showed increased area of GFAP-expressing cells compared with *Braf*$^{+/+}$ brain (n = 8 images from 2 mice, 7 images from 2 mice; ***$p < 0.0001$ by unpaired *t* test). (E, F) Representative confocal images of Iba1 immunolabeling in adult S1 cortex. Scale bars, 100 μm; 10 μm. (G) Both genotypes showed comparable number of Iba1-positive cells in S1 cortex (n = 20 images from 5 mice, 19 images from 5 mice; $p = 0.5530$ by unpaired *t* test). (H) Representative immunoblot image of cortical lysates. (I) p-ERK1/2 expression was increased in mutant lysates (n = 4, 4; ***$p = 0.0005$ by unpaired *t* test). Data are expressed as the mean ± SEM.

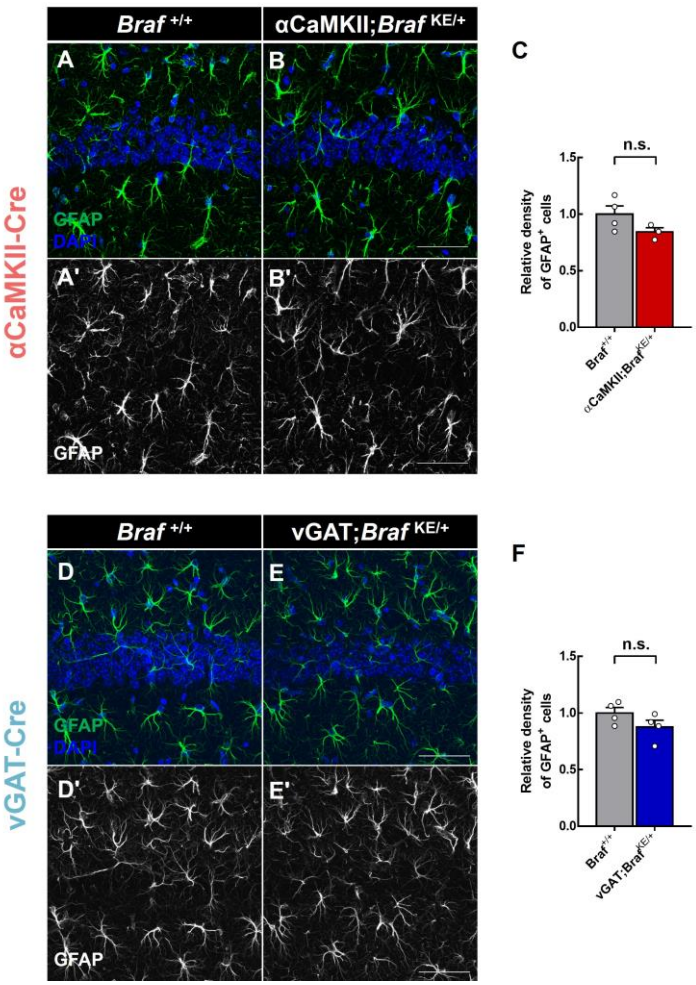

Figure 17. αCaMKII;*Braf*$^{KE/+}$ and vGAT;*Braf*$^{KE/+}$ mice do not exhibit increase of GFAP expression in hippocampus. (A, B) Representative confocal images of GFAP immunolabeling in adult αCaMKII;*Braf*$^{KE/+}$ hippocampus CA1. Scale bars, 50 μm. (C) αCaMKII;*Braf*$^{KE/+}$ brain showed unaltered number of GFAP-expressing cells compared with control brain (n = 4 images from 2 mice, 3 images from 2 mice; p = 0.1430 by unpaired t test). (D, E) Representative confocal images of GFAP immunolabeling in adult vGAT;*Braf*$^{KE/+}$ hippocampus CA1. Scale bars, 50 μm. (F) vGAT;*Braf*$^{KE/+}$ brain showed unaltered number of GFAP-expressing cells compared with control brain (n = 4 images from 2 mice, 4 images from 2 mice; p = 0.1610 by unpaired t test). Data are expressed as the mean ± SEM.

To investigate the molecular basis of BRAF K499E-induced learning and memory deficits as well as astrogliosis, I performed transcriptomic analyses by using RNA sequencing. Comparison between *Braf*$^{+/+}$ and Nestin;*Braf*$^{KE/+}$ mice revealed the differential expression of 864 genes, including 422 up-regulated and 442 down-regulated genes in the hippocampus. The results of the gene ontology analysis showed that upregulated differentially expressed genes (DEGs) were significantly enriched in 'nervous system development', 'protein binding', and 'cell junction'. The downregulated DEGs were mainly enriched in 'regulation of localization', 'protein binding', and 'cell junction'. Notably, gene set enriched analysis (GSEA) revealed that the gene set of reactive astrocytes was significantly enriched in Nestin;*Braf*$^{KE/+}$ mice compared to WT littermates (Figure 18B). In addition, hierarchical clustering heatmap for reactive astrocyte gene set showed the enriched expression of reactive astrocyte-associated genes in the hippocampus of Nestin;*Braf*$^{KE/+}$, including significantly increased genes, *H2-D1, Gfap, Aldoc, S100b, Sulf2, Vgf,* and *Gap43* (Figure 18, A and C).

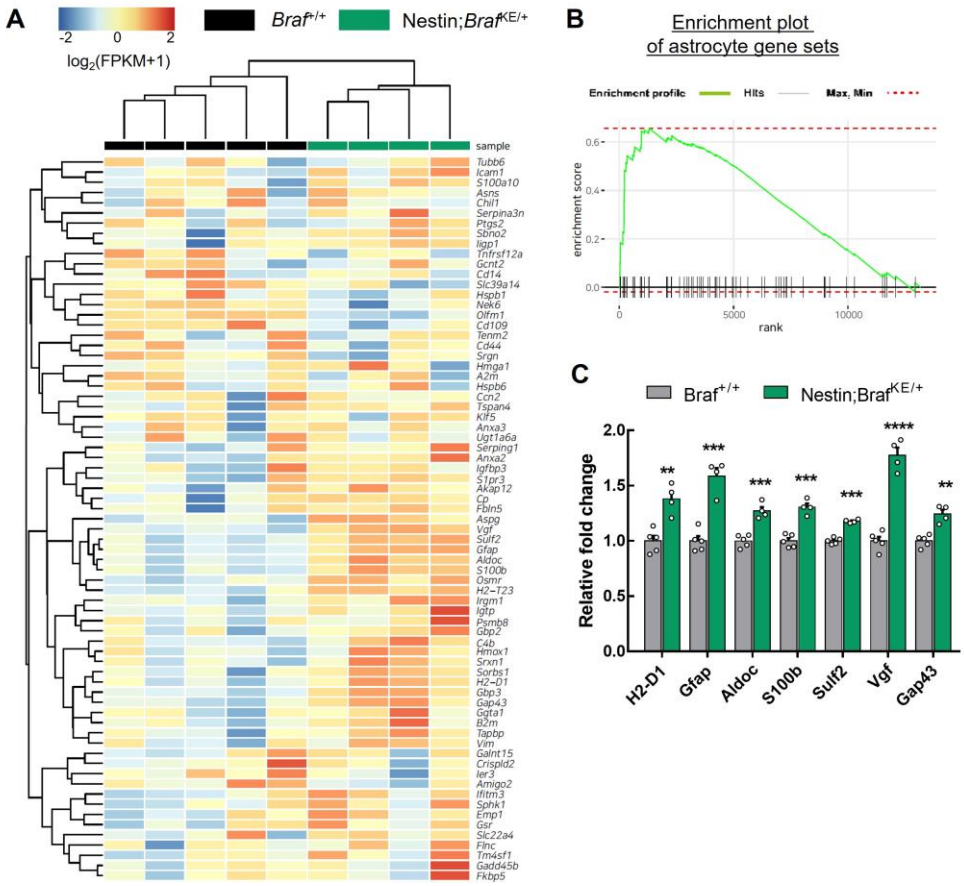

Figure 18. Transcriptome analysis of Nestin;*Braf*$^{KE/+}$ hippocampus exhibit increased expression of reactive astrocyte gene sets. (A) Hierarchical clustering plot for reactive astrocyte genes. (B) Enrichment plot of astrocyte gene sets. (C) Relative fold change of reactive astrocyte genes between *Braf*$^{+/+}$ and Nestin;*Braf*$^{KE/+}$ transcriptome (**p = 0.0020; ***p = 0.0002; ***p = 0.0003; ***p = 0.0002; ****p < 0.0001; ****p < 0.0001; ***p = 0.0009). Data are expressed as the mean ± SEM. *Soowhee Kim analyzed the RNA-seq data (Korea University).*

3. 4 BRAF-driven reactive-like astrogliosis is established during adolescent period

Proliferation is one of the specific aspect of reactive astrogliosis (198). Severe form of reactive astrocytes has proliferating potential, while the mild or moderate reactive astrocytes show hypertrophy without proliferation (183). The increased number of $GFAP^+$ astrocytes might be due to either increased proliferation or alterations in active status. We stained the slices for the proliferation marker Ki67 and found that adult Nestin;*Braf*$^{KE/+}$ mice showed comparable numbers of $Ki67^+$ cells in the hippocampus to those of WT littermates, suggesting that the mutant BRAF does not increase astrocyte proliferation (Figure 19). I then asked whether the reactive-like $GFAP^+$ astrocytes are formed during early developmental stages or progressively increased during postnatal days. At postnatal day 20, the relative areas of $GFAP^+$ cells in the mutant cortex and hippocampus were comparable compared to those in the WT littermates (Figure 20, A to F). Interestingly, at postnatal day 40, there was an increase in the relative density and area of $GFAP^+$ astrocytes in the mutant cortex and hippocampus (Figure 20, G to L). In mice, astrogenesis is initiated around embryonic day 18 and reaches the peak during postnatal day 0 and 5, followed by a gradual diminution until postnatal day 7 (199). Therefore, progressive increment of $GFAP^+$ cells between postnatal day 20 and 40 in Nestin;*Braf*$^{KE/+}$ mice is unlikely due to the aberrantly increased differentiation or proliferation of astrocytes during early development.

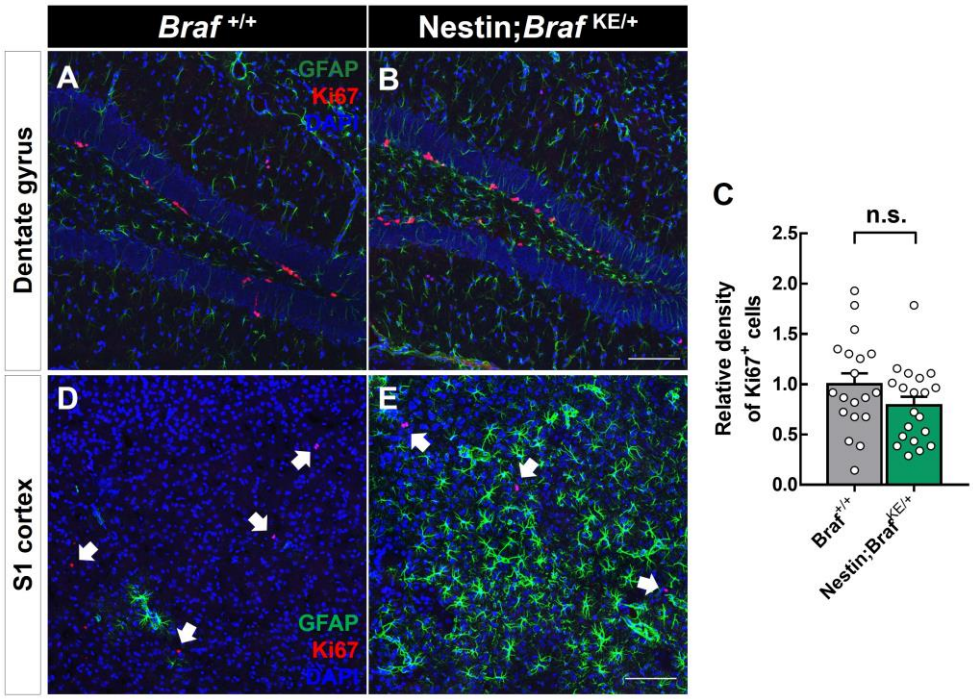

Figure 19. Increased number of GFAP-positive cells in Nestin;*Braf*$^{KE/+}$ mice was not due to astrocyte proliferation in adult period. (A, B) Representative confocal images of Ki67 and GFAP immunolabeling in the adult hippocampus dentate gyrus. Scale bars, 100 μm. (C) Nestin;*Braf*$^{KE/+}$ brain showed unaltered number of Ki67-expressing cells compared with control brain (19 images from 5 mice, 20 images from 5 mice; p = 0.1315 by unpaired t test). (D, E) Representative confocal images of Ki67 and GFAP immunolabeling in the adult S1 cortex. Scale bars, 100 μm. Ki67-immunolabeled cells in both genotypes did not overlapped with GFAP-immunolabeled cells. Data are expressed as the mean ± SEM.

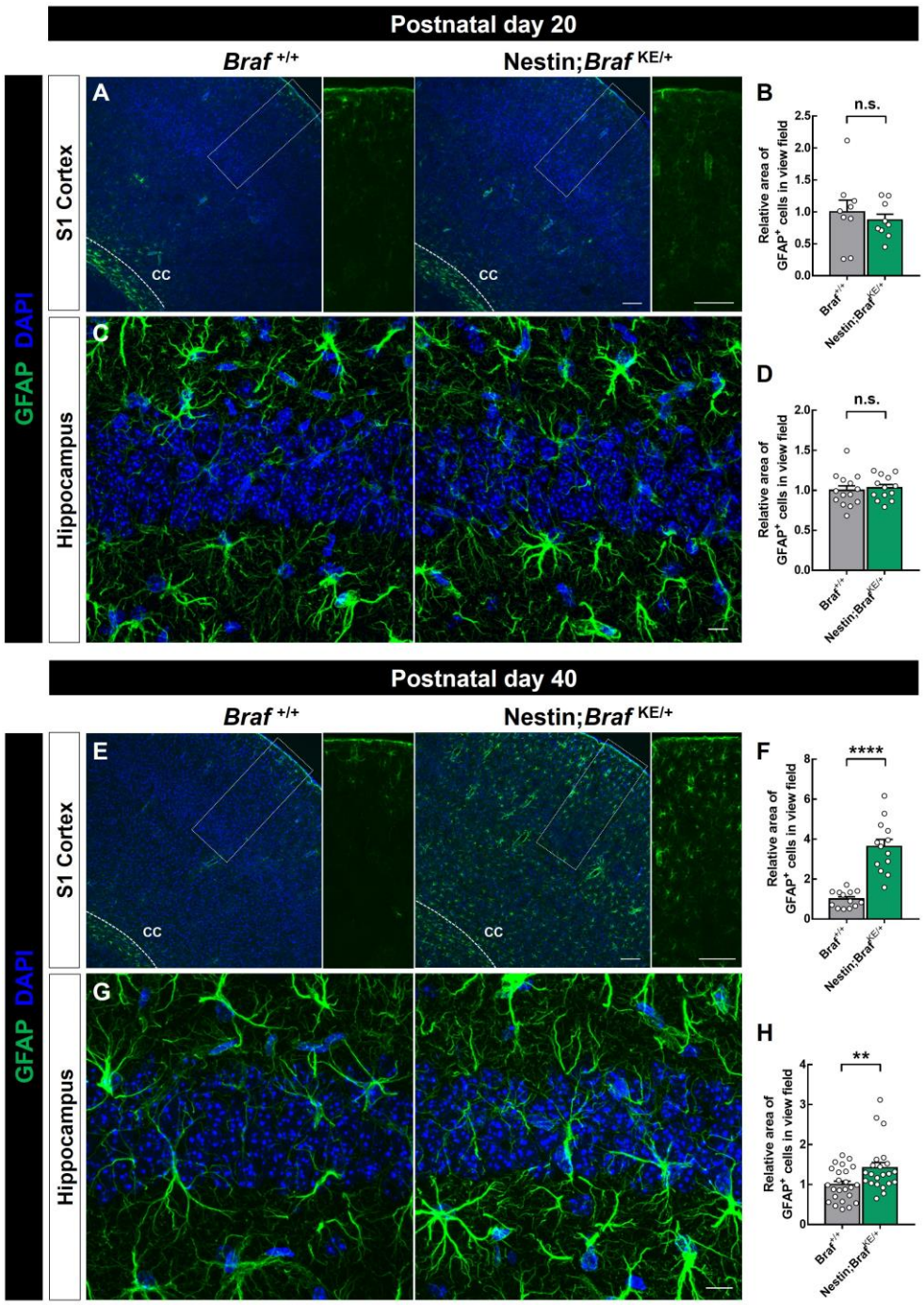

Figure 20. Nestin;*Braf*$^{KE/+}$ mice do not exhibit increase of GFAP expression in early postnatal period in hippocampus. Nestin;*Braf*$^{KE/+}$ mice do not exhibit increase of GFAP expression in early postnatal period in the hippocampus (A) Representative confocal images of GFAP

immunolabeling in Nestin;*Braf*$^{KE/+}$ S1 cortex in postnatal day 20 (P20). Scale bars, 100 μm. (B) P20 Nestin;*Braf*$^{KE/+}$ cortex showed unaltered area of GFAP-expressing cells compared with control brain (n = 9 images from 3 mice, 9 images from 3 mice; p = 0.5415 by unpaired t test). (C) Representative confocal images of GFAP immunolabeling in hippocampus CA1 in P20. Scale bars, 10 μm. (D) P20 Nestin;*Braf*$^{KE/+}$ hippocampus showed unaltered area of GFAP-expressing cells compared with control brain (n = 14 images from 3 mice, 13 images from 3 mice; p = 0.6648 by unpaired t test). (E) Representative confocal images of GFAP immunolabeling in Nestin;*Braf*$^{KE/+}$ S1 cortex in postnatal day 40 (P40). Scale bars, 100 μm. (F) P40 Nestin;*Braf*$^{KE/+}$ brain showed increased area of GFAP-expressing cells in S1 cortex compared with *Braf*$^{+/+}$ brain (n = 13 images from 4 mice, 13 images from 4 mice; ****p < 0.0001 by unpaired t test). (G) Representative confocal images of GFAP immunolabeling in Nestin;*Braf*$^{KE/+}$ hippocampus CA1 in P40. Scale bars, 10 μm. (H) P40 Nestin;*Braf*$^{KE/+}$ brain showed increased area of GFAP-expressing cells compared with P40 *Braf*$^{+/+}$ brain (n = 24 images from 4 mice, 22 images from 4 mice; **p = 0.0091 by unpaired t test). Data are expressed as the mean ± SEM.

3. 5 BRAF K499E in neural stem cell does not affect synaptic properties

To explore biochemical mechanisms that may underlie the cognitive impairment, we assessed expression levels of pre- and postsynaptic proteins from WT and Nestin;*Braf*$^{KE/+}$ hippocampus. Western blotting of whole cell lysates of hippocampus revealed no change in overall expression of synaptic proteins, GRIN1, GRIN2A, GRIN2B, GRIA1, GRIA2, synapsin, vGLUT1, PSD95, gephyrin, and vGAT in Nestin;*Braf*$^{KE/+}$ (Figure 21B). Next, I measured the enrichment of these proteins in LP1 crude synaptosomal membrane fractions. I did not find any significant change in level of synaptic proteins except GRIN1, a NMDA receptor subunit (Figure 21A).

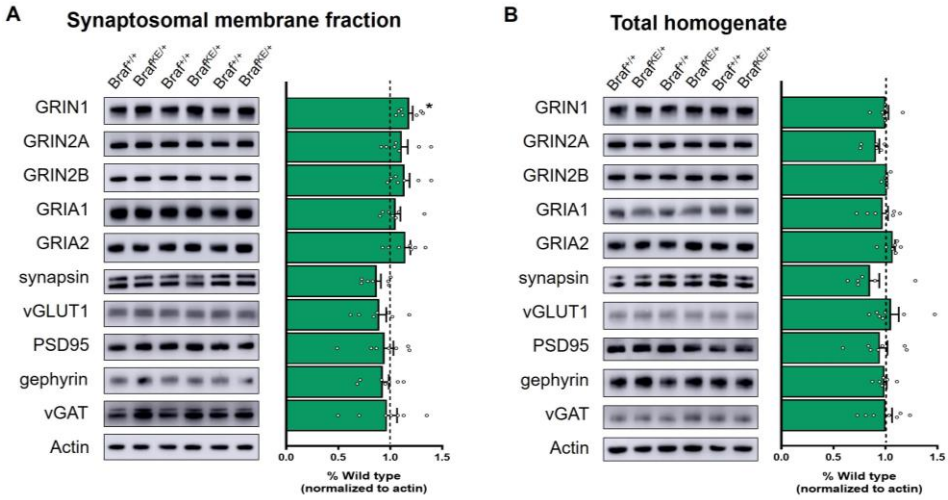

Figure 21. *Braf*^{KE} in neural stem cells does not result in significant alterations in hippocampal synaptic protein expression. (A) Representative Western blot of synaptosomal membrane fraction in *Braf*$^{+/+}$ and Nestin;*Braf*$^{KE/+}$ hippocampus, and summary of results (n = 7, 7). (B) Representative Western blot of total homogenate in *Braf*$^{+/+}$ and Nestin;*Braf*$^{KE/+}$ hippocampus, and summary of results (n = 7, 7). Each histogram shows mean ± SEM of protein levels which are normalized to actin expression. Data are expressed as the mean ± SEM.

3. 6 Braf-mediated RAS-ERK signaling dysregulation in adult astrocytes leads to learning deficits

Taking these observations into account, we hypothesized the astrocyte-specific responsibility of *Braf* in learning and memory. To evaluate the role of astrocytes in the pathophysiology of *Braf*-associated-learning deficits, I injected adeno-associated viral (AAV) vector expressing Braf KE under the control of astrocyte-specific GFAP promoter into the dorsal hippocampus of adult C57BL/6 mice (Figure 22A). At least 3 weeks were allowed for recovery between stereotaxic viral injection and behavioral test. First, I compared the performance of GFAP-BRAF KE-injected mice and control mice in the MWM task to test the effect of BRAF KE expression in astrocytes on hippocampal-dependent spatial learning and memory. GFAP-KE-injected mice took longer to reach the platform during the training session for hidden platform version of MWM compared to control mice (Figure 22B). When spatial memory was assessed after 3 days of training (probe test), GFAP-BRAF KE-injected mice did not prefered target quadrant than other three quadrants, while the control mice significantly prefered target quadrant (Figure 22, C and D). Moreover, GFAP-BRAF KE-injected mice searched farther from the target and less frequently visited the target quadrant than control mice, indicating that expressing BRAF KE in $GFAP^{+}$ astrocytes in the adult hippocampus is sufficient to produce spatial learning impairment (Figure 22, E and F).

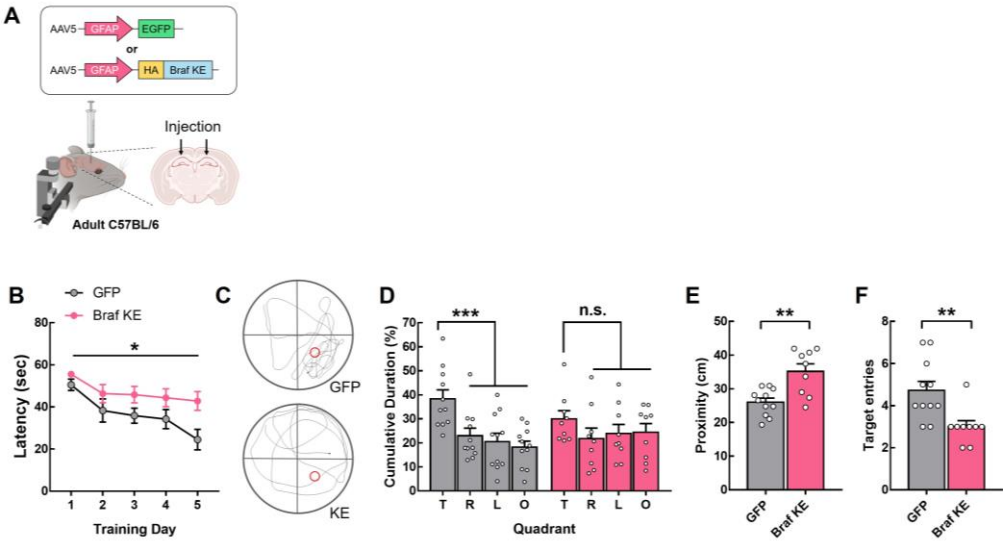

Figure 22. Adult astrocyte-specific *BRAF*^{KE} expression results in hippocampal-dependent learning deficit. (A) Schematic diagram of experiment. AAV5-GFAP-GFP or AAV5-GFAP-HA-BRAF KE virus were injected into hippocampus CA1. (B) Learning curve showing that the latencies to find the hidden platform during the MWM training trials of BRAF KE-injected mice was significantly longer than those of control (n = 11, 9; $F_{1, 18}$ = 4.643, **p* = 0.0450 by Two-way repeated measures ANOVA). (C) Representative swimming trajectory of GFP- or BRAF KE-injected mice during MWM probe test. (D) Quadrant occupancy analysis for the probe test. (n = 11, 9; $F_{3, 40}$ = 0.5299, ****p* = 0.0003 by one-way ANOVA). (E) Proximity to target platform occupied by BRAF KE-injected mice was longer than the GFP-injected mice (n = 11, 9; ***p* = 0.0014 by unpaired *t* test). (F) Number of target zone entries in the probe trial was decreased in BRAF KE-injected mice compared to GFP mice (n = 11, 9; ***p* = 0.0051 by unpaired *t* test). T, target quadrant; R, right quadrant; L, left quadrant; O, opposite quadrant. Data are expressed as the mean ± SEM.

To test the hypothesis that the spatial learning impairment caused by BRAF KE mutation is related to reactive-like astrogliosis, we immunolabeled GFAP protein on hippocampal slices. Notably, area of $GFAP^{+}$ astrocytes was significantly increased in BRAF KE-injected hippocampus (Figure 23, A and B), and I also found significant effect of BRAF KE on astrocytic complexity in Sholl anslysis which is presented by increase of intersects number (Figure 23, C to E). Moreover, the probability of detecting p-ERK1/2 was higher in BRAF-KE-expressing astrocytes than control astrocytes (Figure 23A). These results suggest that the BRAF KE expression in hippocampal astrocyte induces increase of RAS-ERK signaling activity and drives astrocytes to reactive-like state.

Last, immunoblot analyses showed expression of hemagglutinin (HA)-tagged BRAF KE in the hippocampus of mice injected with BRAF KE. p-ERK1/2 protein level was significantly increased in the hippocampus of BRAF KE-injected mice compared to controls, suggesting the BRAF KE-induced overactivation of RAS-ERK signaling pathway (Figure 23, F and G). Consistent with the results of histological immunolabeling, GFAP protein level was also increased in BRAF KE-injected hippocampus (Figure 23, F and H). Therefore, these results suggest that the astrocyte-specific BRAF KE expressing mice also showed overactivated RAS-ERK signaling-mediated reactive-like astrogliosis and hippocampal-dependent learning impairment, as did the Nestin;$Braf^{KE/+}$ mutants.

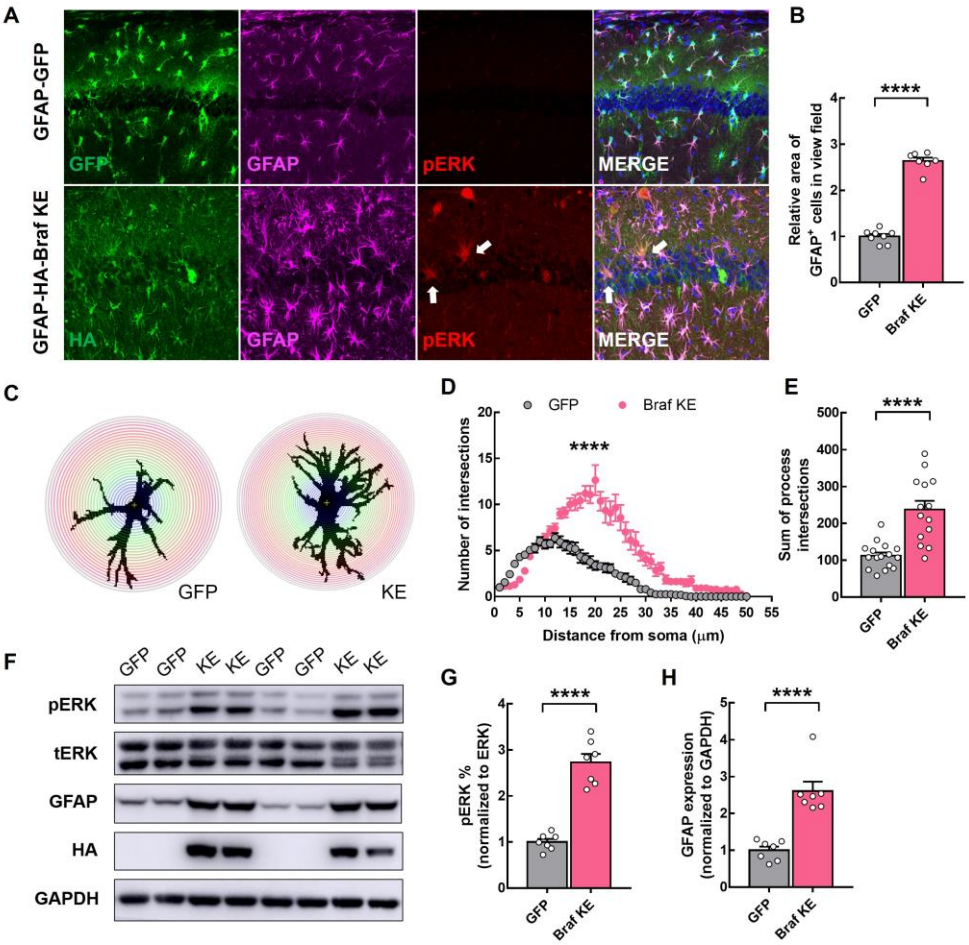

Figure 23. Adult astrocyte-specific *BRAF*^{KE} expression results in reactive-like astrogliosis in hippocampus. (A) Representative IHC images from GFAP-GFP-injected mice and GFAP-HA-BRAF KE-injected mice. Slices were immunostained for HA (green), GFAP (magenta) and p-ERK1/2 (red). Arrows indicate double labeling of GFAP and p-ERK1/2. (B) GFAP-BRAF KE brain showed increased area of GFAP-expressing cells compared with GFAP-GFP brain (n = 8 images from 3 mice, 7 images from 3 mice; ****$p < 0.0001$ by unpaired t test). (C) Representative image for Sholl analysis of an astrocyte in the stratum radiatum from the GFAP-stained image. (D) The number of process intersections and (E) the sum of process intersections of GFAP$^+$ astrocytes were increased in the stratum radiatum of GFAP-BRAF KE injected brain (16 cells from 3 mice, 14 cells from 3 mice;

****$p < 0.0001$ by repeated measures two-way ANOVA; ****$p < 0.0001$ by unpaired *t* test). (F) Representative immunoblot image of hippocampal lysates. (G) p-ERK1/2 expression normalized to total ERK1/2 expression was increased in BRAF KE hippocampal lysates (n = 7, 7; ****$p < 0.0001$ by unpaired *t* test). (H) GFAP expression normalized to GAPDH expression was increased in BRAF KE hippocampal lysates (n = 7, 7; ****$p < 0.0001$ by unpaired *t* test). Data are expressed as the mean ± SEM.

Previous study has shown that the high titer transduction of astrocytes with AAV induces reactive astrocytosis (200). Therefore, we took advantage of targeted Braf muation which is expressed under the condition of tamoxifen-induced CreER^{T2} and LoxP sites to avoid the confound effect of stereotaxic viral injection on reactive astrogliosis. I intraperitoneally injected 100 mg/kg of tamoxifen into GFAP;*Braf*$^{KE/+}$ mice and littermate controls (GFAP-CreER^{T2}) for 5 consecutive days to specifically express *Braf*^{K499E} in adult astrocytes (Figure 24A). To determine whether the adult astrocyte-specific *Braf*^{K499E} affects behavior, I investigated basal locomotive activity of mice as well as learning and memory. In open field test, both genotype of mice displayed normal locomotive activity by presenting comparable level of average velocity and total distance moved (data not shown). As endogenous GFAP expression is prominent in adult hippocampal astrocyte rather than cortical astrocyte, I tested hippocampal learning of GFAP;*Braf*$^{KE/+}$ mice. In MWM, mutant mice showed decreased cumulative occupancy in the quadrant where the platform was located without change in swimming speed (Figure 24, B to D). These results demonstrate that the adult astrocyte-specific *Braf*^{K499E} impairs hippocampal-dependent memory of mice. Next, to examine whether the Braf KE in astrocytes autonomously affects astrocyte itself and induces hypertrophy, I measured GFAP expression. GFAP;*Braf*$^{KE/+}$ mice exhibited increased area of GFAP^{+} cells in hippocampus CA1 after 8 weeks of tamoxifen injection (Figure 24, E to G). The detailed Sholl analysis of individual GFAP^{+} astrocytes showed that the number and sum of intersects were significantly increased in GFAP;*Braf*$^{KE/+}$ mice (Figure 24, I to K). Furthermore, p-ERK1/2 expression was significantly enhanced in GFAP;*Braf*$^{KE/+}$ hippocampal lysates compared to those of control group (Figure 24H). Therefore, these results suggest that the *Braf*^{K499E} expression in astrocytes is sufficient to lead spatial learning impairment which is accompanied by reactive-like astrogliosis as already confirmed in viral vector-injected mice study (Figure 22, 23). Consequently,

two types of astrocyte-specific manipulations provided compelling evidences that the *Braf*-mediated functional alteration of astrocyte is critically involved in the learning impairment associated to RASopathy.

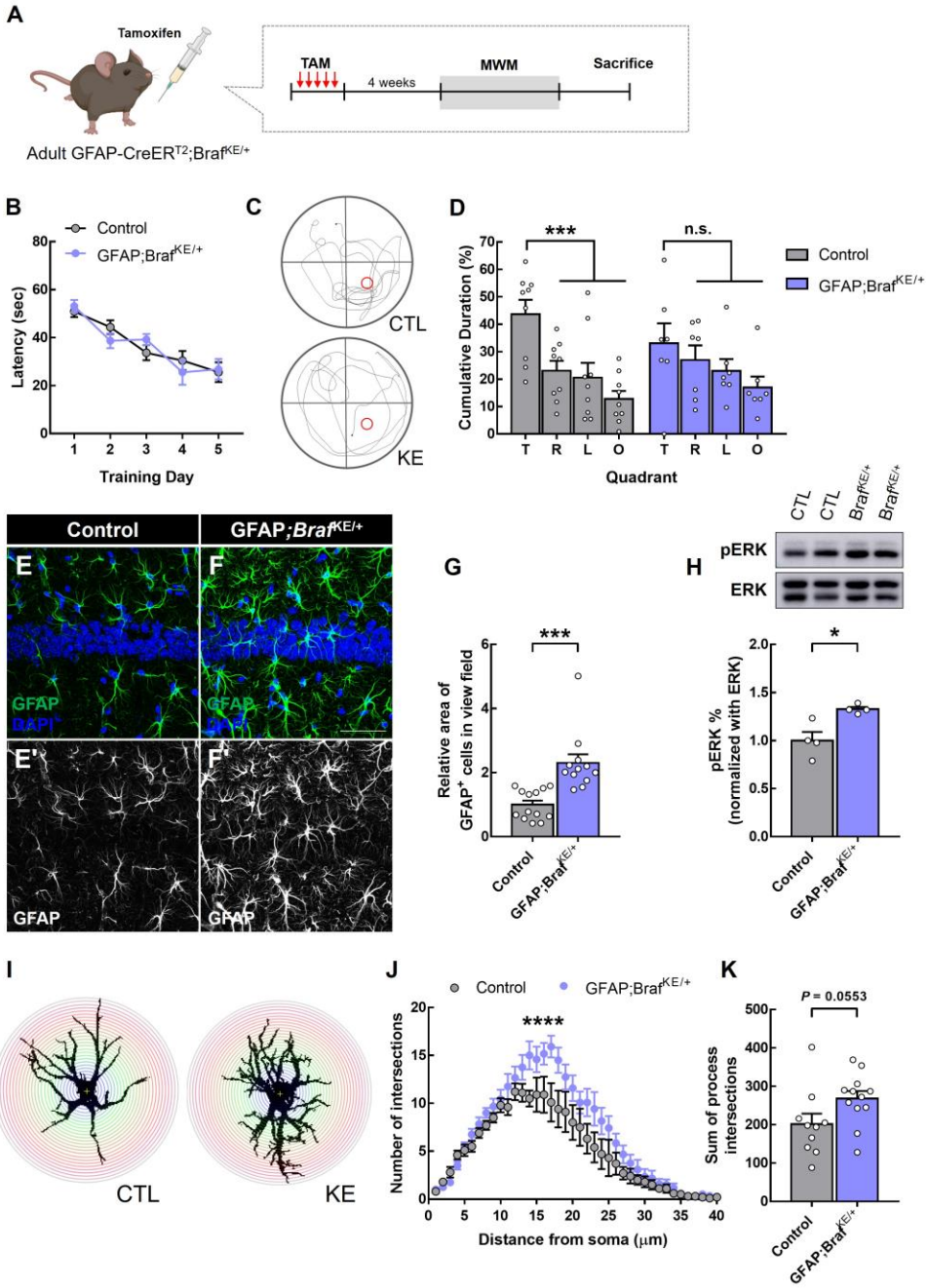

Figure 24. Adult astrocyte-specific *Braf*^{KE} induces reactive astrocytes and hippocampal-dependent learning deficit. (A) Schematic diagram of experiment. Tamoxifen (100 mg/kg, i.p.) was administered once each day for 5 consecutive days to induce Braf K499E expression in adult astrocytes of GFAP-CreER^{T2} and GFAP;*Braf*$^{KE/+}$ mice. (B) Learning curve showing

that the latency to find the hidden platform during the MWM training trials was comparable between control and GFAP;*Braf*$^{KE/+}$ (n = 9, 7). (C) Representative swimming trajectory of WT and αCaMKII;*Braf*$^{KE/+}$ mice in the probe trial of MWM. Platform position during the training trials is indicated by the red-colored circle. (D) Quadrant occupancy analysis for the probe test (n = 9, 7; $F_{3, 32} = 8.836$, ***$p = 0.0002$, $F_{3, 24} = 1.575$, $p = 0.2213$ by one-way ANOVA). (E, F) Representative confocal images of GFAP (green) immunolabeling in adult hippocampus CA1. Scale bars, 50 μm. (G) GFAP;*Braf*$^{KE/+}$ brain showed increased area of GFAP-expressing cells compared with control brain (n = 13 images from 3 mice, 12 images from 3 mice; ***$p = 0.0002$ by unpaired *t* test). (H) Representative image for Sholl analysis of an astrocyte in the stratum radiatum from the GFAP-stained image. (I) The number of process intersections and (J) the sum of process intersections of GFAP^{+} astrocytes were increased in the stratum radiatum of GFAP;*Braf*$^{KE/+}$ mice (10 cells from 3 mice, 12 cells from 3 mice; ****$p < 0.0001$ by two-way ANOVA; $p = 0.0553$ by unpaired *t* test). (K) Representative immunoblot image of hippocampal lysates. p-ERK1/2 expression were increased in GFAP;*Braf*$^{KE/+}$ hippocampal lysates (n = 4, 4; *$p = 0.0131$ by unpaired *t* test). Data are expressed as the mean ± SEM.

3. 7 BRAF KE-expressing astrocyte showed hyperactive calcium fluctuation which is normalized by attenuation of RAS-ERK signaling activity

Unlike neurons, astrocytes do not generate action potentials, but they exhibit spontaneous and evoked intracellular Ca^{2+} concentration increases, which indicate a form of astrocyte excitability (201). Astrocytic Ca^{2+} signaling is reported to have a direct impact on neural circuit modulation by mediating gliotransmitter release, synaptic plasticity and integrity (202, 203). Therefore, it is no wonder that the aberrant regulation of Ca^{2+} homeostasis in astrocytes is implicated in pathophysiology. For instance, it is known that the reactive astrocytes which are induced by inflammatory response produce abnormally increased spontaneous calcium oscillations such as in the case of AD (204-206). However, there is a large variation in Ca^{2+} dynamics of astrocytes in diverse pathological models, indicating various underlying mechanisms for abnormal Ca^{2+} signalings that are dependent on the conditions. Moreover, it remains largely unknown how the astrocyte Ca^{2+} signaling is regulated under noninflammatory condition and whether RAS-ERK signaling is implicated in astrocytic Ca^{2+} signaling and functional impact.

Therefore, I set out to test the presumption that Ca^{2+} fluctuations are altered in BRAF KE-expressing astrocytes. I used AAV5 and the minimal astrocyte-specific gfaABC1D promoter to express fast genetically encoded cytosolic Ca^{2+} indicators, GCaMP6f in astrocytes located in the dorsal CA1 region of the AAV-GFAP-BRAF KE-injected adult mice (Figure 25A). To analyze Ca^{2+} fluctuation, I harvested hippocampal slices 3 weeks after *in vivo* virus microinjections, and imaged fluorescence fluctuations with microscopy from mCherry control and BRAF KE-injected mice. GCaMP6f imaging revealed a significantly increased Ca^{2+} fluctuation peak frequency in each region of interest (ROIs) of BRAF KE-expressing astrocytes (Figure 25, B and C). Thus, this result indicates that the BRAF KE expression lead

to aberrantly hyperactive Ca^{2+} signaling in hippocampal astrocytes.

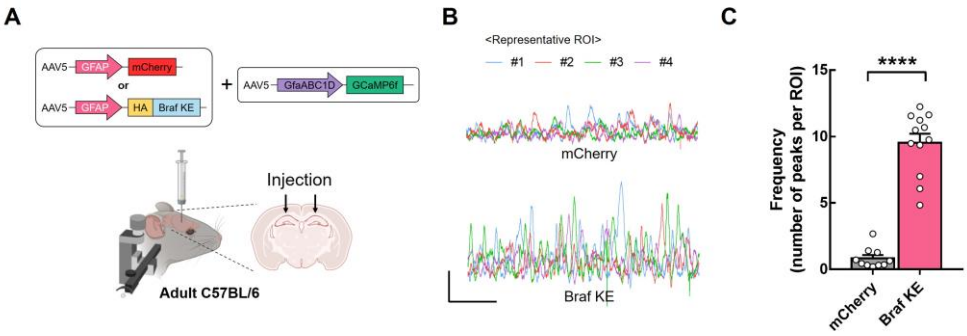

Figure 25. BRAF K499E induces increase of calcium fluctuation in hippocampal astrocytes. (A) Schematic illustrating of the experimental approach. GFAP-mCherry or GFAP-HA-BRAF KE, and gfaABC1D-GCaMP6f virus were injected into hippocampus CA1. (B) Representative traces showing the enhancement in fluorescence of GFAP-BRAF KE-expressing astrocytes. Scale bars, 2 dF/F and 1 minute. (C) The average number of peaks per ROI was significantly increased in GFAP-BRAF KE-injected mice compared to GFAP-mCherry-injected mice (n = 10 images from 5 mice, 12 images from 5 mice; ****$p < 0.0001$ by unpaired *t* test). Data are expressed as the mean ± SEM.

Next, we investigated whether the hyperactive Ca^{2+} signaling in BRAF KE astrocyte is dependent on RAS-ERK signaling activity. To this end, dominant negative mutation K97M of mitogen-activated protein kinase kinase 1 (MEK1), the downstream effector of RAF as well as the oligate upstream activator of ERK, was used. First of all, I transfected human embryonic kidney (HEK) 293T cells with BRAF KE and dominant negative MEK1 (dnMEK1) and measured p-ERK1/2 expression in cell lysates to test whether the dnMEK1 sufficiently alleviates BRAF KE-induced overactivation of RAS-ERK signaling (Figure 26A). Notably, p-ERK1/2 expression of HEK 293T cells cotransfected with BRAF KE and dnMEK1 was significantly lower than in those transfected with BRAF KE only, presenting comparable level with those of BRAF WT-transfected cells (Figure 26B). These results confirmed that the coexpressed dnMEK1 is sufficient to reduce BRAF KE-induced overactivation of RAS-ERK signaling activity.

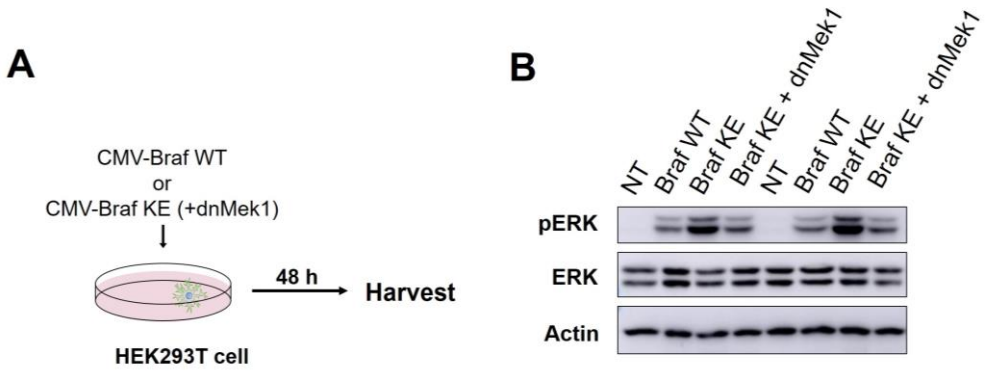

Figure 26. The effect of MEK1 K97M on the BRAF K499E-induced RAS-ERK signaling overactivation. (A) The schematic diagram of experiment. HEK293T cells were transfected with CMV-BRAF WT, CMV-BRAF KE, or CMV-BRAF KE with CMV-MEK1 K97M. (B) Representative Western blot for assessing the RAS-ERK signaling activity in HEK293T cells for p-ERK1/2, total ERK1/2 and actin in cell lysates from the transfected HEK293T cells described in (A). p-ERK1/2 expression was increased in BRAF K499E-transfected cell lysates. Cotransfection of MEK1 K97M with BRAF K499E restored BRAF K499E-induced p-ERK1/2 increase. NT, not transfected;

To verify whether dnMEK1 restores BRAF KE-induced RAS-ERK signaling overactivation and aberrantly hyperactive Ca^{2+} fluctuation *in vivo*, we microinjected AAVs containing astrocyte-specific BRAF WT or BRAF KE, with astrocyte-specific dnMEK1 and GCaMP6f in to dorsal CA1 of adult C57BL6 mice (Figure 27A). First, immunoblot analyses showed significantly increased p-ERK1/2 and GFAP protein level in BRAF KE-expressing hippocampi compared to BRAF WT-expressing hippocampi (Figure 27, B to D). Notably, coexpression of dnMek1 with BRAF KE was able to almost completely restore both increased p-ERK1/2 and GFAP expression to similar level of BRAF WT-expressing hippocampi (Figure 27, B to D). Coexpressing dnMEK1 with BRAF WT in astrocytes did not have noticeable effect. Next, I harvested hippocampal slices 3 weeks after *in vivo* microinjection of virus, and imaged Ca^{2+} fluctuations in four groups of mice via two-photon (2P) confocal microscopy (Figure 27E). 2P imaging revealed that the coexpression of dnMEK1 restore an increased Ca^{2+} fluctuation peak frequency in each region of interest (ROIs) of BRAF KE-expressing astrocytes with no impact on BRAF WT-exressing astrocytes (Figure 27, F and G). These observations indicate that the overactivation of astrocytic RAS-ERK signaling is sufficient to elevate astrocyte Ca^{2+} fluctuation without the involvement of exogenous stimuli.

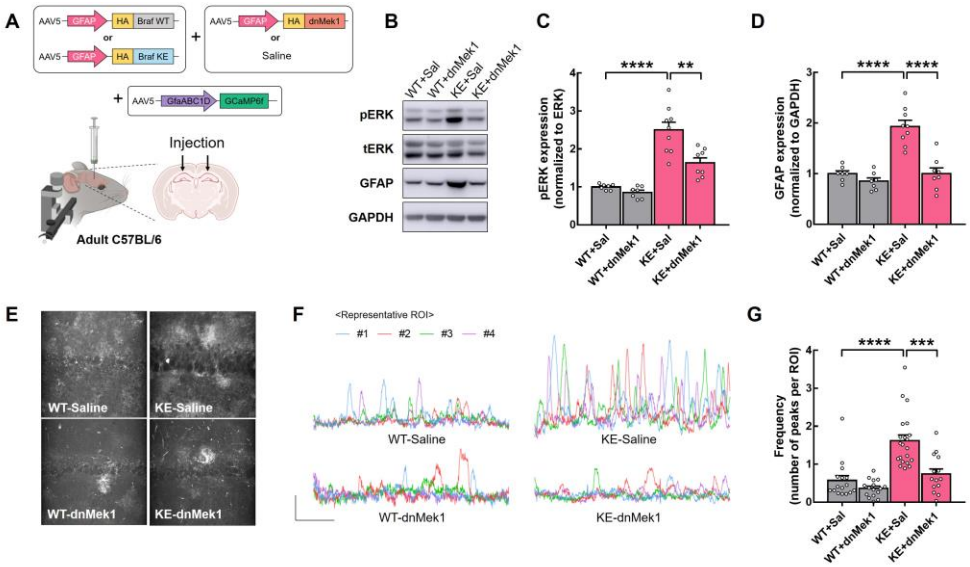

Figure 27. BRAF K499E-induced hyperactive calcium fluctuation in hippocampal astrocytes is depend on the RAS-ERK signaling activity. (A) Schematic illustrating of the experimental approach. GFAP-HA-BRAF WT or GFAP-HA-BRAF KE, GFAP-HA-dnMEK1 and gfaABC1D-GCaMP6f virus were injected into hippocampus CA1. (B) Representative Western blot in hippocampal lysates for p-ERK1/2, total ERK1/2, GFAP and GAPDH. (C) p-ERK1/2 expression which is normalized to total ERK1/2 expression was significantly increased in BRAF KE-injected hippocampi compared to BRAF WT-injected hippocampi (n = 7, 9; ****$p < 0.0001$ by unpaired *t* test). Coinjection of GFAP-dnMEK1 virus with GFAP-BRAF KE virus attenuated the BRAF KE-induced p-ERK1/2 increase (n = 9, 8; **$p = 0.0035$ by unpaired *t* test). (D) GFAP expression which is normalized to GAPDH expression was significantly increased in BRAF KE-injected hippocampi compared to BRAF WT-injected hippocampi (n = 7, 9; ****$p < 0.0001$ by unpaired *t* test). Coinjection of GFAP-dnMEK1 virus with GFAP-BRAF KE virus attenuated the BRAF KE-induced GFAP increase (n = 9, 8; ****$p < 0.0001$ by unpaired *t* test). (E) Representative images of Ca^{2+} fluctuations measured in hippocampal astrocytes from GFAP-BRAF WT or GFAP-BRAF KE virus-injected mice. (F) Representative traces showing the

enhancement in fluorescence of GFAP-BRAF KE-expressing astrocytes which is attenuated by coinjection of GFAP-dnMEK1 virus. Scale bars, dF/F and 1 minute. (G) The average number of peaks per ROI was significantly increased in GFAP-BRAF KE-injected mice compared to GFAP-BRAF WT-injected mice (n = 16 images from 4 mice, 21 images from 5 mice; ****$p < 0.0001$ by unpaired *t* test). Coinjection of GFAP-dnMEK1 with GFAP-BRAF KE attenuated BRAF KE-induced enhancement of Ca^{2+} fluctuation (n = 21 images from 5 mice, 14 images from 4 mice; ***$p = 0.0003$ by unpaired *t* test). Data are expressed as the mean ± SEM.

3. 8 Hyperactive calcium fluctuation in Nestin;*Braf*$^{KE/+}$ astrocytes were attenuated by GFAP-specific dnMEK1 injection

Next, we investigated whether the Nestin;*Braf*$^{KE/+}$ mice also display hyperactive Ca^{2+} fluctuations in astrocytes. To verify astroglial Ca^{2+} signal, we injected gfaABC1D-GCaMP6f virus into dorsal CA1 region of the adult Nestin;*Braf*$^{KE/+}$ mice and littermates (Figure 28A). 3 weeks after in vivo virus microinjections, we harvested hippocampal slices and imaged fluorescence fluctuations with 2P microscopy from Nestin;*Braf*$^{KE/+}$ and littermates. GCaMP6f imaging revealed a significantly increased Ca^{2+} fluctuation peak frequency in each region of interest (ROIs) of Nestin;*Braf*$^{KE/+}$ astrocytes compared to *Braf*$^{+/+}$ astrocytes (Figure 28, E to G). Therefore, this result indicates that in accordance with BRAF KE virus-injected animals, Nestin;*Braf*$^{KE/+}$ mutant mice also exhibit aberrantly hyperactive Ca^{2+} signaling in hippocampal astrocytes.

To test whether dnMEK1 is also able to restores hyperactive Ca^{2+} fluctuation in mutant mice, we microinjected astrocyte-specific dnMEK1 and GCaMP6f into dorsal CA1 of adult Nestin;*Braf*$^{KE/+}$ mice and littermates. First, Western blot analyses showed significantly increased p-ERK1/2 and GFAP protein level in Nestin;*Braf*$^{KE/+}$ hippocampi compared to *Braf*$^{+/+}$ hippocampi (Figure 28, B to D). Notably, expression of GFAP-dnMEK1 was able to attenuate p-ERK1/2 expression. Since dnMEK1 is expressed only in GFAP-specific manner, p-ERK1/2 expression in Nestin;*Braf*$^{KE/+}$ with dnMEK1 virus did not decrease by those of WT, but significantly decreased compared to Nestin;*Braf*$^{KE/+}$ with control virus (Figure 28, B and C). Interestingly, dnMEK1 injection increased GFAP expression in Nestin;*Braf*$^{KE/+}$ mice compared to control virus-injected Nestin;*Braf*$^{KE/+}$ mice (Figure 28, B and D). Next, we harvested hippocampal slices 3 weeks after *in vivo* microinjection of virus, and imaged Ca^{2+} fluctuations in four groups of mice via two-photon (2P) confocal microscopy (Figure 28E). 2P imaging revealed that the expression of GFAP-dnMEK1 restore an

increased Ca^{2+} fluctuation peak frequency in each region of interest (ROIs) of Nestin;*Braf*$^{KE/+}$ astrocytes (Figure 28, F and G). This finding suggests that attenuating overactivation of RAS-ERK signaling in adult period is able to restore the aberrant astrocyte property due to *Braf* mutation that had been expressed since developmental period.

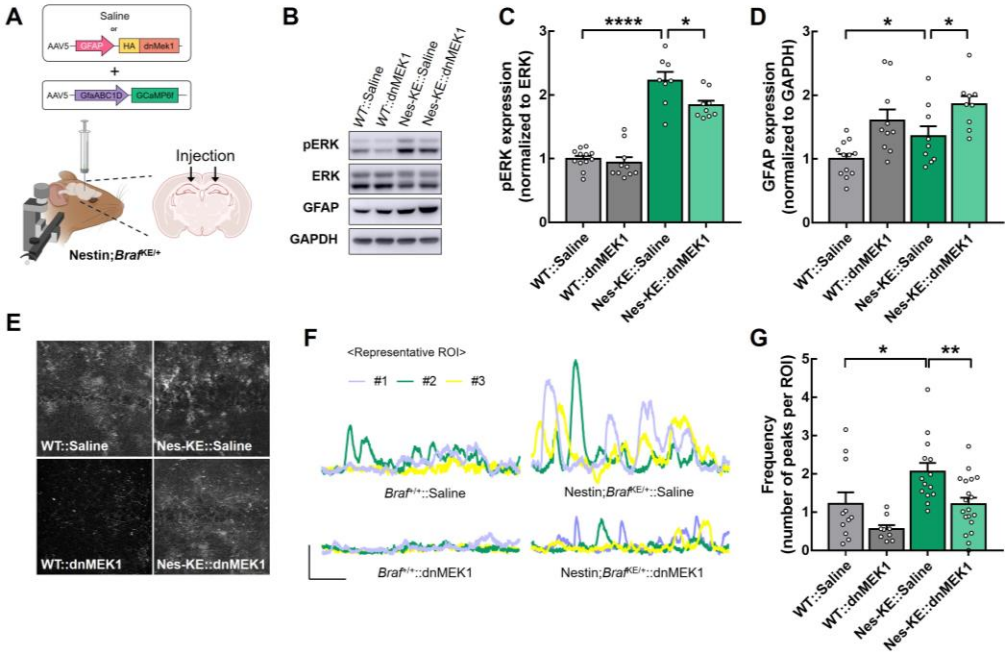

Figure 28. Astrocyte-specific expression of dominant negative MEK1 mutant restores hyperactive astroglial Ca^{2+} fluctuation in Nestin;*Braf*$^{KE/+}$ mice. (A) Schematic illustrating of the experimental approach. GFAP-HA-dnMEK1 and gfaABC1D-GCaMP6f virus were injected into hippocampus CA1 of adult Nestin;*Braf*$^{KE/+}$ mice. (B) Representative Western blot in hippocampal lysates for p-ERK1/2, total ERK1/2, GFAP and GAPDH. (C) p-ERK1/2 expression which is normalized to total ERK1/2 expression was significantly increased in Nestin;*Braf*$^{KE/+}$ hippocampi compared to *Braf*$^{+/+}$ hippocampi (n = 12, 8; ****$p < 0.0001$ by unpaired *t* test). Injection of GFAP-dnMEK1 virus attenuated the BRAF KE-induced p-ERK1/2 increase (n = 8, 9; *$p = 0.0198$ by unpaired *t* test). (D) GFAP expression which is normalized to GAPDH expression was significantly increased in Nestin;*Braf*$^{KE/+}$ hippocampi compared to *Braf*$^{+/+}$ hippocampi (n = 12, 9 *$p = 0.0431$ by unpaired *t* test). Injection of GFAP-dnMEK1 virus elevated GFAP expression in Nestin;*Braf*$^{KE/+}$, compared to control-injected Nestin;*Braf*$^{KE/+}$ mice (n = 9, 9; *$p = 0.0256$ by unpaired *t* test). (E) Representative images of Ca^{2+} fluctuations measured in

hippocampal astrocytes from *Braf*$^{+/+}$ and Nestin;*Braf*$^{KE/+}$ mice. (F) Representative traces showing the enhancement in fluorescence of Nestin;*Braf*$^{KE/+}$ astrocytes which is attenuated by injection of GFAP-dnMEK1 virus. Scale bars, 1 minute. (G) The average number of peaks per ROI was significantly increased in Nestin;*Braf*$^{KE/+}$ mice compared to *Braf*$^{+/+}$ mice (n = 11 images from 4 mice, 14 images from 4 mice; $*p = 0.0339$ by unpaired *t* test). Injection of GFAP-dnMEK1 attenuated BRAF KE-induced enhancement of Ca^{2+} fluctuation (n = 14 images from 4 mice, 19 images from 55 mice; $**p = 0.0043$ by unpaired *t* test). Data are expressed as the mean ± SEM.

3. 9 The learning deficits of Nestin;*Braf*$^{KE/+}$ mice can be reversed by normalizing RAS-ERK signaling solely in astrocytes

Finally, we verified whether attenuating overactivated RAS-ERK signaling solitarily in astrocytes could reverse the impaired spatial learning and memory of Nestin;*Braf*$^{KE/+}$ mice. To restore Braf KE-induced RAS-ERK signaling overactivation in astrocyte-specific manner, I injected AAV vector containing GFAP-dnMEK1 into dorsal hippocampus of adult Nestin;*Braf*$^{KE/+}$ mice (Figure 29A). I then tested spatial memory of AAV-infused Nestin;*Braf*$^{KE/+}$ mice in MWM test. Interestingly, Nestin;*Braf*$^{KE/+}$ mice expressing GFAP-dnMEK1 virus spent significantly longer time in the target quadrant in the probe test 1, indicating comparable performance to control group (*Braf*$^{+/+}$ mice with control virus), while Nestin;*Braf*$^{KE/+}$ mice expressing control virus did not (Figure 29, B and C). Moreover, Nestin;*Braf*$^{KE/+}$ mice expressing GFAP-dnMEK1 virus swam closer from the position in which the platform was located during the training sessions, and visited target quadrant frequently compared to Nestin;*Braf*$^{KE/+}$ mice expressing control virus (Figure 29, D and E). The rescue effect of GFAP-dnMEK1 in Nestin;*Braf*$^{KE/+}$ mice was consistently observed in probe test 2, while GFAP-dnMEK1 virus in *Braf*$^{+/+}$ mice inversely disrupted the task performances, indicating suitable activity of RAS-ERK signaling in adult astrocytes are critical for learning and memory (Figure 29, F to I). In conclusion, the findings that the learnind deficits of Nestin;*Braf*$^{KE/+}$ mice can be reversed with astrocyte-specific RAS-ERK signaling attenuation suggest the prominent role of astrocyte in *Braf*-related learning deficits, and shows that these learning deficits are reversible in adult period.

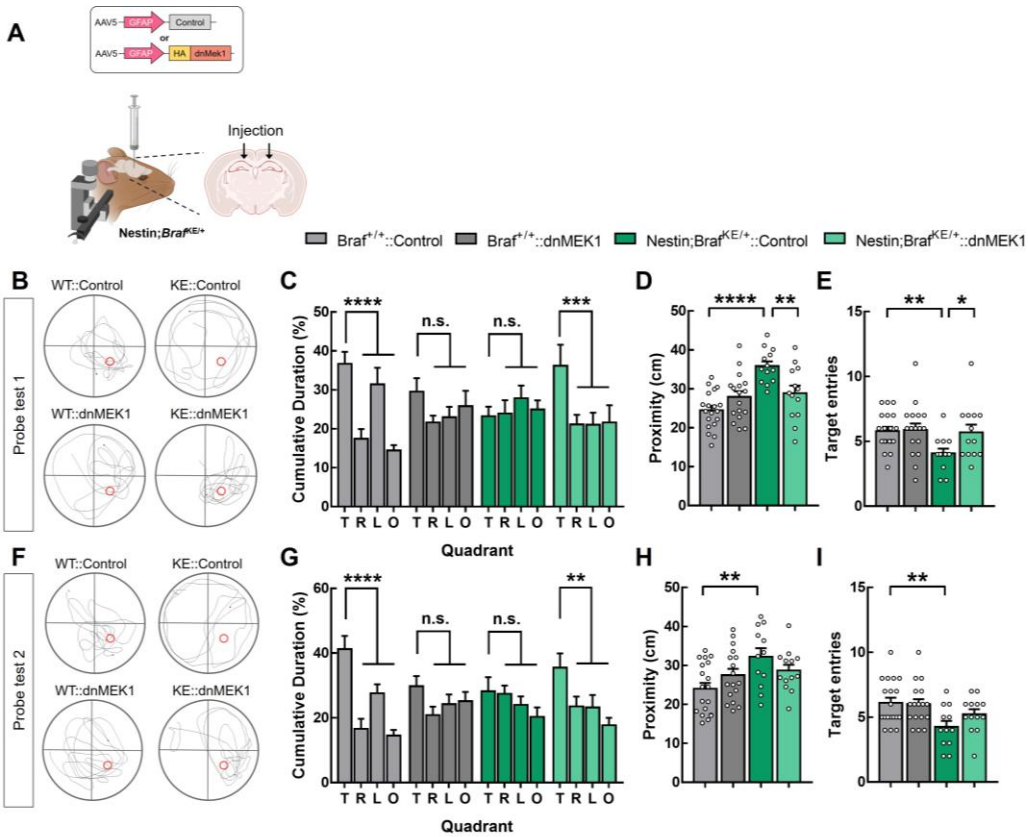

Figure 29. Astrocyte-specific expression of dominant negative Mek1 mutant restores hippocampal learning deficits in adult Nestin;*Braf*$^{KE/+}$ mice. (A) Schematic illustrating of the experimental approach. GFAP-control (mcherry or GFP) or GFAP-HA-dnMek1 virus were injected into hippocampus CA1 of Nestin;*Braf*$^{KE/+}$ mice. (B) Representative swimming trajectory of WT and Nestin;*Braf*$^{KE/+}$ mice in the probe test 1 of MWM. Platform position during the training trials is indicated by the red-colored circle. (C) *Braf*$^{KE/+}$ mice with control virus and Nestin;*Braf*$^{KE/+}$ mice with GFAP-dnMEK1 virus significantly prefered target quadrant compared to other quadrants (n = 19, 17, 13, 13; $F_{3, 72} = 12.99$, ****$p < 0.0001$; $F_{3, 64} = 1.294$, $p = 0.2842$; $F_{3, 48} = 0.4916$, $p = 0.6898$; $F_{3, 48} = 6.589$, ***$p = 0.0008$ by one-way ANOVA). (D) Proximity during the probe test 1 was significantly increased in Nestin;*Braf*$^{KE/+}$ mice with control virus compared to *Braf*$^{KE/+}$ mice with control virus. Injection of GFAP-dnMEK1 virus

significantly decreased proximity of Nestin;*Braf*$^{KE/+}$ mice (n = 19, 17, 13, 13; ****p < 0.0001; **p = 0.0056 by unpaired t test). (E) Number of target zone entries during the probe test 1 was significantly decreased in Nestin;*Braf*$^{KE/+}$ mice with control virus compared to *Braf*$^{KE/+}$ mice with control virus. Injection of GFAP-dnMEK1 virus significantly increased target entries of Nestin;*Braf*$^{KE/+}$ mice (n = 19, 17, 13, 13; **p = 0.0018; *p = 0.0292). (F) Representative swimming trajectory of WT and Nestin;*Braf*$^{KE/+}$ mice in the probe test 2 of MWM. Platform position during the training trials is indicated by the red-colored circle. (G) *Braf*$^{KE/+}$ mice with control virus and Nestin;*Braf*$^{KE/+}$ mice with GFAP-dnMEK1 virus significantly prefered target quadrant compared to other quadrants (n = 19, 17, 12, 13; $F_{3, 72}$ = 16.12, ****p < 0.0001; $F_{3, 64}$ = 1.6, p = 0.1981; $F_{3, 44}$ = 1.28, p = 0.2929; $F_{3, 48}$ = 4.611, **p = 0.0065 by one-way ANOVA). (H) Proximity during the probe test 2 was significantly increased in Nestin;*Braf*$^{KE/+}$ mice with control virus compared to *Braf*$^{KE/+}$ mice with control virus (n = 19, 17, 12, 13; **p = 0.0035 by unpaired t test). Injection of GFAP-dnMEK1 virus tended to decrease proximity of Nestin;*Braf*$^{KE/+}$ mice. (I) Number of target zone entries during the probe test 2 was significantly decreased in Nestin;*Braf*$^{KE/+}$ mice with control virus compared to *Braf*$^{KE/+}$ mice with control virus. Injection of GFAP-dnMEK1 virus tended to increase target entries of Nestin;*Braf*$^{KE/+}$ mice (n = 19, 17, 12, 13; **p = 0.0056 by unpaired t test). Data are expressed as the mean ± SEM.

Discussion

In the present study, I have demonstrated that the overactive RAS-ERK signaling induced by RASopathy-associated *Braf*^{KE} mutation results in aberrant astrocytic properties such as reactive-like astrogliosis and hyperactive intracellular Ca^{2+} signaling, and impairs hippocampal memory. First, I found that the *Braf*^{KE} mutation in Nestin^{+} neural stem cells, but not in αCaMKII^{+} excitatory or vGAT^{+} inhibitory neurons, resulted in hippocampal learning deficits in mice. Then, I observed *Braf*^{KE}-induced reactive-like astrogliosis in multiple models including mice and human cortical organoids. *Braf*^{KE} mutation in neural stem cells induced reactive-like astrogliosis which is presented by hypertrophy and upregulated reactive transcripts in mice, and BRAF KE-containing human forebrain organoid displayed specific aspects of reactive-like astrogliosis with enormous enhancement of RAS-ERK signaling activity in astrocytic populations. Notably, *Braf*^{KE} variant even in adult astrocytes is sufficient to induce an impairment of hippocampal learning and memory which is accompanied by hypertrophy and hyperactive Ca^{2+} fluctuations in astrocytes. Eventually, these impairments were restored by astrocyte-specific attenuation of RAS-ERK signaling activity, suggesting that astrocyte is the cell type that is responsible for the cognitive impairment.

Although RAS-ERK signaling is a ubiquitous signaling pathway, a number of studies have reported that the dysregulation of this signaling has distinct effects on each cell type in central nervous system. For example, it has been shown that expressing Noonan syndrome-associated SHP2 mutant only in excitatory neurons, but not in inhibitory neurons, resulted in cognitive impairments (122). On the other hand, haploinsufficiency of *Nf1* enhanced RAS-ERK signaling primarily in GABAergic neurons (80, 84). Similarly, mice with Noonan syndrome-associated *KRAS* mutation displayed distinct cellular and physiological phenotypes specific to each neuronal cell type (99, 174). The results showing that *Braf*^{KE} in excitatory or in inhibitory neurons

did not induce learning deficits or reactive-like astrogliosis demonstrate that astrocytes are responsible for *Braf*-mediated cognitive impairments in Nestin;*Braf*$^{KE/+}$ mice. Since the Nestin promotor drives expression of mutant *Braf* in most cell types in central and peripheral nervous systems, possibility for involvements of other cell types cannot be ruled out. However, results in diverse models strongly support that is an astrocyte-autonomous phenomenon. Consistently, expressing *Braf*^{KE} only in GFAP^{+} adult astrocytes is sufficient to induce learning deficits, and attenuation of the overactivated RAS-ERK signaling in astrocytes by injecting *Gfap-dnMek1* restored aberrant astrocytic Ca^{2+} increase and learning deficit in Nestin;*Braf*$^{KE/+}$ mice, demonstrating that all the evidence suggests that astrocyte is the cause of *Braf*-mediated defects. It is interesting that even in αCaMKII^{+} excitatory or vGAT^{+} inhibitory neurons, the ERK level is increased due to *Braf*^{KE}, but the learning and memory is unaffected. In this regard, determining how RAS-ERK signaling network is composed in astrocytes requires further investigation. The αCaMKII-Cre transgenic mice express Cre recombinase in hippocampus at postnatal day 17 of age, while the vGAT-Cre mice express Cre recombinase since embryonic period (207, 208). Because of the possibilities for little difference in expression amount and onset depend on Cre promoters, it would be worthwhile to investigating the implications of neuronal types with other Cre lines that express Cre recombinase since early neuronal developmental period.

In recent years, the crucial roles of astrocytes in cognition and in brain diseases such as neurodegenerative disorders and neurodevelopmental diseases have emerged (209-213). Several studies have reported that the RAS-ERK signaling is involved in astrocytes' biological processes, such as development and death. For example, gain-of-function mutation of *Mek1* or *Raf1* induced increased number of glial cells in mouse cortex and hippocampus (107, 108). In another cases, RAS-ERK signaling contributes to initiation of astrocyte apoptosis in harmful condition (214, 215). However,

how the RAS-ERK signaling is involved in regulatory system of astroglial properties was poorly understood. There are emerging evidences for critical roles of astrocytic Ca^{2+} in physiological and pathological conditions (212, 213, 216), little is known about the involvement of RAS-ERK signaling in regulating astrocytic Ca^{2+} signaling. Previous study has reported that the growth factors which activate various cascades involving RAS-ERK pathway increase the size of the intracellular Ca^{2+} store in the astrocytes and Ca^{2+} responses to neurotransmitters, and that these effects were suppressed by pro-inflammatory cytokines (217). Interestingly, cytokines suppressed growth factor-induced RAS-ERK pathway-dependent immediate early gene promoter activation, but not phosphorylation of ERK, demonstrating that the astrocytic Ca^{2+} is modulated by gene regulation downstream of ERK (217). Among the varied mechanisms for Ca^{2+} increases in astrocytes, canonical phospholipase C (PLC)/inositol 1,4,5-triphosphate (IP_3) pathway is the most widely accepted mechanism. IP_3 receptors (IP_3R) on the endoplasmic reticulum (ER) are ligand gated calcium channels, and upon ligand binding, release Ca^{2+} that is stored in high concentrations within the ER (218, 219). Of note, transcriptome analyses showed that the level of astrocyte-abundant IP_3R transcript (*ITPR2*) was significantly increased in BRAF KE organoid (data not shown). Therefore, there is high probability of contributions of IP_3R pathway in BRAF-mediated increased Ca^{2+} fluctuations.

It has been also posited that the reactive astrocytes drive excessive gliotransmitter release in pathological conditions, and negatively influence intrinsic neuron excitability and thereby lead to impairments in synaptic plasticity (210, 220). For example, reactive astrocytes increase astrocytic GABA release, and then cause strong inhibitory effect that induces impairments of neurotransmitter release, synaptic plasticity and memory in AD mouse model (210). In Huntington's disease, astrocytes displayed hyperactive Ca^{2+}-dependent glutamate release, and excessive accumulation of extracellular glutamate causes overpotentiation of neuronal activity and

cytotoxicity (221, 222). It is reasonable to speculate that *Braf*^{KE} astrocytes exhibit altered gliotransmitter release and might affect synaptic plasticity. Indeed, Nestin;*Braf*$^{KE/+}$ mice showed impaired LTP in Schaffer collateral pathway (data not shown), there is a limitation of this work that has not revealed exactly which gliotransmitter is released in mice.

According to the findings in this chapter, *BRAF* has certain roles in astrocytes rather than in neurons, specific to the timepoint after postnatal day 20. So far, it remained unclear how does *BRAF* functions in such a spatio-temporal manner. Recently, transcriptome analysis revealed that the amount of *BRAF* expression is largely less compared to other major components of RAS-ERK signaling in hippocampal neurons, which could explain the minimal effect of *BRAF* in neurons (122). Unexpectedly, expression amount of *BRAF* is similar between in neurons and in astrocytes (223). Therefore, it could be speculated that the *BRAF* dominantly functions in astrocytes rather than in neurons in physiological condition. Gliogenesis begins around embryonic day 18, and astrocytes develop their characteristic complex morphology at postnatal day 21 to day 28 in brain (224). Therefore, it could be assumed that the *BRAF* has a certain role in astrocytes after postnatal day 20 since *BRAF* affects astroglial properties of mature astrocytes including astrocyte reactivity and Ca^{2+} fluctuations.

Another possibility for cell type-specificity of *BRAF* mutant is involvement of other proteins or pathways which interact with *BRAF*, excepts for RAS-ERK pathway. Previous study has shown that the *NF1* interacts with hyperpolarization-activated cyclic nucleotide-gated channel 1 (HCN1) through its N terminus, and that mutations in *NF1* affect HCN channel function and induce learning deficits in mice (121). The regulation of HCN channels could be RAS-independent, because it was not affected by MEK inhibitors (225). BRAF interact with 14-3-3, a family of conserved regulatory molecules that binds specific serine- or threonine-phosphorylated motifs in diverse signalling proteins (226). Sequencially, 14-3-3 protein acts

as positive regulator of Sirt2, a family of protein deacylases and ADP-ribosyltransferases. Interestingly, Sirt2 controls reactive astrogliosis in disease condition, and has previously been demonstrated that the inhibition of Sirt2 reduces astrocyte reactivity markers (211, 227). Therefore, BRAF-14-3-3-Sirt2 interaction could also be involved in BRAF KE-induced phenotypes which seem to be predominantly presented in astrocytes.

In this study, decreasing ERK activity in astrocytes even in adult period could rescue memory deficits in Nestin;*Braf*$^{KE/+}$ mice where Braf K499E begins to be expressed in early developmental stage. However, other property such as increase of GFAP expression was not restored, suggesting that the memory deficits could be attenuated by rescuing only essential properties of astrocytes such as Ca^{2+} regulation, although not all aspects of the astrocyte were restored as normal. In this case, neuronal function may be restored via normalization of the gliotransmitter release or uptake due to recovered astrocytic Ca^{2+} signaling.

An important limitation of this study is a lack of the direct observation of the transgene expression in neural stem cell-derived cell types such as neuron and glia of Nestin;*Braf*$^{KE/+}$ brain, because the transgene locus does not contain any tag. However, I have seen the increased p-ERK1/2 expression in both neurons and astrocytes by immunolabeling (data not shown), considering the transgene was expressed and functioned properly in both cell types.

Taken together, these observations suggest that the *Braf*-related cognitive impairments are mediated mainly by astrocytic contributions, possibly because of RAS-ERK signaling activity-dependent modulation of astrocyte reactivity and Ca^{2+} signaling. Therefore, to my knowledge, these results are the first to demonstrate that the reactive-like astrogliosis may underlies the severe cognitive deficits in RASopathy.

General conclusion

In this dissertation, I investigated the mechanisms underlying learning and memory impairments in two types of RASopathy mouse models to find out the distinct roles that contribute to the cell type-specific pathological mechanisms in RASopathy-related cognitive deficits.

In chapter 1, I reviewed the distinct impacts of different components of the RAS-ERK signaling pathway associated with different RASopathies on CNS development. The schematic illustration that summarizes the chapter 1 contents is presented in **Figure 30**. In chapter 2, I found that both inhibitory and excitatory neurons are involved in *KRAS*-associated learning impairments in adult via distinct mechanisms. In chapter 3, I demonstrated that the reactive-like astrogliosis may underlies the severe cognitive deficits in *BRAF*-related RASopathy. The cell type-specificity of *KRAS* and *BRAF* that is identified in chapter 2 and 3 is also shown in Figure 30.

So far, it remained unclear how some RASopathy-related genes have dominant role in neurons and others have role in glia. Therefore, how $KRAS^{G12V}$-mediated RAS-ERK overactivation induces learning deficits in adult hippocampal neuron types, while the $BRAF^{K499E}$-mediated RAS-ERK overactivation induces learning deficits in astrocytes, but not in neuron types is not yet solved in my dissertation. One possibility is an absolute difference in the level of expression in neuron between *KRAS* and *BRAF*. Previous study provided the RNA-seq transcriptome data that analyzed expression level of RASopathy-associated genes, such as *Braf*, *Hras*, *Kras*, *Ptpn11*, and *Nf1* in mouse hippocampal neurons (122). Interestingly, expression amount of *Braf* is largely lower than that of *Kras* in both excitatory and inhibitory neurons. Therefore, *Kras* may have had a greater influence in neuron types due to the enriched expression compared to *Braf* expression in neuron. Furthermore, it also would be worthwhile to compare

the expression of RASopathy-associated genes in glial types.

Therapeutic treatments for the cognitive impairments presented in RASopathy individuals are not available yet. Considering the ubiquitous existence of RAS-ERK signaling pathway in various cell types, directly regulating RAS-ERK activity may have unknown confounding effects. Therefore, it would be better to target mechanism-based specific molecules in a disease-specific manner. From that perspective, this dissertation suggests the available information for the clinical treatments for *KRAS*-, and *BRAF*-related cognitive deficits in RASopathies.

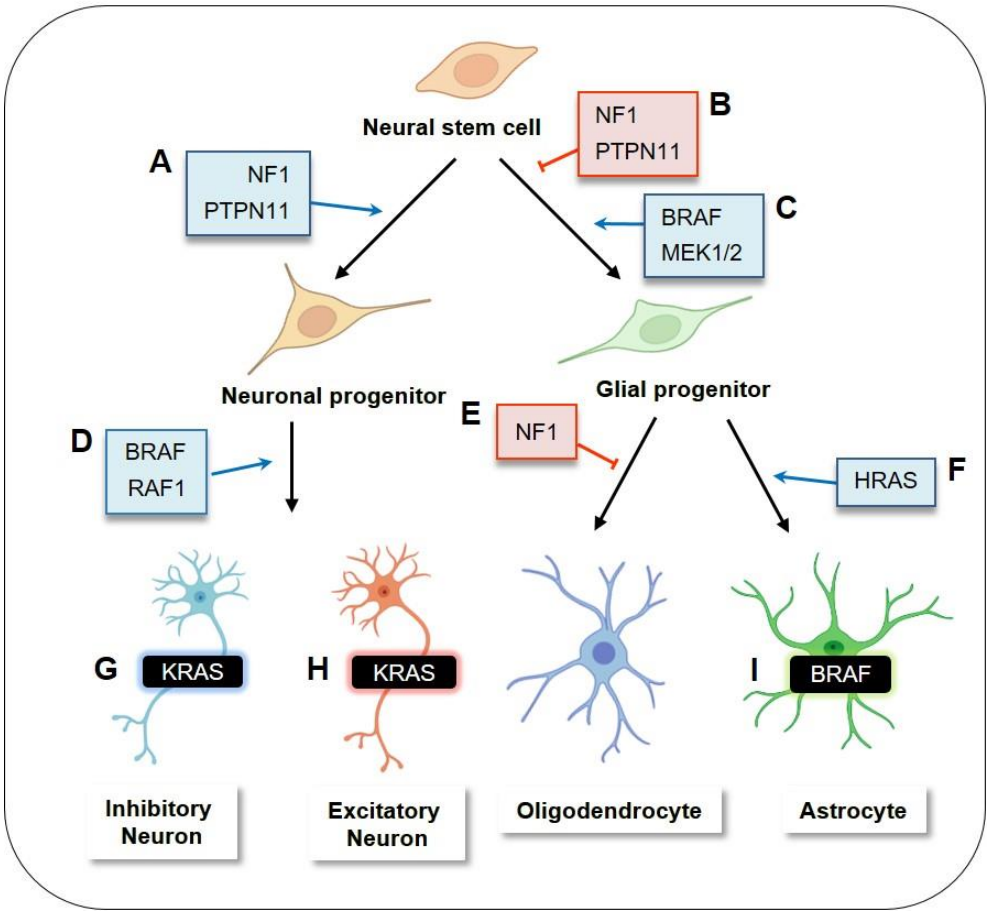

Figure 30. Cell type-specific contributions of RAS-ERK signaling components. (A) NF1 inactivation led to decreased neurogenesis in neonatal and adult mouse brains (85). PTPN11 positively regulates neurogenesis at the expense of gliogenesis (96).(B) NF1 negatively regulates gliogenesis, thus NF1 inactivation increases the number of glial progenitor cells and gliogenesis (79, 85, 89, 120, 228). PTPN11 suppresses gliogenesis by directly interacting with the JAK-STAT pathway, which promotes gliogenesis (92, 96). (C) Hyperactivation of RAF1 induces the increase of glial lineage populations, including oligodendrocyte progenitor cells and astrocytes (107). MEK is required for gliogenesis, and the hyperfunction of MEK1 leads to increase in glial populations (108, 109). (D) BRAF and RAF1 positively regulate neuronal differentiation, and the

disruption of BRAF or RAF1 impairs the ability of progenitor cells to differentiate into mature neurons in mouse brain (102, 105). In consistent, iPSC containing hyperactivated BRAF mutant showed early maturation of neurons (147). (E) Oligodendroglial lineage potential is restricted by NF1 in the adult hippocampus, and inactivation of NF1 allows the adult hippocampus to generate oligodendrocytes (85). (F) Hyperactivated HRAS leads to an acceleration of astroglial maturation (163, 167). Blue and red arrows indicate positive and negative regulation, respectively. (G, H) KRAS in both inhibitory and excitatory neurons has cell type-specific function. (I) BRAF in astrocytes has cell type-specific function.

Bibliography

1. Kolch W. Meaningful relationships: the regulation of the Ras/Raf/MEK/ERK pathway by protein interactions. *The Biochemical journal.* 2000;351 Pt 2(289-305.
2. Boguski MS, and McCormick F. Proteins regulating Ras and its relatives. *Nature.* 1993;366(6456):643-54.
3. Ryu HH, and Lee YS. Cell type-specific roles of RAS-MAPK signaling in learning and memory: Implications in neurodevelopmental disorders. *Neurobiol Learn Mem.* 2016.
4. Rauen KA. The RASopathies. *Annual review of genomics and human genetics.* 2013;14(355-69.
5. Innocenti M, Tenca P, Frittoli E, Faretta M, Tocchetti A, Di Fiore PP, and Scita G. Mechanisms through which Sos-1 coordinates the activation of Ras and Rac. *The Journal of cell biology.* 2002;156(1):125-36.
6. Zhao L, and Brinton RD. Vasopressin-induced cytoplasmic and nuclear calcium signaling in embryonic cortical astrocytes: dynamics of calcium and calcium-dependent kinase translocation. *The Journal of neuroscience : the official journal of the Society for Neuroscience.* 2003;23(10):4228-39.
7. Deak M, Clifton AD, Lucocq LM, and Alessi DR. Mitogen- and stress-activated protein kinase-1 (MSK1) is directly activated by MAPK and SAPK2/p38, and may mediate activation of CREB. *The EMBO journal.* 1998;17(15):4426-41.
8. Shilyansky C, Lee YS, and Silva AJ. Molecular and cellular mechanisms of learning disabilities: a focus on NF1. *Annu Rev Neurosci.* 2010;33(221-43.
9. Kim YE, and Baek ST. Neurodevelopmental Aspects of RASopathies. *Molecules and cells.* 2019;42(6):441-7.
10. Tidyman WE, and Rauen KA. The RASopathies: developmental syndromes of Ras/MAPK pathway dysregulation. *Current opinion in genetics & development.* 2009;19(3):230-6.
11. Jindal GA, Goyal Y, Burdine RD, Rauen KA, and Shvartsman SY. RASopathies: unraveling mechanisms with animal models. *Disease models & mechanisms.* 2015;8(8):769-82.
12. Ferner RE, Huson SM, Thomas N, Moss C, Willshaw H, Evans DG, Upadhyaya M, Towers R, Gleeson M, Steiger C, et al. Guidelines for the diagnosis and management of individuals with neurofibromatosis 1. *Journal of medical genetics.* 2007;44(2):81-8.
13. Rosman NP, and Pearce J. The brain in multiple neurofibromatosis (von Recklinghausen's disease): a suggested neuropathological basis for the associated mental defect. *Brain : a journal of neurology.* 1967;90(4):829-38.
14. Listernick R, Charrow J, Greenwald MJ, and Esterly NB. Optic

gliomas in children with neurofibromatosis type 1. *The Journal of pediatrics.* 1989;114(5):788-92.
15. Krab LC, Aarsen FK, de Goede-Bolder A, Catsman-Berrevoets CE, Arts WF, Moll HA, and Elgersma Y. Impact of neurofibromatosis type 1 on school performance. *Journal of child neurology.* 2008;23(9):1002-10.
16. Shilyansky C, Karlsgodt KH, Cummings DM, Sidiropoulou K, Hardt M, James AS, Ehninger D, Bearden CE, Poirazi P, Jentsch JD, et al. Neurofibromin regulates corticostriatal inhibitory networks during working memory performance. *Proceedings of the National Academy of Sciences of the United States of America.* 2010;107(29):13141-6.
17. Cichowski K, and Jacks T. NF1 tumor suppressor gene function: narrowing the GAP. *Cell.* 2001;104(4):593-604.
18. Zhu Y, and Parada LF. Neurofibromin, a tumor suppressor in the nervous system. *Experimental cell research.* 2001;264(1):19-28.
19. Brems H, and Legius E. Legius syndrome, an Update. Molecular pathology of mutations in SPRED1. *The Keio journal of medicine.* 2013;62(4):107-12.
20. Williams VC, Lucas J, Babcock MA, Gutmann DH, Korf B, and Maria BL. Neurofibromatosis type 1 revisited. *Pediatrics.* 2009;123(1):124-33.
21. Tartaglia M, Kalidas K, Shaw A, Song X, Musat DL, van der Burgt I, Brunner HG, Bertola DR, Crosby A, Ion A, et al. PTPN11 mutations in Noonan syndrome: molecular spectrum, genotype-phenotype correlation, and phenotypic heterogeneity. *American journal of human genetics.* 2002;70(6):1555-63.
22. Razzaque MA, Nishizawa T, Komoike Y, Yagi H, Furutani M, Amo R, Kamisago M, Momma K, Katayama H, Nakagawa M, et al. Germline gain-of-function mutations in RAF1 cause Noonan syndrome. *Nature genetics.* 2007;39(8):1013-7.
23. Pandit B, Sarkozy A, Pennacchio LA, Carta C, Oishi K, Martinelli S, Pogna EA, Schackwitz W, Ustaszewska A, Landstrom A, et al. Gain-of-function RAF1 mutations cause Noonan and LEOPARD syndromes with hypertrophic cardiomyopathy. *Nature genetics.* 2007;39(8):1007-12.
24. Tartaglia M, Pennacchio LA, Zhao C, Yadav KK, Fodale V, Sarkozy A, Pandit B, Oishi K, Martinelli S, Schackwitz W, et al. Gain-of-function SOS1 mutations cause a distinctive form of Noonan syndrome. *Nature genetics.* 2007;39(1):75-9.
25. Schubbert S, Zenker M, Rowe SL, Boll S, Klein C, Bollag G, van der Burgt I, Musante L, Kalscheuer V, Wehner LE, et al. Germline KRAS mutations cause Noonan syndrome. *Nature genetics.* 2006;38(3):331-6.
26. Carta C, Pantaleoni F, Bocchinfuso G, Stella L, Vasta I, Sarkozy A, Digilio C, Palleschi A, Pizzuti A, Grammatico P, et al. Germline missense mutations affecting KRAS Isoform B are associated with a severe Noonan syndrome phenotype. *American journal of human genetics.* 2006;79(1):129-35.

27. Nava C, Hanna N, Michot C, Pereira S, Pouvreau N, Niihori T, Aoki Y, Matsubara Y, Arveiler B, Lacombe D, et al. Cardio-facio-cutaneous and Noonan syndromes due to mutations in the RAS/MAPK signalling pathway: genotype-phenotype relationships and overlap with Costello syndrome. *Journal of medical genetics.* 2007;44(12):763-71.
28. Peiris A, and Ball MJ. Chiari (type 1) malformation and syringomyelia in a patient with Noonan's syndrome. *Journal of neurology, neurosurgery, and psychiatry.* 1982;45(8):753-4.
29. Kobayashi I, Aikawa T, Takemiya T, Maruyama S, and Takano K. Noonan's syndrome with syringomyelia. *The Japanese journal of psychiatry and neurology.* 1986;40(1):101-4.
30. Gorke W. [Cerebral defects in Noonan's syndrome (author's transl)]. *Klinische Padiatrie.* 1980;192(6):577-81.
31. Noonan JA. Hypertelorism with Turner phenotype. A new syndrome with associated congenital heart disease. *American journal of diseases of children (1960).* 1968;116(4):373-80.
32. Raman Unnithan R, Bahuleyan CG, and Matnew Roy VC. Noonan syndrome. *The Journal of the Association of Physicians of India.* 1985;33(2):177-9.
33. Saito Y, Sasaki M, Hanaoka S, Sugai K, and Hashimoto T. A case of Noonan syndrome with cortical dysplasia. *Pediatric neurology.* 1997;17(3):266-9.
34. Cesarini L, Alfieri P, Pantaleoni F, Vasta I, Cerutti M, Petrangeli V, Mariotti P, Leoni C, Ricci D, Vicari S, et al. Cognitive profile of disorders associated with dysregulation of the RAS/MAPK signaling cascade. *American journal of medical genetics Part A.* 2009;149a(2):140-6.
35. Pierpont EI, Pierpont ME, Mendelsohn NJ, Roberts AE, Tworog-Dube E, and Seidenberg MS. Genotype differences in cognitive functioning in Noonan syndrome. *Genes, brain, and behavior.* 2009;8(3):275-82.
36. Aoki Y, Niihori T, Banjo T, Okamoto N, Mizuno S, Kurosawa K, Ogata T, Takada F, Yano M, Ando T, et al. Gain-of-function mutations in RIT1 cause Noonan syndrome, a RAS/MAPK pathway syndrome. *American journal of human genetics.* 2013;93(1):173-80.
37. Lee DA, Portnoy S, Hill P, Gillberg C, and Patton MA. Psychological profile of children with Noonan syndrome. *Developmental medicine and child neurology.* 2005;47(1):35-8.
38. Razzaque MA, Komoike Y, Nishizawa T, Inai K, Furutani M, Higashinakagawa T, and Matsuoka R. Characterization of a novel KRAS mutation identified in Noonan syndrome. *American journal of medical genetics Part A.* 2012;158a(3):524-32.
39. Roberts AE, Allanson JE, Tartaglia M, and Gelb BD. Noonan syndrome. *Lancet (London, England).* 2013;381(9863):333-42.
40. van der Burgt I, Thoonen G, Roosenboom N, Assman-Hulsmans C, Gabreels F, Otten B, and Brunner HG. Patterns of cognitive functioning in school-aged children with Noonan syndrome associated with variability in phenotypic expression. *The Journal of*

pediatrics. 1999;135(6):707-13.
41. Niihori T, Aoki Y, Narumi Y, Neri G, Cave H, Verloes A, Okamoto N, Hennekam RC, Gillessen-Kaesbach G, Wieczorek D, et al. Germline KRAS and BRAF mutations in cardio-facio-cutaneous syndrome. *Nature genetics.* 2006;38(3):294-6.
42. Rodriguez-Viciana P, Tetsu O, Tidyman WE, Estep AL, Conger BA, Cruz MS, McCormick F, and Rauen KA. Germline mutations in genes within the MAPK pathway cause cardio-facio-cutaneous syndrome. *Science (New York, NY).* 2006;311(5765):1287-90.
43. Narumi Y, Aoki Y, Niihori T, Neri G, Cave H, Verloes A, Nava C, Kavamura MI, Okamoto N, Kurosawa K, et al. Molecular and clinical characterization of cardio-facio-cutaneous (CFC) syndrome: overlapping clinical manifestations with Costello syndrome. *American journal of medical genetics Part A.* 2007;143a(8):799-807.
44. Reynolds JF, Neri G, Herrmann JP, Blumberg B, Coldwell JG, Miles PV, and Opitz JM. New multiple congenital anomalies/mental retardation syndrome with cardio-facio-cutaneous involvement--the CFC syndrome. *American journal of medical genetics.* 1986;25(3):413-27.
45. Neri G, Sabatino G, Bertini E, and Genuardi M. The CFC syndrome--report of the first two cases outside the United States. *American journal of medical genetics.* 1987;27(4):767-71.
46. Chrzanowska K, Fryns JP, and Van den Berghe H. Cardio-facio-cutaneous (CFC) syndrome: report of a new patient. *American journal of medical genetics.* 1989;33(4):471-3.
47. Ades LC, Sillence DO, and Rogers M. Cardiofaciocutaneous syndrome. *Clinical dysmorphology.* 1992;1(3):145-50.
48. Young TL, Ziylan S, and Schaffer DB. The ophthalmologic manifestations of the cardio-facio-cutaneous syndrome. *Journal of pediatric ophthalmology and strabismus.* 1993;30(1):48-52.
49. Krajewska-Walasek M, Chrzanowska K, and Jastrzbska M. The cardio-facio-cutaneous (CFC) syndrome--two possible new cases and review of the literature. *Clinical dysmorphology.* 1996;5(1):65-72.
50. Yoon G, Rosenberg J, Blaser S, and Rauen KA. Neurological complications of cardio-facio-cutaneous syndrome. *Developmental medicine and child neurology.* 2007;49(12):894-9.
51. Somer M, Peippo M, Aalto-Korte K, Ritvanen A, and Niemi KM. Cardio-facio-cutaneous syndrome: three additional cases and review of the literature. *American journal of medical genetics.* 1992;44(5):691-5.
52. Grebe TA, and Clericuzio C. Neurologic and gastrointestinal dysfunction in cardio-facio-cutaneous syndrome: identification of a severe phenotype. *American journal of medical genetics.* 2000;95(2):135-43.
53. Manci EA, Martinez JE, Horenstein MG, Gardner TM, Ahmed A, Mancao MC, Gremse DA, Gardner DM, Nimityongskul P, Maertens P, et al. Cardiofaciocutaneous syndrome (CFC) with congenital

peripheral neuropathy and nonorganic malnutrition: an autopsy study. *American journal of medical genetics Part A.* 2005;137(1):1-8.
54. Baraitser M, and Patton MA. A Noonan-like short stature syndrome with sparse hair. *Journal of medical genetics.* 1986;23(2):161-4.
55. Armour CM, and Allanson JE. Further delineation of cardio-facio-cutaneous syndrome: clinical features of 38 individuals with proven mutations. *Journal of medical genetics.* 2008;45(4):249-54.
56. Papadopoulou E, Sifakis S, Sol-Church K, Klein-Zighelboim E, Stabley DL, Raissaki M, Gripp KW, and Kalmanti M. CNS imaging is a key diagnostic tool in the evaluation of patients with CFC syndrome: two cases and literature review. *American journal of medical genetics Part A.* 2011;155a(3):605-11.
57. Wieczorek D, Majewski F, and Gillessen-Kaesbach G. Cardio-facio-cutaneous (CFC) syndrome--a distinct entity? Report of three patients demonstrating the diagnostic difficulties in delineation of CFC syndrome. *Clinical genetics.* 1997;52(1):37-46.
58. Roberts A, Allanson J, Jadico SK, Kavamura MI, Noonan J, Opitz JM, Young T, and Neri G. The cardiofaciocutaneous syndrome. *Journal of medical genetics.* 2006;43(11):833-42.
59. Schulz AL, Albrecht B, Arici C, van der Burgt I, Buske A, Gillessen-Kaesbach G, Heller R, Horn D, Hubner CA, Korenke GC, et al. Mutation and phenotypic spectrum in patients with cardio-facio-cutaneous and Costello syndrome. *Clinical genetics.* 2008;73(1):62-70.
60. Aoki Y, Niihori T, Kawame H, Kurosawa K, Ohashi H, Tanaka Y, Filocamo M, Kato K, Suzuki Y, Kure S, et al. Germline mutations in HRAS proto-oncogene cause Costello syndrome. *Nature genetics.* 2005;37(10):1038-40.
61. Kerr B, Delrue MA, Sigaudy S, Perveen R, Marche M, Burgelin I, Stef M, Tang B, Eden OB, O'Sullivan J, et al. Genotype-phenotype correlation in Costello syndrome: HRAS mutation analysis in 43 cases. *Journal of medical genetics.* 2006;43(5):401-5.
62. Estep AL, Tidyman WE, Teitell MA, Cotter PD, and Rauen KA. HRAS mutations in Costello syndrome: detection of constitutional activating mutations in codon 12 and 13 and loss of wild-type allele in malignancy. *American journal of medical genetics Part A.* 2006;140(1):8-16.
63. Zenker M, Lehmann K, Schulz AL, Barth H, Hansmann D, Koenig R, Korinthenberg R, Kreiss-Nachtsheim M, Meinecke P, Morlot S, et al. Expansion of the genotypic and phenotypic spectrum in patients with KRAS germline mutations. *Journal of medical genetics.* 2007;44(2):131-5.
64. Der Kaloustian VM, Moroz B, McIntosh N, Watters AK, and Blaichman S. Costello syndrome. *American journal of medical genetics.* 1991;41(1):69-73.
65. Zampino G, Mastroiacovo P, Ricci R, Zollino M, Segni G, Martini-Neri ME, and Neri G. Costello syndrome: further clinical delineation, natural history, genetic definition, and nosology. *American journal of*

medical genetics. 1993;47(2):176-83.
66. Gripp KW, Scott CI, Jr., Nicholson L, and Figueroa TE. Second case of bladder carcinoma in a patient with Costello syndrome. *American journal of medical genetics.* 2000;90(3):256-9.
67. Gripp KW, Scott CI, Jr., Nicholson L, McDonald-McGinn DM, Ozeran JD, Jones MC, Lin AE, and Zackai EH. Five additional Costello syndrome patients with rhabdomyosarcoma: proposal for a tumor screening protocol. *American journal of medical genetics.* 2002;108(1):80-7.
68. Fryns JP, Vogels A, Haegeman J, Eggermont E, and van den Berghe H. Costello syndrome: a postnatal growth retardation syndrome with distinct phenotype. *Genetic counseling (Geneva, Switzerland).* 1994;5(4):337-43.
69. Johnson JP, Golabi M, Norton ME, Rosenblatt RM, Feldman GM, Yang SP, Hall BD, Fries MH, and Carey JC. Costello syndrome: phenotype, natural history, differential diagnosis, and possible cause. *The Journal of pediatrics.* 1998;133(3):441-8.
70. Kerr B, Eden OB, Dandamudi R, Shannon N, Quarrell O, Emmerson A, Ladusans E, Gerrard M, and Donnai D. Costello syndrome: two cases with embryonal rhabdomyosarcoma. *Journal of medical genetics.* 1998;35(12):1036-9.
71. van Eeghen AM, van Gelderen I, and Hennekam RC. Costello syndrome: report and review. *American journal of medical genetics.* 1999;82(2):187-93.
72. Say B, Gucsavas M, Morgan H, and York C. The Costello syndrome. *American journal of medical genetics.* 1993;47(2):163-5.
73. Delrue MA, Chateil JF, Arveiler B, and Lacombe D. Costello syndrome and neurological abnormalities. *American journal of medical genetics Part A.* 2003;123a(3):301-5.
74. Okamoto N, Chiyo H, Imai K, Otani K, and Futagi Y. A Japanese patient with the Costello syndrome. *Human genetics.* 1994;93(5):605-6.
75. Lakkis MM, Golden JA, O'Shea KS, and Epstein JA. Neurofibromin deficiency in mice causes exencephaly and is a modifier for Splotch neural tube defects. *Developmental biology.* 1999;212(1):80-92.
76. Brannan CI, Perkins AS, Vogel KS, Ratner N, Nordlund ML, Reid SW, Buchberg AM, Jenkins NA, Parada LF, and Copeland NG. Targeted disruption of the neurofibromatosis type-1 gene leads to developmental abnormalities in heart and various neural crest-derived tissues. *Genes & development.* 1994;8(9):1019-29.
77. Jacks T, Shih TS, Schmitt EM, Bronson RT, Bernards A, and Weinberg RA. Tumour predisposition in mice heterozygous for a targeted mutation in Nf1. *Nature genetics.* 1994;7(3):353-61.
78. Gutmann DH, Loehr A, Zhang Y, Kim J, Henkemeyer M, and Cashen A. Haploinsufficiency for the neurofibromatosis 1 (NF1) tumor suppressor results in increased astrocyte proliferation. *Oncogene.* 1999;18(31):4450-9.
79. Rizvi TA, Akunuru S, de Courten-Myers G, Switzer RC, 3rd,

Nordlund ML, and Ratner N. Region-specific astrogliosis in brains of mice heterozygous for mutations in the neurofibromatosis type 1 (Nf1) tumor suppressor. *Brain research.* 1999;816(1):111-23.
80. Costa RM, Federov NB, Kogan JH, Murphy GG, Stern J, Ohno M, Kucherlapati R, Jacks T, and Silva AJ. Mechanism for the learning deficits in a mouse model of neurofibromatosis type 1. *Nature.* 2002;415(6871):526-30.
81. Silva AJ, Frankland PW, Marowitz Z, Friedman E, Laszlo GS, Cioffi D, Jacks T, and Bourtchuladze R. A mouse model for the learning and memory deficits associated with neurofibromatosis type I. *Nature genetics.* 1997;15(3):281-4.
82. Costa RM, Yang T, Huynh DP, Pulst SM, Viskochil DH, Silva AJ, and Brannan CI. Learning deficits, but normal development and tumor predisposition, in mice lacking exon 23a of Nf1. *Nature genetics.* 2001;27(4):399-405.
83. Zhu Y, Romero MI, Ghosh P, Ye Z, Charnay P, Rushing EJ, Marth JD, and Parada LF. Ablation of NF1 function in neurons induces abnormal development of cerebral cortex and reactive gliosis in the brain. *Genes & development.* 2001;15(7):859-76.
84. Cui Y, Costa RM, Murphy GG, Elgersma Y, Zhu Y, Gutmann DH, Parada LF, Mody I, and Silva AJ. Neurofibromin regulation of ERK signaling modulates GABA release and learning. *Cell.* 2008;135(3):549-60.
85. Wang Y, Kim E, Wang X, Novitch BG, Yoshikawa K, Chang LS, and Zhu Y. ERK inhibition rescues defects in fate specification of Nf1-deficient neural progenitors and brain abnormalities. *Cell.* 2012;150(4):816-30.
86. Zhu Y, Harada T, Liu L, Lush ME, Guignard F, Harada C, Burns DK, Bajenaru ML, Gutmann DH, and Parada LF. Inactivation of NF1 in CNS causes increased glial progenitor proliferation and optic glioma formation. *Development (Cambridge, England).* 2005;132(24):5577-88.
87. Lush ME, Li Y, Kwon CH, Chen J, and Parada LF. Neurofibromin is required for barrel formation in the mouse somatosensory cortex. *The Journal of neuroscience : the official journal of the Society for Neuroscience.* 2008;28(7):1580-7.
88. Sanchez-Ortiz E, Cho W, Nazarenko I, Mo W, Chen J, and Parada LF. NF1 regulation of RAS/ERK signaling is required for appropriate granule neuron progenitor expansion and migration in cerebellar development. *Genes & development.* 2014;28(21):2407-20.
89. Hegedus B, Dasgupta B, Shin JE, Emnett RJ, Hart-Mahon EK, Elghazi L, Bernal-Mizrachi E, and Gutmann DH. Neurofibromatosis-1 regulates neuronal and glial cell differentiation from neuroglial progenitors in vivo by both cAMP- and Ras-dependent mechanisms. *Cell stem cell.* 2007;1(4):443-57.
90. Sun GJ, Zhou Y, Ito S, Bonaguidi MA, Stein-O'Brien G, Kawasaki NK, Modak N, Zhu Y, Ming GL, and Song H. Latent tri-lineage potential of adult hippocampal neural stem cells revealed by Nf1 inactivation.

Nature neuroscience. 2015;18(12):1722-4.
91. Li Y, Li Y, McKay RM, Riethmacher D, and Parada LF. Neurofibromin modulates adult hippocampal neurogenesis and behavioral effects of antidepressants. *The Journal of neuroscience : the official journal of the Society for Neuroscience.* 2012;32(10):3529-39.
92. Ke Y, Zhang EE, Hagihara K, Wu D, Pang Y, Klein R, Curran T, Ranscht B, and Feng GS. Deletion of Shp2 in the brain leads to defective proliferation and differentiation in neural stem cells and early postnatal lethality. *Molecular and cellular biology.* 2007;27(19):6706-17.
93. Zhu Y, Park J, Hu X, Zheng K, Li H, Cao Q, Feng GS, and Qiu M. Control of oligodendrocyte generation and proliferation by Shp2 protein tyrosine phosphatase. *Glia.* 2010;58(12):1407-14.
94. Ehrman LA, Nardini D, Ehrman S, Rizvi TA, Gulick J, Krenz M, Dasgupta B, Robbins J, Ratner N, Nakafuku M, et al. The protein tyrosine phosphatase Shp2 is required for the generation of oligodendrocyte progenitor cells and myelination in the mouse telencephalon. *The Journal of neuroscience : the official journal of the Society for Neuroscience.* 2014;34(10):3767-78.
95. Zheng H, Yu WM, Waclaw RR, Kontaridis MI, Neel BG, and Qu CK. Gain-of-function mutations in the gene encoding the tyrosine phosphatase SHP2 induce hydrocephalus in a catalytically dependent manner. *Science signaling.* 2018;11(522).
96. Gauthier AS, Furstoss O, Araki T, Chan R, Neel BG, Kaplan DR, and Miller FD. Control of CNS cell-fate decisions by SHP-2 and its dysregulation in Noonan syndrome. *Neuron.* 2007;54(2):245-62.
97. Lee YS, Ehninger D, Zhou M, Oh JY, Kang M, Kwak C, Ryu HH, Butz D, Araki T, Cai Y, et al. Mechanism and treatment for learning and memory deficits in mouse models of Noonan syndrome. *Nature neuroscience.* 2014;17(12):1736-43.
98. Araki T, Mohi MG, Ismat FA, Bronson RT, Williams IR, Kutok JL, Yang W, Pao LI, Gilliland DG, Epstein JA, et al. Mouse model of Noonan syndrome reveals cell type- and gene dosage-dependent effects of Ptpn11 mutation. *Nature medicine.* 2004;10(8):849-57.
99. Papale A, d'Isa R, Menna E, Cerovic M, Solari N, Hardingham N, Cambiaghi M, Cursi M, Barbacid M, Leocani L, et al. Severe Intellectual Disability and Enhanced Gamma-Aminobutyric Acidergic Synaptogenesis in a Novel Model of Rare RASopathies. *Biological psychiatry.* 2016.
100. Schreiber J, Grimbergen LA, Overwater I, Vaart TV, Stedehouder J, Schuhmacher AJ, Guerra C, Kushner SA, Jaarsma D, and Elgersma Y. Mechanisms underlying cognitive deficits in a mouse model for Costello Syndrome are distinct from other RASopathy mouse models. *Scientific reports.* 2017;7(1):1256.
101. Kushner SA, Elgersma Y, Murphy GG, Jaarsma D, van Woerden GM, Hojjati MR, Cui Y, LeBoutillier JC, Marrone DF, Choi ES, et al. Modulation of presynaptic plasticity and learning by the H-ras/extracellular signal-regulated kinase/synapsin I signaling

pathway. *The Journal of neuroscience : the official journal of the Society for Neuroscience.* 2005;25(42):9721-34.
102. Pfeiffer V, Gotz R, Xiang C, Camarero G, Braun A, Zhang Y, Blum R, Heinsen H, Nieswandt B, and Rapp UR. Ablation of BRaf impairs neuronal differentiation in the postnatal hippocampus and cerebellum. *PloS one.* 2013;8(3):e58259.
103. Galabova-Kovacs G, Catalanotti F, Matzen D, Reyes GX, Zezula J, Herbst R, Silva A, Walter I, and Baccarini M. Essential role of B-Raf in oligodendrocyte maturation and myelination during postnatal central nervous system development. *The Journal of cell biology.* 2008;180(5):947-55.
104. Urosevic J, Sauzeau V, Soto-Montenegro ML, Reig S, Desco M, Wright EM, Canamero M, Mulero F, Ortega S, Bustelo XR, et al. Constitutive activation of B-Raf in the mouse germ line provides a model for human cardio-facio-cutaneous syndrome. *Proceedings of the National Academy of Sciences of the United States of America.* 2011;108(12):5015-20.
105. Pfeiffer V, Gotz R, Camarero G, Heinsen H, Blum R, and Rapp UR. Impaired neuronal maturation of hippocampal neural progenitor cells in mice lacking CRAF. *PLoS One.* 2018;13(3):e0192067.
106. Preiss T, and Hentze MW. From factors to mechanisms: translation and translational control in eukaryotes. *Current opinion in genetics & development.* 1999;9(5):515-21.
107. Holter MC, Hewitt LT, Koebele SV, Judd JM, Xing L, Bimonte-Nelson HA, Conrad CD, Araki T, Neel BG, Snider WD, et al. The Noonan Syndrome-linked Raf1L613V mutation drives increased glial number in the mouse cortex and enhanced learning. *PLoS genetics.* 2019;15(4):e1008108.
108. Aoidi R, Houde N, Landry-Truchon K, Holter M, Jacquet K, Charron L, Krishnaswami SR, Yu BD, Rauen KA, Bisson N, et al. Mek1(Y130C) mice recapitulate aspects of human cardio-facio-cutaneous syndrome. *Disease models & mechanisms.* 2018;11(3).
109. Li X, Newbern JM, Wu Y, Morgan-Smith M, Zhong J, Charron J, and Snider WD. MEK Is a Key Regulator of Gliogenesis in the Developing Brain. *Neuron.* 2012;75(6):1035-50.
110. Krab LC, Goorden SM, and Elgersma Y. Oncogenes on my mind: ERK and MTOR signaling in cognitive diseases. *Trends in genetics : TIG.* 2008;24(10):498-510.
111. Bentires-Alj M, Kontaridis MI, and Neel BG. Stops along the RAS pathway in human genetic disease. *Nature medicine.* 2006;12(3):283-5.
112. Costa RM, and Silva AJ. Molecular and cellular mechanisms underlying the cognitive deficits associated with neurofibromatosis 1. *Journal of child neurology.* 2002;17(8):622-6; discussion 7-9, 46-51.
113. Li W, Cui Y, Kushner SA, Brown RA, Jentsch JD, Frankland PW, Cannon TD, and Silva AJ. The HMG-CoA reductase inhibitor lovastatin reverses the learning and attention deficits in a mouse model of neurofibromatosis type 1. *Current biology : CB.*

2005;15(21):1961-7.
114. Rabchevsky AG, Weinitz JM, Coulpier M, Fages C, Tinel M, and Junier MP. A role for transforming growth factor alpha as an inducer of astrogliosis. *The Journal of neuroscience : the official journal of the Society for Neuroscience.* 1998;18(24):10541-52.
115. Zhuo L, Theis M, Alvarez-Maya I, Brenner M, Willecke K, and Messing A. hGFAP-cre transgenic mice for manipulation of glial and neuronal function in vivo. *Genesis (New York, NY : 2000).* 2001;31(2):85-94.
116. Zhou Q, and Anderson DJ. The bHLH transcription factors OLIG2 and OLIG1 couple neuronal and glial subtype specification. *Cell.* 2002;109(1):61-73.
117. Lee DY, Yeh TH, Emnett RJ, White CR, and Gutmann DH. Neurofibromatosis-1 regulates neuroglial progenitor proliferation and glial differentiation in a brain region-specific manner. *Genes & development.* 2010;24(20):2317-29.
118. Bennett MR, Rizvi TA, Karyala S, McKinnon RD, and Ratner N. Aberrant growth and differentiation of oligodendrocyte progenitors in neurofibromatosis type 1 mutants. *The Journal of neuroscience : the official journal of the Society for Neuroscience.* 2003;23(18):7207-17.
119. Kim HA, Ling B, and Ratner N. Nf1-deficient mouse Schwann cells are angiogenic and invasive and can be induced to hyperproliferate: reversion of some phenotypes by an inhibitor of farnesyl protein transferase. *Molecular and cellular biology.* 1997;17(2):862-72.
120. Dasgupta B, and Gutmann DH. Neurofibromin regulates neural stem cell proliferation, survival, and astroglial differentiation in vitro and in vivo. *The Journal of neuroscience : the official journal of the Society for Neuroscience.* 2005;25(23):5584-94.
121. Omrani A, van der Vaart T, Mientjes E, van Woerden GM, Hojjati MR, Li KW, Gutmann DH, Levelt CN, Smit AB, Silva AJ, et al. HCN channels are a novel therapeutic target for cognitive dysfunction in Neurofibromatosis type 1. *Molecular psychiatry.* 2015;20(11):1311-21.
122. Ryu HH, Kim T, Kim JW, Kang M, Park P, Kim YG, Kim H, Ha J, Choi JE, Lee J, et al. Excitatory neuron-specific SHP2-ERK signaling network regulates synaptic plasticity and memory. *Science signaling.* 2019;12(571).
123. Ryu HH, Kang M, Park J, Park SH, and Lee YS. Enriched expression of NF1 in inhibitory neurons in both mouse and human brain. *Molecular brain.* 2019;12(1):60.
124. Tartaglia M, and Gelb BD. Noonan syndrome and related disorders: genetics and pathogenesis. *Annual review of genomics and human genetics.* 2005;6(45-68.
125. Romano AA, Allanson JE, Dahlgren J, Gelb BD, Hall B, Pierpont ME, Roberts AE, Robinson W, Takemoto CM, and Noonan JA. Noonan syndrome: clinical features, diagnosis, and management guidelines. *Pediatrics.* 2010;126(4):746-59.

126. Tartaglia M, Mehler EL, Goldberg R, Zampino G, Brunner HG, Kremer H, van der Burgt I, Crosby AH, Ion A, Jeffery S, et al. Mutations in PTPN11, encoding the protein tyrosine phosphatase SHP-2, cause Noonan syndrome. *Nature genetics.* 2001;29(4):465-8.
127. Sarkozy A, Digilio MC, and Dallapiccola B. Leopard syndrome. *Orphanet journal of rare diseases.* 2008;3(13.
128. Chen PC, Wakimoto H, Conner D, Araki T, Yuan T, Roberts A, Seidman C, Bronson R, Neel B, Seidman JG, et al. Activation of multiple signaling pathways causes developmental defects in mice with a Noonan syndrome-associated Sos1 mutation. *The Journal of clinical investigation.* 2010;120(12):4353-65.
129. Nakamura T, Gulick J, Pratt R, and Robbins J. Noonan syndrome is associated with enhanced pERK activity, the repression of which can prevent craniofacial malformations. *Proceedings of the National Academy of Sciences of the United States of America.* 2009;106(36):15436-41.
130. Hernandez-Porras I, Fabbiano S, Schuhmacher AJ, Aicher A, Canamero M, Camara JA, Cusso L, Desco M, Heeschen C, Mulero F, et al. K-RasV14I recapitulates Noonan syndrome in mice. *Proceedings of the National Academy of Sciences of the United States of America.* 2014;111(46):16395-400.
131. Wu X, Simpson J, Hong JH, Kim KH, Thavarajah NK, Backx PH, Neel BG, and Araki T. MEK-ERK pathway modulation ameliorates disease phenotypes in a mouse model of Noonan syndrome associated with the Raf1(L613V) mutation. *The Journal of clinical investigation.* 2011;121(3):1009-25.
132. Araki T, Chan G, Newbigging S, Morikawa L, Bronson RT, and Neel BG. Noonan syndrome cardiac defects are caused by PTPN11 acting in endocardium to enhance endocardial-mesenchymal transformation. *Proceedings of the National Academy of Sciences of the United States of America.* 2009;106(12):4736-41.
133. Liu X, Zheng H, Li X, Wang S, Meyerson HJ, Yang W, Neel BG, and Qu CK. Gain-of-function mutations of Ptpn11 (Shp2) cause aberrant mitosis and increase susceptibility to DNA damage-induced malignancies. *Proceedings of the National Academy of Sciences of the United States of America.* 2016;113(4):984-9.
134. Yoshida R, Hasegawa T, Hasegawa Y, Nagai T, Kinoshita E, Tanaka Y, Kanegane H, Ohyama K, Onishi T, Hanew K, et al. Protein-tyrosine phosphatase, nonreceptor type 11 mutation analysis and clinical assessment in 45 patients with Noonan syndrome. *The Journal of clinical endocrinology and metabolism.* 2004;89(7):3359-64.
135. Keilhack H, David FS, McGregor M, Cantley LC, and Neel BG. Diverse biochemical properties of Shp2 mutants. Implications for disease phenotypes. *J Biol Chem.* 2005;280(35):30984-93.
136. Neel BG, Gu H, and Pao L. The 'Shp'ing news: SH2 domain-containing tyrosine phosphatases in cell signaling. *Trends Biochem Sci.* 2003;28(6):284-93.

137. Ernst M, and Jenkins BJ. Acquiring signalling specificity from the cytokine receptor gp130. *Trends in genetics : TIG.* 2004;20(1):23-32.
138. Feng GS. Shp-2 tyrosine phosphatase: signaling one cell or many. *Experimental cell research.* 1999;253(1):47-54.
139. Chong ZZ, and Maiese K. The Src homology 2 domain tyrosine phosphatases SHP-1 and SHP-2: diversified control of cell growth, inflammation, and injury. *Histology and histopathology.* 2007;22(11):1251-67.
140. Marin TM, Clemente CF, Santos AM, Picardi PK, Pascoal VD, Lopes-Cendes I, Saad MJ, and Franchini KG. Shp2 negatively regulates growth in cardiomyocytes by controlling focal adhesion kinase/Src and mTOR pathways. *Circulation research.* 2008;103(8):813-24.
141. Neel BG. Structure and function of SH2-domain containing tyrosine phosphatases. *Seminars in cell biology.* 1993;4(6):419-32.
142. Qu CK. The SHP-2 tyrosine phosphatase: signaling mechanisms and biological functions. *Cell research.* 2000;10(4):279-88.
143. Cai Z, Feng GS, and Zhang X. Temporal requirement of the protein tyrosine phosphatase Shp2 in establishing the neuronal fate in early retinal development. *The Journal of neuroscience : the official journal of the Society for Neuroscience.* 2010;30(11):4110-9.
144. Huang YS, Cheng CY, Chueh SH, Hueng DY, Huang YF, Chu CM, Wu ST, Tai MC, Liang CM, Liao MH, et al. Involvement of SHP2 in focal adhesion, migration and differentiation of neural stem cells. *Brain & development.* 2012;34(8):674-84.
145. Papale A, d'Isa R, Menna E, Cerovic M, Solari N, Hardingham N, Cambiaghi M, Cursi M, Barbacid M, Leocani L, et al. Severe Intellectual Disability and Enhanced Gamma-Aminobutyric Acidergic Synaptogenesis in a Novel Model of Rare RASopathies. *Biological psychiatry.* 2017;81(3):179-92.
146. Anastasaki C, Estep AL, Marais R, Rauen KA, and Patton EE. Kinase-activating and kinase-impaired cardio-facio-cutaneous syndrome alleles have activity during zebrafish development and are sensitive to small molecule inhibitors. *Human molecular genetics.* 2009;18(14):2543-54.
147. Yeh E, Dao DQ, Wu ZY, Kandalam SM, Camacho FM, Tom C, Zhang W, Krencik R, Rauen KA, Ullian EM, et al. Patient-derived iPSCs show premature neural differentiation and neuron type-specific phenotypes relevant to neurodevelopment. *Molecular psychiatry.* 2017.
148. Yeh TH, Lee DY, Gianino SM, and Gutmann DH. Microarray analyses reveal regional astrocyte heterogeneity with implications for neurofibromatosis type 1 (NF1)-regulated glial proliferation. *Glia.* 2009;57(11):1239-49.
149. Wiese S, Pei G, Karch C, Troppmair J, Holtmann B, Rapp UR, and Sendtner M. Specific function of B-Raf in mediating survival of embryonic motoneurons and sensory neurons. *Nature neuroscience.*

2001;4(2):137-42.
150. Wojnowski L, Zimmer AM, Beck TW, Hahn H, Bernal R, Rapp UR, and Zimmer A. Endothelial apoptosis in Braf-deficient mice. *Nature genetics.* 1997;16(3):293-7.
151. Chen AP, Ohno M, Giese KP, Kuhn R, Chen RL, and Silva AJ. Forebrain-specific knockout of B-raf kinase leads to deficits in hippocampal long-term potentiation, learning, and memory. *Journal of neuroscience research.* 2006;83(1):28-38.
152. Moriya M, Inoue S, Miyagawa-Tomita S, Nakashima Y, Oba D, Niihori T, Hashi M, Ohnishi H, Kure S, Matsubara Y, et al. Adult mice expressing a Braf Q241R mutation on an ICR/CD-1 background exhibit a cardio-facio-cutaneous syndrome phenotype. *Human molecular genetics.* 2015;24(25):7349-60.
153. Andreadi C, Cheung LK, Giblett S, Patel B, Jin H, Mercer K, Kamata T, Lee P, Williams A, McMahon M, et al. The intermediate-activity (L597V)BRAF mutant acts as an epistatic modifier of oncogenic RAS by enhancing signaling through the RAF/MEK/ERK pathway. *Genes & development.* 2012;26(17):1945-58.
154. Inoue S, Moriya M, Watanabe Y, Miyagawa-Tomita S, Niihori T, Oba D, Ono M, Kure S, Ogura T, Matsubara Y, et al. New BRAF knockin mice provide a pathogenetic mechanism of developmental defects and a therapeutic approach in cardio-facio-cutaneous syndrome. *Human molecular genetics.* 2014;23(24):6553-66.
155. Gripp KW, Hopkins E, Sol-Church K, Stabley DL, Axelrad ME, Doyle D, Dobyns WB, Hudson C, Johnson J, Tenconi R, et al. Phenotypic analysis of individuals with Costello syndrome due to HRAS p.G13C. *American journal of medical genetics Part A.* 2011;155a(4):706-16.
156. Abe Y, Aoki Y, Kuriyama S, Kawame H, Okamoto N, Kurosawa K, Ohashi H, Mizuno S, Ogata T, Kure S, et al. Prevalence and clinical features of Costello syndrome and cardio-facio-cutaneous syndrome in Japan: findings from a nationwide epidemiological survey. *American journal of medical genetics Part A.* 2012;158a(5):1083-94.
157. Costello JM. A new syndrome: mental subnormality and nasal papillomata. *Australian paediatric journal.* 1977;13(2):114-8.
158. Gripp KW, Lin AE, Stabley DL, Nicholson L, Scott CI, Jr., Doyle D, Aoki Y, Matsubara Y, Zackai EH, Lapunzina P, et al. HRAS mutation analysis in Costello syndrome: genotype and phenotype correlation. *American journal of medical genetics Part A.* 2006;140(1):1-7.
159. Gibbs JB, Sigal IS, Poe M, and Scolnick EM. Intrinsic GTPase activity distinguishes normal and oncogenic ras p21 molecules. *Proceedings of the National Academy of Sciences of the United States of America.* 1984;81(18):5704-8.
160. Bertola DR, Pereira AC, Brasil AS, Albano LM, Kim CA, and Krieger JE. Further evidence of genetic heterogeneity in Costello syndrome: involvement of the KRAS gene. *Journal of human genetics.* 2007;52(6):521-6.
161. Gripp KW, and Lin AE. Costello syndrome: a Ras/mitogen activated

protein kinase pathway syndrome (rasopathy) resulting from HRAS germline mutations. *Genetics in medicine : official journal of the American College of Medical Genetics.* 2012;14(3):285-92.
162. Lin AE, Alexander ME, Colan SD, Kerr B, Rauen KA, Noonan J, Baffa J, Hopkins E, Sol-Church K, Limongelli G, et al. Clinical, pathological, and molecular analyses of cardiovascular abnormalities in Costello syndrome: a Ras/MAPK pathway syndrome. *American journal of medical genetics Part A.* 2011;155a(3):486-507.
163. Krencik R, Hokanson KC, Narayan AR, Dvornik J, Rooney GE, Rauen KA, Weiss LA, Rowitch DH, and Ullian EM. Dysregulation of astrocyte extracellular signaling in Costello syndrome. *Science translational medicine.* 2015;7(286):286ra66.
164. Rooney GE, Goodwin AF, Depeille P, Sharir A, Schofield CM, Yeh E, Roose JP, Klein OD, Rauen KA, Weiss LA, et al. Human iPS Cell-Derived Neurons Uncover the Impact of Increased Ras Signaling in Costello Syndrome. *The Journal of neuroscience : the official journal of the Society for Neuroscience.* 2016;36(1):142-52.
165. Gripp KW, Hopkins E, Doyle D, and Dobyns WB. High incidence of progressive postnatal cerebellar enlargement in Costello syndrome: brain overgrowth associated with HRAS mutations as the likely cause of structural brain and spinal cord abnormalities. *American journal of medical genetics Part A.* 2010;152a(5):1161-8.
166. Schuhmacher AJ, Guerra C, Sauzeau V, Canamero M, Bustelo XR, and Barbacid M. A mouse model for Costello syndrome reveals an Ang II-mediated hypertensive condition. *The Journal of clinical investigation.* 2008;118(6):2169-79.
167. Viosca J, Schuhmacher AJ, Guerra C, and Barco A. Germline expression of H-Ras(G12V) causes neurological deficits associated to Costello syndrome. *Genes, brain, and behavior.* 2009;8(1):60-71.
168. Paquin A, Hordo C, Kaplan DR, and Miller FD. Costello syndrome H-Ras alleles regulate cortical development. *Developmental biology.* 2009;330(2):440-51.
169. Ozkan ED, Creson TK, Kramar EA, Rojas C, Seese RR, Babyan AH, Shi Y, Lucero R, Xu X, Noebels JL, et al. Reduced cognition in Syngap1 mutants is caused by isolated damage within developing forebrain excitatory neurons. *Neuron.* 2014;82(6):1317-33.
170. Hancock JF. Ras proteins: different signals from different locations. *Nature reviews Molecular cell biology.* 2003;4(5):373-84.
171. Rocks O, Peyker A, and Bastiaens PI. Spatio-temporal segregation of Ras signals: one ship, three anchors, many harbors. *Current opinion in cell biology.* 2006;18(4):351-7.
172. Muñoz-Maldonado C, Zimmer Y, and Medová M. A Comparative Analysis of Individual RAS Mutations in Cancer Biology. *Frontiers in oncology.* 2019;9(1088.
173. Kang M, Ryu HH, and Lee YS. Comparisons of behavior and synaptic plasticity among three C57BL/6 substrains. *Animal Cells and Systems.* 2015;19(3):181-7.
174. Ryu HH, Kang M, Hwang KD, Jang HB, Kim SJ, and Lee YS. Neuron

type-specific expression of a mutant KRAS impairs hippocampal-dependent learning and memory. *Scientific reports.* 2020;10(1):17730.
175. Vong L, Ye C, Yang Z, Choi B, Chua S, Jr., and Lowell BB. Leptin action on GABAergic neurons prevents obesity and reduces inhibitory tone to POMC neurons. *Neuron.* 2011;71(1):142-54.
176. Langston RF, and Wood ER. Associative recognition and the hippocampus: differential effects of hippocampal lesions on object-place, object-context and object-place-context memory. *Hippocampus.* 2010;20(10):1139-53.
177. Maren S. Neurobiology of Pavlovian fear conditioning. *Annual review of neuroscience.* 2001;24(897-931.
178. Lee YS, and Silva AJ. The molecular and cellular biology of enhanced cognition. *Nat Rev Neurosci.* 2009;10(2):126-40.
179. Seok SH, Na YR, Han JH, Kim TH, Jung H, Lee BH, Emelyanov A, Parinov S, and Park JH. Cre/loxP-regulated transgenic zebrafish model for neural progenitor-specific oncogenic Kras expression. *Cancer science.* 2010;101(1):149-54.
180. Kim D, Herdeis L, Rudolph D, Zhao Y, Böttcher J, Vides A, Ayala-Santos CI, Pourfarjam Y, Cuevas-Navarro A, Xue JY, et al. Pan-KRAS inhibitor disables oncogenic signalling and tumour growth. *Nature.* 2023.
181. Garnett MJ, and Marais R. Guilty as charged: B-RAF is a human oncogene. *Cancer cell.* 2004;6(4):313-9.
182. Lim CS, Kang X, Mirabella V, Zhang H, Bu Q, Araki Y, Hoang ET, Wang S, Shen Y, Choi S, et al. BRaf signaling principles unveiled by large-scale human mutation analysis with a rapid lentivirus-based gene replacement method. *Genes & development.* 2017;31(6):537-52.
183. Chun H, Im H, Kang YJ, Kim Y, Shin JH, Won W, Lim J, Ju Y, Park YM, Kim S, et al. Severe reactive astrocytes precipitate pathological hallmarks of Alzheimer's disease via H2O2− production. *Nature neuroscience.* 2020;23(12):1555-66.
184. Morris R. Developments of a water-maze procedure for studying spatial learning in the rat. *Journal of neuroscience methods.* 1984;11(1):47-60.
185. Adviento B, Corbin IL, Widjaja F, Desachy G, Enrique N, Rosser T, Risi S, Marco EJ, Hendren RL, Bearden CE, et al. Autism traits in the RASopathies. *Journal of medical genetics.* 2014;51(1):10-20.
186. Suzuki S, Namiki J, Shibata S, Mastuzaki Y, and Okano H. The neural stem/progenitor cell marker nestin is expressed in proliferative endothelial cells, but not in mature vasculature. *The journal of histochemistry and cytochemistry : official journal of the Histochemistry Society.* 2010;58(8):721-30.
187. Pierpont ME, Magoulas PL, Adi S, Kavamura MI, Neri G, Noonan J, Pierpont EI, Reinker K, Roberts AE, Shankar S, et al. Cardio-facio-cutaneous syndrome: clinical features, diagnosis, and management guidelines. *Pediatrics.* 2014;134(4):e1149-62.

188. Seth S, Biswas T, Biswas B, Roy A, and Datta AK. Cardiofaciocutaneous Syndrome: Case Report of a Rare Disorder. *Journal of clinical and diagnostic research : JCDR.* 2016;10(11):Sd01-sd2.
189. Kavamura MI, Peres CA, Alchorne MM, and Brunoni D. CFC index for the diagnosis of cardiofaciocutaneous syndrome. *American journal of medical genetics.* 2002;112(1):12-6.
190. Kang M, and Lee YS. The impact of RASopathy-associated mutations on CNS development in mice and humans. *Molecular brain.* 2019;12(1):96.
191. Angara K, Pai EL-L, Bilinovich SM, Stafford AM, Nguyen JT, Li KX, Paul A, Rubenstein JL, and Vogt D. Nf1 deletion results in depletion of the Lhx6 transcription factor and a specific loss of parvalbumin(+) cortical interneurons. *Proceedings of the National Academy of Sciences of the United States of America.* 2020;117(11):6189-95.
192. Holter MC, Hewitt LT, Nishimura KJ, Knowles SJ, Bjorklund GR, Shah S, Fry NR, Rees KP, Gupta TA, Daniels CW, et al. Hyperactive MEK1 Signaling in Cortical GABAergic Neurons Promotes Embryonic Parvalbumin Neuron Loss and Defects in Behavioral Inhibition. *Cerebral Cortex.* 2021;31(6):3064-81.
193. Escartin C, Galea E, Lakatos A, O'Callaghan JP, Petzold GC, Serrano-Pozo A, Steinhäuser C, Volterra A, Carmignoto G, Agarwal A, et al. Reactive astrocyte nomenclature, definitions, and future directions. *Nature neuroscience.* 2021;24(3):312-25.
194. Hol EM, and Pekny M. Glial fibrillary acidic protein (GFAP) and the astrocyte intermediate filament system in diseases of the central nervous system. *Current opinion in cell biology.* 2015;32(121-30.
195. Michetti F, D'Ambrosi N, Toesca A, Puglisi MA, Serrano A, Marchese E, Corvino V, and Geloso MC. The S100B story: from biomarker to active factor in neural injury. *Journal of neurochemistry.* 2019;148(2):168-87.
196. Liu LR, Liu JC, Bao JS, Bai QQ, and Wang GQ. Interaction of Microglia and Astrocytes in the Neurovascular Unit. *Frontiers in immunology.* 2020;11(1024.
197. Zhang Y, Xu S, Liang KY, Li K, Zou ZP, Yang CL, Tan K, Cao X, Jiang Y, Gao TM, et al. Neuronal mTORC1 Is Required for Maintaining the Nonreactive State of Astrocytes. *J Biol Chem.* 2017;292(1):100-11.
198. Sofroniew MV. Molecular dissection of reactive astrogliosis and glial scar formation. *Trends in neurosciences.* 2009;32(12):638-47.
199. Reemst K, Noctor SC, Lucassen PJ, and Hol EM. The Indispensable Roles of Microglia and Astrocytes during Brain Development. *Frontiers in human neuroscience.* 2016;10(566.
200. Ortinski PI, Dong J, Mungenast A, Yue C, Takano H, Watson DJ, Haydon PG, and Coulter DA. Selective induction of astrocytic gliosis generates deficits in neuronal inhibition. *Nature neuroscience.* 2010;13(5):584-91.
201. Cornell-Bell AH, Finkbeiner SM, Cooper MS, and Smith SJ.

Glutamate induces calcium waves in cultured astrocytes: long-range glial signaling. *Science.* 1990;247(4941):470-3.
202. Guerra-Gomes S, Sousa N, Pinto L, and Oliveira JF. Functional Roles of Astrocyte Calcium Elevations: From Synapses to Behavior. *Frontiers in cellular neuroscience.* 2017;11(427.
203. Tanaka M, Shih PY, Gomi H, Yoshida T, Nakai J, Ando R, Furuichi T, Mikoshiba K, Semyanov A, and Itohara S. Astrocytic Ca2+ signals are required for the functional integrity of tripartite synapses. *Molecular brain.* 2013;6(6.
204. Delekate A, Füchtemeier M, Schumacher T, Ulbrich C, Foddis M, and Petzold GC. Metabotropic P2Y1 receptor signalling mediates astrocytic hyperactivity in vivo in an Alzheimer's disease mouse model. *Nature communications.* 2014;5(5422.
205. Kuchibhotla KV, Lattarulo CR, Hyman BT, and Bacskai BJ. Synchronous hyperactivity and intercellular calcium waves in astrocytes in Alzheimer mice. *Science.* 2009;323(5918):1211-5.
206. Lines J, Baraibar AM, Fang C, Martin ED, Aguilar J, Lee MK, Araque A, and Kofuji P. Astrocyte-neuronal network interplay is disrupted in Alzheimer's disease mice. *Glia.* 2022;70(2):368-78.
207. Tsien JZ, Chen DF, Gerber D, Tom C, Mercer EH, Anderson DJ, Mayford M, Kandel ER, and Tonegawa S. Subregion- and cell type-restricted gene knockout in mouse brain. *Cell.* 1996;87(7):1317-26.
208. Saito K, Kakizaki T, Hayashi R, Nishimaru H, Furukawa T, Nakazato Y, Takamori S, Ebihara S, Uematsu M, Mishina M, et al. The physiological roles of vesicular GABA transporter during embryonic development: a study using knockout mice. *Molecular brain.* 2010;3(40.
209. Chun H, Im H, Kang YJ, Kim Y, Shin JH, Won W, Lim J, Ju Y, Park YM, Kim S, et al. Severe reactive astrocytes precipitate pathological hallmarks of Alzheimer's disease via H(2)O(2)(-) production. *Nature neuroscience.* 2020;23(12):1555-66.
210. Jo S, Yarishkin O, Hwang YJ, Chun YE, Park M, Woo DH, Bae JY, Kim T, Lee J, Chun H, et al. GABA from reactive astrocytes impairs memory in mouse models of Alzheimer's disease. *Nature medicine.* 2014;20(8):886-96.
211. Scuderi C, Stecca C, Bronzuoli MR, Rotili D, Valente S, Mai A, and Steardo L. Sirtuin modulators control reactive gliosis in an in vitro model of Alzheimer's disease. *Front Pharmacol.* 2014;5(89-.
212. Wang Q, Kong Y, Wu DY, Liu JH, Jie W, You QL, Huang L, Hu J, Chu HD, Gao F, et al. Impaired calcium signaling in astrocytes modulates autism spectrum disorder-like behaviors in mice. *Nature communications.* 2021;12(1):3321.
213. Allen M, Huang BS, Notaras MJ, Lodhi A, Barrio-Alonso E, Lituma PJ, Wolujewicz P, Witztum J, Longo F, Chen M, et al. Astrocytes derived from ASD individuals alter behavior and destabilize neuronal activity through aberrant Ca(2+) signaling. *Molecular psychiatry.* 2022;27(5):2470-84.
214. Liao SL, Ou YC, Lin SY, Kao TK, Pan HC, Chang CY, Lai CY, Lu HC,

Wang WY, and Chen CJ. Signaling cascades mediate astrocyte death induced by zinc. *Toxicology letters.* 2011;204(2-3):108-17.
215. Xu L, Wang L, Wen Z, Wu L, Jiang Y, Yang L, Xiao L, Xie Y, Ma M, Zhu W, et al. Caveolin-1 is a checkpoint regulator in hypoxia-induced astrocyte apoptosis via Ras/Raf/ERK pathway. *American journal of physiology Cell physiology.* 2016;310(11):C903-10.
216. Saito K, Shigetomi E, Yasuda R, Sato R, Nakano M, Tashiro K, Tanaka KF, Ikenaka K, Mikoshiba K, Mizuta I, et al. Aberrant astrocyte Ca(2+) signals "AxCa signals" exacerbate pathological alterations in an Alexander disease model. *Glia.* 2018;66(5):1053-67.
217. Morita M, Higuchi C, Moto T, Kozuka N, Susuki J, Itofusa R, Yamashita J, and Kudo Y. Dual regulation of calcium oscillation in astrocytes by growth factors and pro-inflammatory cytokines via the mitogen-activated protein kinase cascade. *The Journal of neuroscience : the official journal of the Society for Neuroscience.* 2003;23(34):10944-52.
218. Billups D, Billups B, Challiss RA, and Nahorski SR. Modulation of Gq-protein-coupled inositol trisphosphate and Ca2+ signaling by the membrane potential. *The Journal of neuroscience : the official journal of the Society for Neuroscience.* 2006;26(39):9983-95.
219. Petravicz J, Fiacco TA, and McCarthy KD. Loss of IP3 receptor-dependent Ca2+ increases in hippocampal astrocytes does not affect baseline CA1 pyramidal neuron synaptic activity. *The Journal of neuroscience : the official journal of the Society for Neuroscience.* 2008;28(19):4967-73.
220. Wu Z, Guo Z, Gearing M, and Chen G. Tonic inhibition in dentate gyrus impairs long-term potentiation and memory in an Alzheimer's [corrected] disease model. *Nature communications.* 2014;5(4159.
221. Lee W, Reyes RC, Gottipati MK, Lewis K, Lesort M, Parpura V, and Gray M. Enhanced Ca(2+)-dependent glutamate release from astrocytes of the BACHD Huntington's disease mouse model. *Neurobiology of disease.* 2013;58(192-9.
222. Tong X, Ao Y, Faas GC, Nwaobi SE, Xu J, Haustein MD, Anderson MA, Mody I, Olsen ML, Sofroniew MV, et al. Astrocyte Kir4.1 ion channel deficits contribute to neuronal dysfunction in Huntington's disease model mice. *Nature neuroscience.* 2014;17(5):694-703.
223. Cahoy JD, Emery B, Kaushal A, Foo LC, Zamanian JL, Christopherson KS, Xing Y, Lubischer JL, Krieg PA, Krupenko SA, et al. A transcriptome database for astrocytes, neurons, and oligodendrocytes: a new resource for understanding brain development and function. *The Journal of neuroscience : the official journal of the Society for Neuroscience.* 2008;28(1):264-78.
224. Bayraktar OA, Fuentealba LC, Alvarez-Buylla A, and Rowitch DH. Astrocyte development and heterogeneity. *Cold Spring Harbor perspectives in biology.* 2014;7(1):a020362.
225. Poolos NP, Bullis JB, and Roth MK. Modulation of h-Channels in Hippocampal Pyramidal Neurons by p38 Mitogen-Activated Protein Kinase. *The Journal of Neuroscience.* 2006;26(30):7995-8003.

226. Park E, Rawson S, Li K, Kim B-W, Ficarro SB, Pino GG-D, Sharif H, Marto JA, Jeon H, and Eck MJ. Architecture of autoinhibited and active BRAF-MEK1-14-3-3 complexes. *Nature.* 2019;575(7783):545-50.
227. Li D, Liu N, Zhao HH, Zhang X, Kawano H, Liu L, Zhao L, and Li HP. Interactions between Sirt1 and MAPKs regulate astrocyte activation induced by brain injury in vitro and in vivo. *Journal of neuroinflammation.* 2017;14(1):67.
228. Gutmann DH, Aylsworth A, Carey JC, Korf B, Marks J, Pyeritz RE, Rubenstein A, and Viskochil D. The diagnostic evaluation and multidisciplinary management of neurofibromatosis 1 and neurofibromatosis 2. *Jama.* 1997;278(1):51-7.

국문 초록

신경세포와 교세포의 Ras 경로 과활성화가 Ras 관련 신경발달장애 생쥐 모델의 기억장애에 미치는 영향

강 민 경
서울대학교 대학원
의과대학 의과학과

RAS-ERK 신호 전달 경로는 여러 세포에 존재한다고 알려져 있는 신호 전달 경로로써 세포의 생존과 분화, 시냅스 전달, 그리고 학습과 기억 등 중추신경계에서 다양한 뇌 기능에 관여한다. 이 경로에 관여하는 유전자들의 돌연변이에 의해서 다양한 질병이 발생하게 되는데 이들을 총칭하여 RASopathy라고 부르고, 신경섬유종 1형, 누난 증후군, 심장-얼굴-피부 증후군, 그리고 코스텔로 증후군 등이 이에 속한다. RASopathy와 연관되어 있는 돌연변이들은 대부분 RAS-ERK 신호 전달 경로를 과활성시키며 대부분의 RASopathy 케이스는 공통적인 특징을 보이는데, 그중 하나가 바로 인지 기능 장애이다. 다양한 생쥐 모델을 이용한 최근 연구들은 RAS-ERK 신호 전달 경로 구성 유전자들이 세포 타입 특이성에 따라 각기 다른 분자, 세포적 병리 생리학적 기전을 가진다고 보고한 바 있다. 본 학위 논문에서는 RASopathy 연관 인지 기능 장애의 병리기전에 있어 신경세포와 성상교세포가 각기 다른 역할을 수행할 것이라는 가설을 설정하였다. 이를 확인하기 위해 두 가지 종류의 RASopathy 생쥐 모델, *KRAS*^{G12V}와 *BRAF*^{K499E}에서 인지 장애를 유발하는 세포 타입 특이적 메커니즘에 대해 연구하였다.

Chapter 1에서는, 환자와 생쥐 모델의 중추신경계 발달과 인지 기능에 있어 RASopathy 관련 돌연변이의 특징적인 역할을 리뷰하였고, RAS-ERK 신호 전달 경로 유전자들의 병리적 기전에 관한 문헌들을 정리하였다.

Chapter 2에서는 $KRAS^{G12V}$ 발현을 통한 RAS-ERK 신호 전달 경로의 신경세포 타입 특이적 조절이 해마 인지 기능에 미치는 영향에 대해 연구하였고, $KRAS^{G12V}$의 발현이 흥분성 신경세포와 억제성 신경세포 모두에서 각기 다른 이유로 학습과 기억 장애를 유발하는 것을 확인하였다. 억제성 신경세포에서 $KRAS^{G12V}$는 억제성 시냅스 전달를 증가시켰으며, 시냅스 가소성을 손상시켰다. 이에 반해 흥분성 신경세포에서 $KRAS^{G12V}$는 신경세포 사멸을 유발하였다. 이러한 결과는 억제성 신경세포와 흥분성 신경세포 두 가지 모두가 서로 다른 메커니즘을 통해 KRAS와 연관된 인지 기능 장애에 관여하고 있다는 것을 의미한다.

Chapter 3에서는 비이상적인 Braf 신호가 어떻게 인지 기능에 영향을 미치는지 RASopathy 연관 Braf 돌연변이를 이용하여 연구하였다. 신경 줄기 세포 특이적으로 $Braf^{K499E}$를 발현하는 생쥐는 심각한 학습 장애를 보였지만 흥분성 혹은 억제성 신경세포 특이적으로 $Braf^{K499E}$를 발현하는 생쥐는 정상적으로 학습했다. $Braf^{K499E}$는 RAS-ERK 신호 전달 경로를 과활성화 시켰으며, 성상교세포를 반응성 상태로 변화시켰다. 특히, 성체 시기에서 성상교세포 특이적인 돌연변이 BRAF의 발현 역시 세포적, 행동적 장애를 유도할 수 있었고, 성상교세포 내부의 칼슘 신호가 비이상적으로 증가되어 있음을 확인하였다. 마지막으로, 발달 단계부터 $Braf^{K499E}$를 발현하는 생쥐의 성체 시기에 성상교세포 특이적으로만 RAS-ERK 신호 전달 경로를 정상화 시켰을 때 학습 장애가 회복되는 것을 확인하였다.

결론적으로, 본 학위 논문에서는 RASopathy 연관 유전자들이 여러 중추신경계 세포 타입의 기능적 특성에 각기 다른 영향을 미치며, 이는 RASopathy 환자들의 세포 타입 특이적 병리기전을 뒷받침한다. *KRAS*로 인해 매개되는 학습 장애에서 신경세포의 기여를, 그리고 *BRAF*로 인해 매개되는 학습 장애에서는 성상교세포의 기여를 확인함으로써, 각 유전자 특이적인 조건에서 신경세포와 성상교세포 모두가 RASopathy 연관 인지 기능 장애의 원인이라는 결론을 얻었다. 또한, 본 학위 논문의 연구는 이 연구에서 다루지 않은 다른 RASopathy 연관 인지 기능 장애의 메커니즘에 대해 새로운 이해와 통찰을 제공할 수 있을 것으로 기대한다.

핵심어: RAS-ERK 신호 전달 경로, 신경 발달 질환, 학습과 기억, 해마
학번: 2017-37022